IITRI

CASE FILE COPY

IITRI-B6058-40
(Final Report)

PROTECTIVE COATINGS FOR

REFRACTORY METALS IN ROCKET ENGINES

National Aeronautics and
Space Administration
Washington, D. C.   20546

Contract No. NAS7-431

IITRI-B6058-40
(Final Report)

PROTECTIVE COATINGS FOR

REFRACTORY METALS IN ROCKET ENGINES

National Aeronautics and
Space Administration
Washington, D. C.   20546

Contract No. NAS7-431

IIT RESEARCH INSTITUTE
Technology Center
Chicago, Illinois   60616

PROTECTIVE COATINGS FOR

REFRACTORY METALS IN ROCKET ENGINES

IITRI-B6058-40
(Final Report)

13 January 1968 to 13 March 1969

Contract No. NAS7-431

Submitted to:

NASA Headquarters
Washington, D. C. 20546

RPL/Liquid Propulsion Technology
F. E. Compitello

5 August 1969

FOREWORD

This is Report No. IITRI-B6058-40 of IITRI Project B6058 under Contract NAS7-431, entitled "Protective Coatings for Refractory Metals in Rocket Engines," and covers work performed during the period 13 January 1968 to 13 March 1969. Also summarized in this report is information included in previous reports B6058-26 and B6058-13.

Personnel who contributed to this project included: V. L. Hill, Manager, Coatings Research, who was the IITRI Project Manager; and M. J. Malatesta, Assistant Metallurgist, who acted as Project Engineer on this program. The cooperation of R. Cannova of the Jet Propulsion Laboratory, Project Monitor, is gratefully acknowledged. Y. Harada of the Ceramics Research Division, IITRI, and Dr. E. V. Clougherty of ManLabs, Inc., kindly supplied carbide-graphite composites and borides, respectively, for corrosion evaluation.

Data are recorded in IITRI Logbooks C16959, C17539, and C17767.

V. L. Hill
Manager, Coatings Research

N. M. Parikh
Director, Metals Research

ABSTRACT

The objective of this program is to develop coating systems of refractory metals for use on rocket nozzles for liquid propellants containing both fluorides and oxygen.

Tungsten, iridium, Ir-33 w/o Re, rhenium, ATJ graphite, HfC-20 v/o C, TaC-20 v/o C, and ZrB_2-SiC-C were evaluated in oxygen, fluorine, hydrogen fluoride, fluorine-oxygen, and hydrogen fluoride-oxygen atmospheres at 3000°-5500°F. In all environments iridium and iridium-33Re had the lowest recession rates to their respective melting points of 4450°F and 4750°F; rhenium had the lowest recession rates in the combined environments at 5000°F. Materials which form solid oxides were not resistant to the combined environments.

Development of Ir-Re/Re duplex coatings by slurry techniques was investigated based on previous work on Ir/Re duplex coatings. Sintering studies showed that Ir-20Re coatings could be developed using the same technique used for unalloyed iridium.

Sintered carbide coatings based on Hf-10Ta for use on Ta-10W substrates were investigated. High density coatings could not be sintered at carbon contents above 4.5 w/o carbon. A duplex coating process and subsequent carburization was effective in producing 20 mil coatings with carbon contents above 5.5 w/o.

Eight rocket nozzles were coated for engine firing tests. Four of these nozzles are to be fired in hydrazine-nitrogen tetroxide, and the remaining in a fluorine-containing propellant system. Tungsten nozzles coated with Ir, Ir/Re, and Ir-20Re/Re and Ta-10W nozzles with Ir/Re and (Hf-10Ta)C duplex coatings have been submitted.

TABLE OF CONTENTS

LIST OF ILLUSTRATIONS

LIST OF ILLUSTRATIONS (Continued)

LIST OF TABLES

LIST OF TABLES (Continued)

PROTECTIVE COATINGS FOR

REFRACTORY METALS IN ROCKET ENGINES

I.   INTRODUCTION

The objective of this program was to investigate and develop materials and coating systems for use in liquid rocket combustion products at temperatures above 4000°F. Current emphasis is on the development of material systems for use in the combustion products of fluorine fuels. These environments require materials capable of resisting the combined effects of both fluorine compounds and oxygen. Effort in this program was intended to define the refractory materials capable of withstanding these environments at temperatures above 4000°F. Subsequently, the compatibility data was translated into the development of processes for fabricating rocket nozzles of resistant materials for rocket engine firing tests.

Effort was directed toward four tasks: (1) corrosion tests of selected materials in oxygen, fluorine, hydrogen fluoride, fluorine-oxygen, and hydrogen fluoride-oxygen environments, (2) development of Ir-33Re/Re duplex coatings, (3) development of carbide coatings, and (4) coating of small rocket nozzles. These tasks were extensions of previous work to define materials and coating systems for use in combined fluorine-oxygen environments. The coatings applied to rocket nozzle components for evaluation in hydrocarbon and fluorine engines were based on coatings developed during previous and current work.

Evaluation of materials in fluorine-oxygen and hydrogen fluoride-oxygen environments extended the work in fluorine and hydrogen fluoride atmospheres to the combined environments. Materials evaluated included graphites, graphite-carbide composites, borides, iridium, rhenium, and iridium-rhenium alloys. In these

evaluations, tungsten was used as the reference material because of its lower cost and because of extensive data available on fluorine corrosion. The exposure temperatures and fluorine-oxygen ratios were based on data on the combustion products of typical fluorine-containing propellant systems.

Effort on Ir-33Re/Re duplex coatings was an extension of previous work on Ir/Re duplex coatings. In the latter, addition of appreciable amounts of rhenium altered the sintering characteristics of the Ir-33Cu slurry used for iridium coatings. The Ir-Re coatings generally contained porosity that was not present in the iridium coatings of the same slurry composition, and under the same sintering conditions. Modifications of the metallic vehicle concentrations and sintering conditions required to obtain high-density Ir-33Re coatings were investigated.

Development of carbide coatings was an extension of the feasibility studies conducted on hafnium carbide based coatings (IITRI-B6058-26). Slurry coating studies, in which silicon was the metallic vehicle, evaluated the effect of slurry composition, powder particle size, and sintering conditions on carbide coatings, particularly those at 5-6 wt% C. The objective was to develop dense coatings in the 10 to 20 mil range, based on HfC and modified with TaC or other additions which improve the oxidation-corrosion behavior.

II.   EXPERIMENTAL PROCEDURE AND RESULTS

A.   Oxidation-Corrosion Testing

Prior to this program, very limited data were available in literature on the corrosion of refractory materials in fluorine or hydrogen fluoride. A review of the available information was presented previously in IITRI-B6058-13.[1] Most of the data were for oxides, graphite, or the refractory metals tantalum and tungsten, and were generally obtained in static tests or by thermody-

namic calculations. Comprehensive data on corrosion at high gas velocities and/or over a range of temperatures, did not exist.

During previous phases in this program, a number of refractory materials were evaluated in high-velocity fluorine and hydrogen fluoride environments at 2500 to 5200°F.[1,2] Materials evaluated include refractory metals and alloys, graphites, carbides, borides, and composite materials. The majority of these tests were conducted in argon-6.5% fluorine and argon-10% hydrogen fluoride. Generally, the results demonstrated that the corrosion rate of most materials was less in hydrogen fluoride than in fluorine. Also, many materials exhibited decreasing corrosion rate with increasing temperature in fluorine at a constant gas-flow rate. This effect was due to a decrease in the stability of the fluoride reaction products at high temperatures.

Corrosion testing during the current program consisted of the following:

1. Extension of corrosion data for selected materials in fluorine and hydrogen fluoride to higher temperatures than previously investigated.

2. Measurement of the rate of oxidation of these materials at 3000-5800°F.

3. Evaluation of these materials in combined fluorine-oxygen and hydrogen fluoride-oxygen atmospheres.

Corrosion data previously obtained in fluorine and hydrogen fluoride were limited to 4000°F for nonmetals and about 5200°F for refractory metals. This was due to the input power of the 2.5 kw induction unit.

During the current program, a 5 kw induction unit was installed in the fluorine corrosion test facility. This permitted evaluation of graphite, carbides, and borides at temperatures to 5000°F, and refractory metals to about 5800°F. Accordingly, corrosion data in 6.5 v/o fluorine and 10 v/o hydrogen fluoride were obtained up to these temperatures or to the melting points for the materials evaluated in the current program.

Measurement of oxidation rates was intended to provide a means of comparison of the surface recession rates in the individual gases with the combined atmospheres. Oxidation data existed in the literature for the tungsten and graphite materials tested in this program. However, these data did not include the temperature ranges, gas flow rates, or oxygen pressures of interest. Therefore, all of the materials evaluated in this program were exposed in argon containing 0.56 to 5.4 v/o oxygen at temperatures to 5800°F. As will be discussed subsequently, the oxygen concentrations employed were predicated on the volumetric concentrations used for the combined tests.

The environments selected for evaluation of materials in combined fluorine-oxygen and hydrogen fluoride-oxygen were based on both the previous data in fluorine and hydrogen fluoride and information on the reaction products of OF_2/B_2H_6 combustion obtained from the Jet Propulsion Laboratory. In the combined tests, fluorine and hydrogen fluoride concentrations were fixed at 6.5 and 10 v/o, respectively, to provide a comparison with previous corrosion data. Oxygen ratios were then selected based on combustion data for an OF_2/B_2H_6 engine operating at a chamber pressure of 100 psi and mixture ratios of 4 and 6. These mixture ratios correspond to maximum specific impulse and maximum flame temperature, respectively. Under these combustion conditions, the ratios of the mole fractions of hydrogen fluoride to atomic oxygen were 20:1 and 4:1 for mixture ratios of 4 and 6, respectively. The corresponding ratios of atomic fluorine to atomic oxygen were 1.6:1 and 1.2:1. Combining these ratios with the fixed concentrations of 6.5 v/o fluorine and 10 v/o hydrogen fluoride, the oxygen concentrations were, therefore, 0.56 and 2.3 v/o in tests with 10 v/o hydrogen fluoride, and 4.0 and 5.4 v/o in tests with 6.5 v/o fluorine. These ratios were used for all combined fluorine-oxygen and hydrogen fluoride-oxygen tests. A summary of volumetric concentration, and corresponding flow rates, for all oxidation-corrosion atmospheres is presented in Table I. Since all tests were at a total flow rate of 10 cfh, conversion of volume present to flow rate in cfh is obtained by simply dividing by 10.

TABLE I

COMPOSITION OF ATMOSPHERES
EMPLOYED FOR OXIDATION-CORROSION TESTS

Test Atmosphere	Corrodent Concentration, v/o*	Corrodent Gas Flow Rate, cfh	
		Fluorine or Hydrogen Fluoride	Oxygen
Oxygen	2.3	--	0.23
	4.0	--	0.40
	5.4	--	0.54
Fluorine	6.5	0.65	--
HF	10	1.0	--
Fluorine-Oxygen	$6.5F_2-4.00_2$	0.65	0.40
	$6.5F_2-5.40_2$	0.65	0.54
HF-Oxygen	$10HF-0.560_2$	1.0	0.056
	$10HF-2.30_2$	1.0	0.23

[+]Total flow rate 10 cfh.

*Remainder argon.

5

1.   Testing Methods

During previous work on this program,[1] a test facil-
ity was constructed capable of evaluating the corrosion resist-
ance of refractory materials in flowing fluorine at temperatures
to 5200°F under variable flow conditions. This facility and the
test methods developed previously were also employed for corro-
sion tests in this program. The test facility is shown in Fig-
ure 1. Test samples 0.5 x 0.5 x 0.125 in. thick were heated by
self-inductance in a thick-walled stainless steel chamber using
a 2.5 kw induction unit. Thus, the maximum temperature limit
was defined by the material under test and the input power. Met-
als were tested at temperatures to 5200°F and nonmetallic materi-
als (carbides, graphite) to 4000°F. A 5 kw induction unit was
installed in the corrosion facility during the current program.
This modification permitted testing of metals to about 5800°F,
and nonmetals to about 5000°F. Temperature measurements were
made optically through a top sight glass which permitted visual
observation of specimen deterioration during exposure.

A schematic diagram of the test chamber is shown in
Figure 2. Argon and the corrosive gases are metered in precision
flow meters and premixed before entering the nozzle assembly.
Fluorine is passed through a sodium bifluoride trap to remove re-
sidual hydrogen fluoride prior to entering the fluorine-flow
meter. This is necessary to eliminate reaction with the pyrex
flow meter. Kel F flow meters are used for metering hydrogen
fluoride. The nozzle assembly consists of thick-walled stainless
tubing swaged to obtain a 0.036 in. exit nozzle. During testing,
the nozzle exit was maintained at a distance of 1 in. from the
test specimen. Test specimens are supported in the induction
coil by a 0.125 in. tungsten rod, which is split to minimize the
contact area and stabilize the test specimen. Exiting reaction
products are passed through an activated charcoal absorption
column prior to exhausting through a laboratory hood.
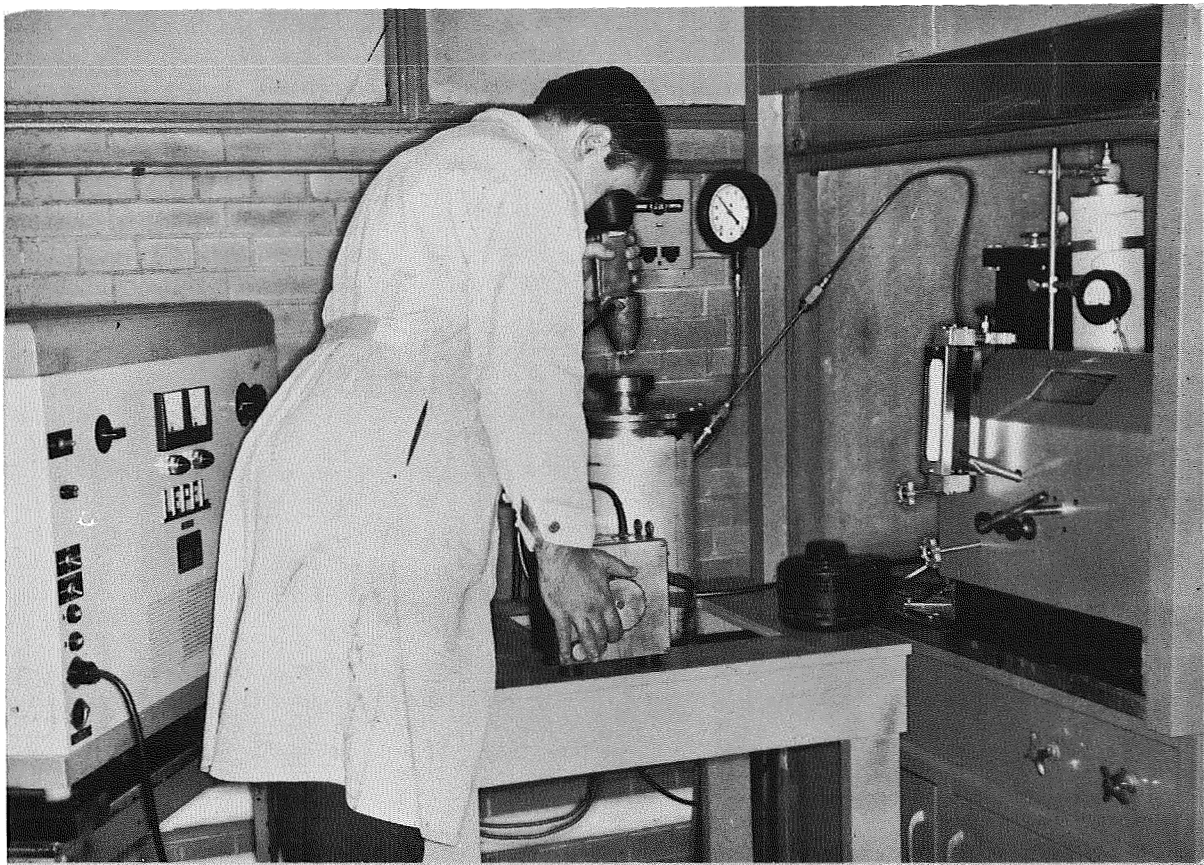
Neg. No. 30766

Fig. 1 - Equipment for Fluorine Corrosion Experiments.

LEGEND

1 TO VACUUM SYSTEM
2 TO EXHAUST SYSTEM
3 VACUUM PRESSURE
  GAGE
4 SIGHT PORT
5 GAS INLET
6 INDUCTION COIL
7 SAMPLE SUPPORT ROD
8 INDUCTION COIL
  POWER FEED
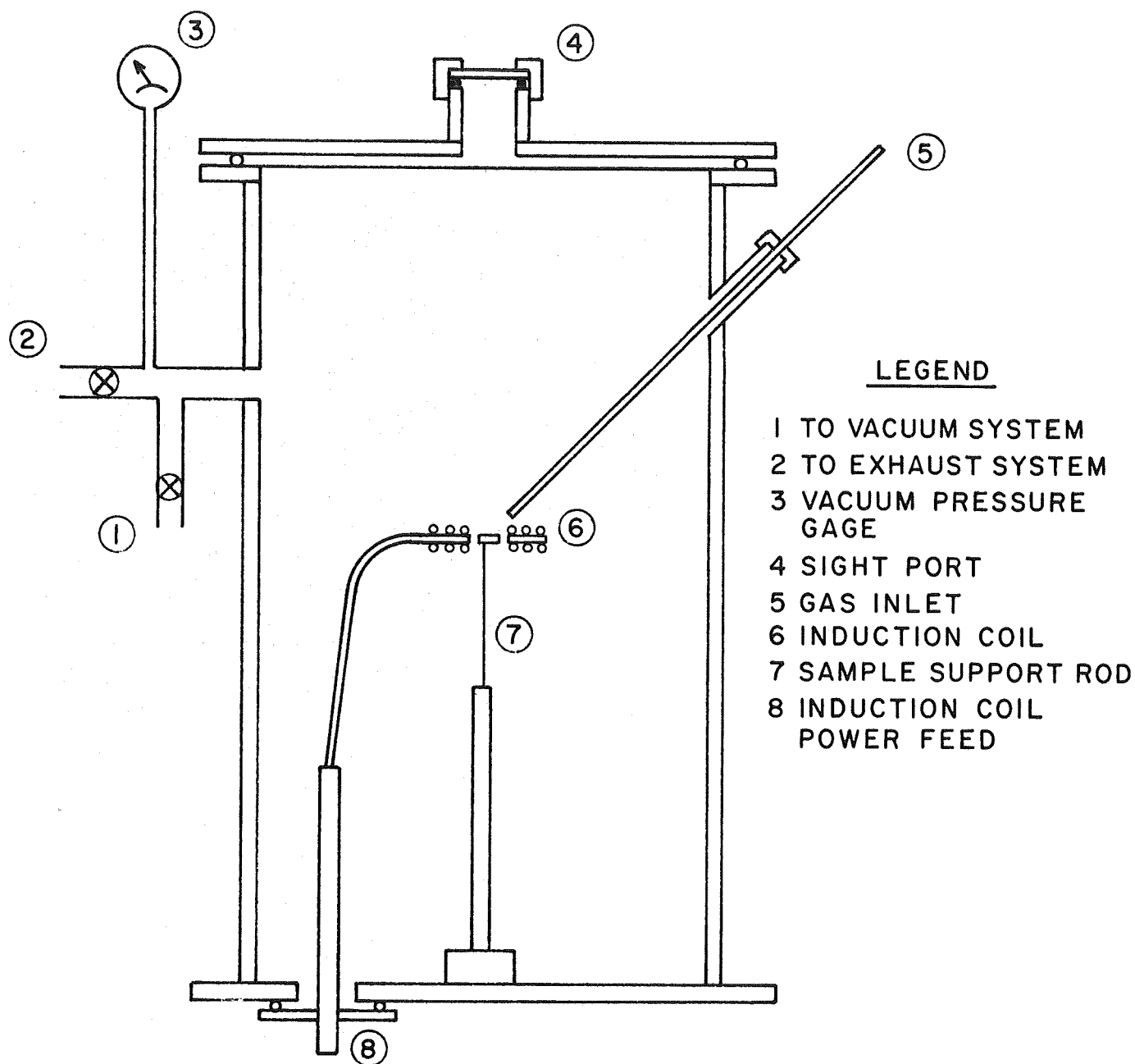
Fig. 2 - Schematic Diagram of Fluorine Reaction Chamber.

The following conditions for corrosion tests were constant during most of the tests: (1) nozzle distance, 1 in.; (2) total flow rate, 10 cfh; (3) exposure time, 5 min; and (4) nozzle exit velocity, 400 fps. Deviations were made only in specific cases where the effects of variations were examined. The test procedure was constant for the various corrosion tests. Test samples were heated to the exposure temperature with only the argon flowing. After stabilization of the sample temperature, the fluorine, hydrogen fluoride, and/or oxygen was introduced. Normally, this did not result in significant variation of the sample temperature since argon represented the major portion of the gas stream. In some cases, it was necessary to reduce the exposure time to 3 min because of extensive attack of the test sample, but this generally occurred only in tests with the highest concentrations of fluorine-oxygen. It is possible that the shorter exposure time may have influenced data scatter for some of the materials. On the other hand, increased exposure times were also employed for iridium alloys because of very low weight loss. Exposure times of up to 10 min were used for these alloys to obtain a higher total weight loss for recession rate calculations.

The surface recession rates contained in this report were calculated from weight loss of the normally 0.5 x 0.5 x 0.125 in. thick test samples, assuming a linear time dependence of the weight loss. Surface recession rates were therefore obtained by the following calculation:

$$\text{Recession rate (mils/min)} = \frac{\Delta w}{2.54\ A\rho t} \times 10^3$$

where

Δw = weight loss (g)
ρ = actual sample density (g/cm^3)
A = effective sample area (cm^2)
t = exposure time (min)

The effective surface area was obtained using one of the 0.5 x 0.5 in. surfaces (location of direct gas impingement) and the four 0.5 x 0.125 in. edges of the test sample. This is consistent with the observed location of attack on all test samples. Attack of the corrodent gases was usually not uniform over the test sample; material removed was maximum at the center of the 0.5 x 0.5 in. surface where direct gas impingement occurred. Thus, test samples tended to have a concave top surface after exposure. This concave top surface is described as "cratering" in the following discussion.

The effect of nozzle distance on the surface recession of tungsten in argon-6.5 v/o fluorine at 4000°F is summarized in Table II and plotted in Figure 3. As expected, the corrosion rate increases with decreasing nozzle distance, since less bypass and higher gas velocity should obtain at a decreased nozzle distance. The results indicate that only minor variations in corrosion rates existed for nozzle distances of around 1 in. Therefore, a 1 in. torch distance for samples near the nominal size is optimum to obtain the objective of the highest possible gas velocity and nozzle like. At the 1 in. nozzle distance the gas velocity across the sample surface should be only slightly less than the nozzle exit velocity (400 fps).

Also plotted in Figure 3 is the maximum recession rate obtained by micrometer measurements of the minimum thickness of the test samples after exposure. Although these measurements are probably not as accurate as weight loss, it is apparent that "cratering" increases rapidly at distances less than 1.5 in. This suggests that the fluorine-tungsten reaction rates are very rapid. If this were not the case, cratering would be less significant since material removal would tend to be more uniform over the test sample. The factor for conversion from the average surface recession to the maximum depth for a 1 in. nozzle distance is approximately 2.5 to 3. This value compares reasonably well for most of the materials tested in this program, at least for those materials with average corrosion rates above approximately 1.5 mils/min.

TABLE II

EFFECT OF NOZZLE DISTANCE
ON THE CORROSION RATE OF TUNGSTEN
IN ARGON-6.5 v/o FLUORINE MIXTURES AT 4000°F*

Nozzle Distance, in.	Weight Loss, g	Specific Weight Loss, $mg/cm^2/min$	Calculated Average Surface Recession Rate, mils/min	Maximum Measured Surface Recession, mils/min
0.75	1.904	140.0	2.9	9.3
1.0	1.787	128.6	2.6	6.8
1.25	1.739	130.5	2.7	6.2
1.25	1.896	137.0	2.8	6.3
1.5	1.587	119.5	2.4	4.6
1.75	1.504	109.0	2.2	3.8
1.75	1.690	120.5	2.5	4.3
2.5	1.518	109.0	2.2	3.0
3.0	1.166	90.5	1.8	2.5
3.0	1.274	94.5	1.9	2.4

* Total flow rate 10 cfh; fluorine flow rate 0.65 cfh.
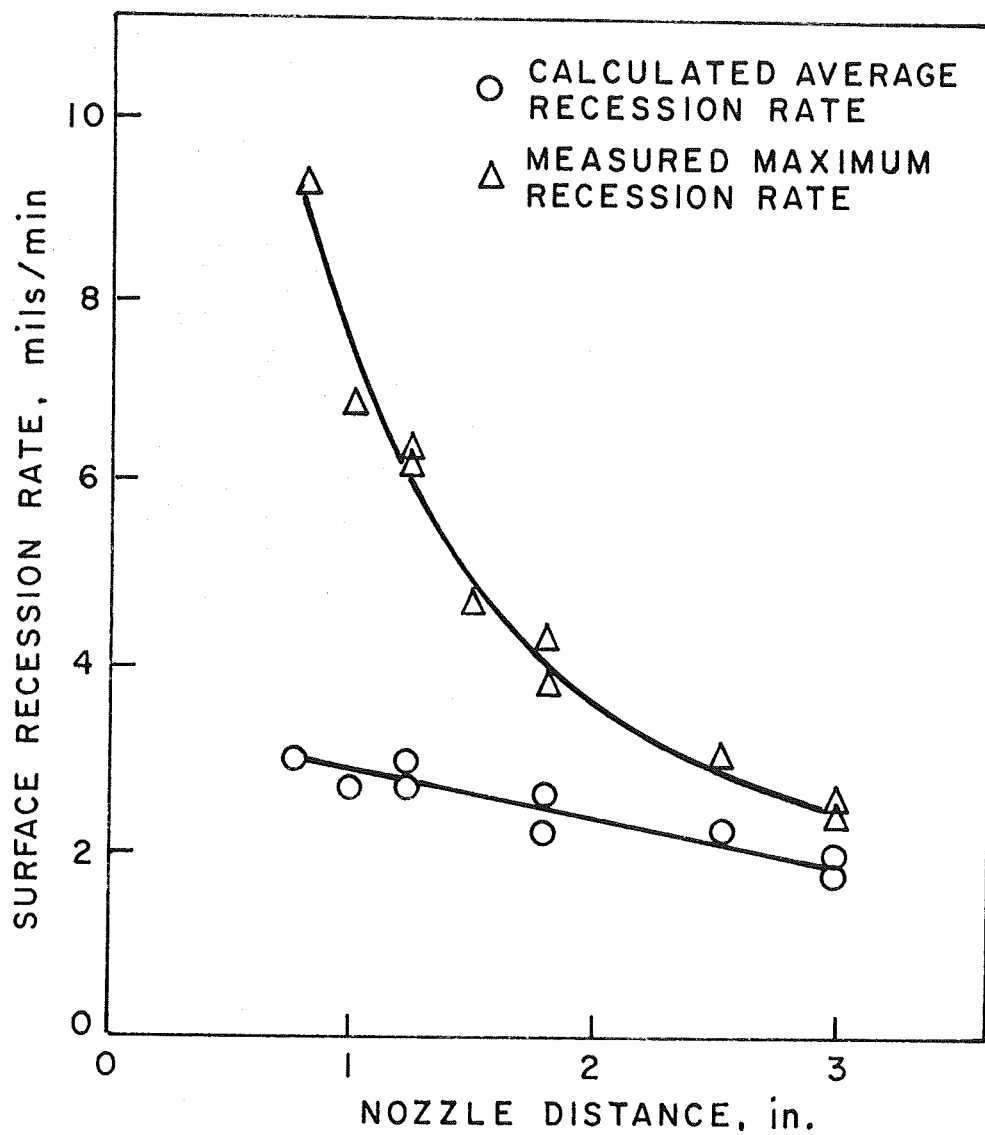
Fig. 3 - Effect of Nozzle Distance on the Corrosion
Rate of Tungsten in Argon-6.5 v/o Fluorine.

Figure 3 indicates the difficulty in measuring the cor-
rosion rate of gas-metal reactions by micrometer measurement of
the surface recession on a flat test sample. The geometry of the
test sample becomes important in the recession rate determination.
Obviously, one reason for the observed "cratering" is the gas
stream-sample geometry relationship for a fixed L/d ratio nozzle.
As the nozzle distance is decreased, the area of projection of
the major portion of the gas stream on the test sample is also
decreased. Furthermore, flow through the nozzle is probably not
uniform; a velocity gradient exists across the nozzle. Both of
these factors result in a decrease in the concentration of unre-
acted fluorine at the edges of the test sample. Since the corro-
sion rate is a function of the fluorine mass-flow rate and the
reaction rates are apparently rapid, preferential attack occurs
at the center of the test sample where the fluorine concentration
is at a maximum. This will occur if the reaction time is small
compared to the dwell time of fluorine molecules on the reaction
surface.

The above discussion indicates that the primary parame-
ter is the flow rate of fluorine per unit area. Measurement of
the recession rate at the point of most rapid attack (center) re-
sults in a recession rate that is too high in relationship to the
average rate of delivery of the reactive gas. A better measure
of the recession rate under specified flow conditions is to aver-
age the corrosion over the effective area of attack. Obviously,
this can lead to a calculated rate which is too low if the effec-
tive surface area of the sample is such that all of the available
reactant gas is used in the reaction. This is not the case for
the test conditions described herein, since calculations, assum-
ing a reaction product WF_6, indicate that more than one-half of
the available reactant gas remains after reaction with the test
samples.

A summary of the high-temperature materials tested dur-
ing the current program is given in Table III. The melting points

TABLE III

MATERIALS SELECTED FOR
CORROSION AND OXIDATION EVALUATION

| Material | Melting Point | | Emittance | Reference |
	°C	°F		
Tungsten	3410	6170	0.35	3
Rhenium	3180	5755	0.40	3
Iridium	2454	4450	0.30	3
Ir-33Re	2800	5070	0.35	4
ATJ Graphite	3727	6740	0.85	5
HfC-33 v/o C	3150	5734	0.85[*]	6
TaC-20 v/o C	3450	6274	0.85[*]	7
ZrB_2-SiC-C	2400[+]	4350	0.85[*]	3

[+]Estimate based on decomposition temperature of SiC.

[*]Estimated.

listed are the best available data for the various materials. In some cases, accurate melting point data are unavailable, particularly for the more complex materials. Consequently, the listed values for these materials are estimated from data on their components.

Exposure temperatures for fluorine and hydrogen fluoride corrosion tests given in this report are optical temperatures corrected for emittance of the material. Optical corrections were applied to all exposure temperatures based on the emittance values given in Table III. In the case of carbide and boride composites, accurate emittance data were unavailable. As a result, the estimated emittance may have been high, as will be discussed with the data for these materials.

Corrosion rates in fluorine and hydrogen fluoride measured previously, along with additional data in these gases obtained in the current program, are given in graphic and tabular form. This is intended to provide a comparison of the corrosion rates in the various corrodent gases.

A study establishing whether the corrodent gases could be safely premixed upstream of the nozzle was conducted prior to fluorine-oxygen and hydrogen fluoride-oxygen corrosion tests. Previously, hydrogen was injected at the nozzle exit in fluorine-hydrogen tests. However, upon attaching an injection assembly at the nozzle exit,[2] lower corrosion rates resulted, apparently caused by a modification of the gas flow path. Accordingly, a series of corrosion tests were conducted on tungsten primarily at 4000°F to compare the corrosion rates with premixed gases and injected oxygen. The oxidation rate was measured by introducing oxygen both through the nozzle and the injector.

The results of premixing and injection tests are summarized in Table IV and plotted in Figure 4. Surface recession data in Figure 4 illustrate lower corrosion rates were obtained in the combined atmosphere with the injector assembly. Thus, the

TABLE IV

CORROSION BEHAVIOR OF TUNGSTEN
IN FLOWING INJECTED AND PREMIXED FLUORINE-OXYGEN[a]

Exposure Temp., °F	Fluorine Concentration, v/o	Oxygen Concentration, v/o	Weight Loss, g	Specific Weight Loss, mg/cm²/min	Surface Recession Rate, mils/min
Injected Oxygen[b]					
3000	-	3.25	0.323	23.2	0.47
4000	-	1.08	0.179	13.0	0.26
4000	-	1.63	0.278	20.0	0.40
4000	-	3.25	0.453	32.7	0.66
4000	-	6.5	0.623	56.5	1.10
5000	-	3.25	0.515	37.4	0.76
4000	6.5	-	1.033	74.8	1.52
4000	6.5	1.08	1.078	78.4	1.59
4000	6.5	1.63	1.138	82.1	1.66
4000	6.5	3.25	1.361	99.6	2.03
Nozzle (Premixed) Tests[c]					
4000	-	1.08	0.570	45.2	0.92
4000	-	1.63	0.671	50.1	1.04
4000	-	3.25	0.898	114.5	2.32
4000	-	4.0	1.083	131.0	2.66
4000	6.5	1.08	1.886	142.0	2.88
4000	6.5	1.08	1.771	127.2	2.58
4000	6.5	1.63	1.888	135.0	2.76
4000	6.5	3.25	2.128	195.0	3.90
4000	6.5	3.28	2.566	186.1	3.81
4000	6.5	4.0	1.785	215.0	4.38

[a] Total flow rate - 10 cfh (400 fps).

[b] Fluorine through nozzle--oxygen through injector.

[c] Fluorine and/or oxygen through nozzle.

16
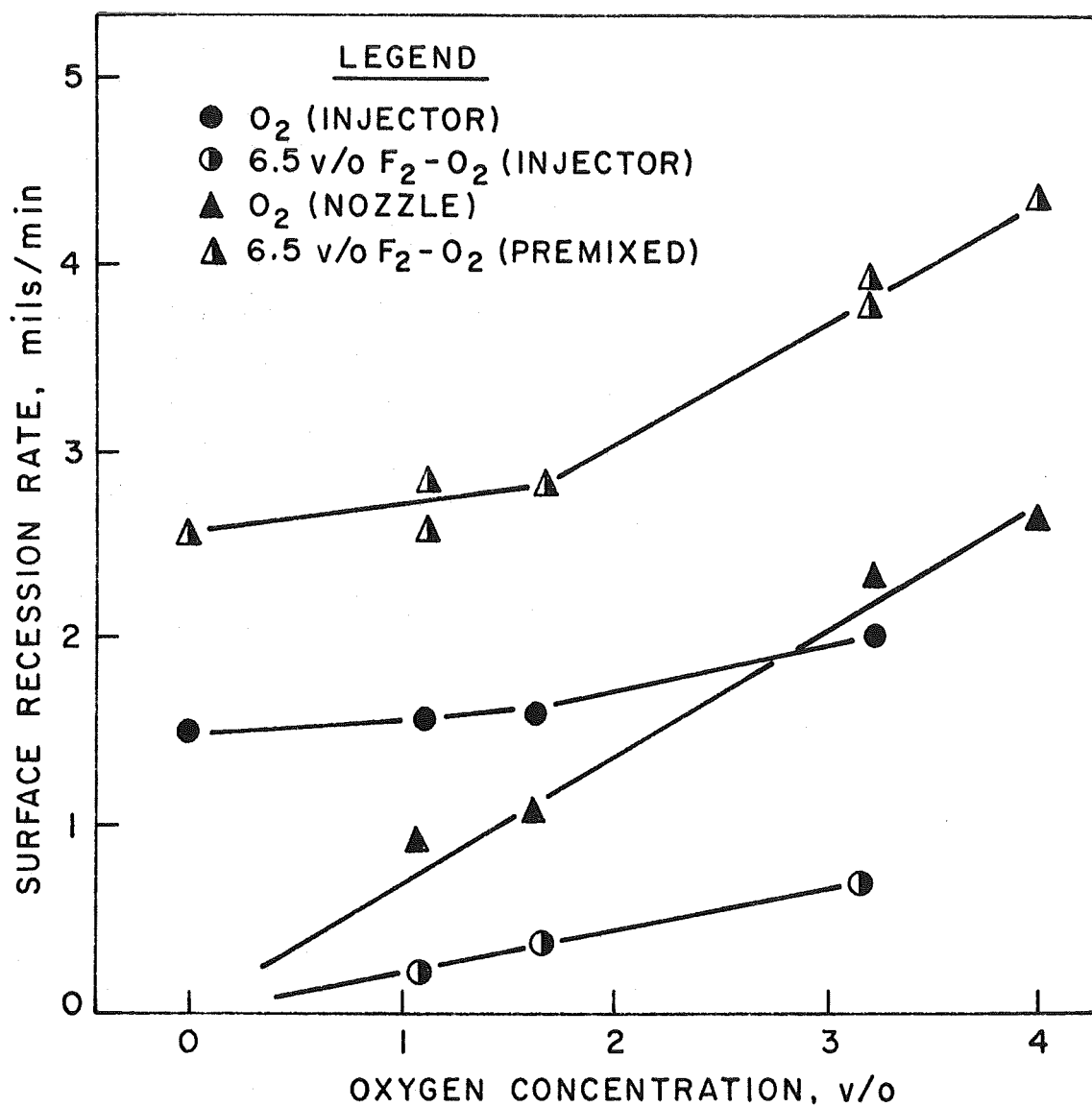
Fig. 4 - Surface Recession Rate of Tungsten at 4000°F in Injected and Premixed 6.5 v/o Fluorine-Oxygen.

results in fluorine-oxygen correlated with previous data in fluorine-hydrogen.

Since no difficulties arose by premixing fluorine and oxygen upstream of the nozzle, all subsequent tests in combined atmospheres, including both fluorine-oxygen and hydrogen fluoride-oxygen tests, were conducted using premixed gases. The individual gases were metered in their respective supply lines and combined at the inlet of the nozzle assembly. No difficulties were encountered with this technique during either fluorine-oxygen or hydrogen fluoride-oxygen tests.

Although the data in Figure 4 are limited, some interesting results are apparent in the combined environments for both premixed gases and injected oxygen. Addition of up to 1.6 v/o oxygen to 6.5 v/o fluorine had little effect on the surface recession rate. Both fluorine-oxygen curves show a change in slope at 1.6 v/o oxygen, and the slope above 1.6 v/o oxygen is about equivalent to that of the oxidation curves. Furthermore, the recession rate in the combined environment is less than the algebraic sum of the individual recession rates. These results suggested that at low oxygen concentrations, the fluorine-oxygen ratio may be as important in the corrosion mechanism as the total combined flow rate.

2.   Experimental Results

Oxidation-corrosion tests were performed to compare the relative resistance of several material classes, which had shown variable behavior in oxygen and fluorine, in combined atmospheres under the conditions described in the previous section. The materials selected included four refractory metals: ATJ graphite, two graphite-carbide composites,[8] and a boride composite developed for oxidation and thermal shock resistance.[9]

The refractory metals included iridium, Ir-33Re, rhenium, and tungsten. Iridium and Ir-33Re were selected because both had previously demonstrated resistance to fluorine and hydrogen-

18

fluoride at high temperatures[2] and were known to be resistant
to oxygen. Rhenium was chosen because of its usefulness as an
alloying element in the Ir-Re system and moderate resistance to
fluorine and oxygen. Tungsten was selected primarily as a ref-
erence material in spite of poor resistance to both fluorine and
oxygen.

ATJ graphite, HfC-33 v/o C, TaC-20 v/o C, and ZrB_2-
SiC-C, which had previously been evaluated in fluorine and hy-
drogen fluoride, constituted the remaining test materials.
Graphites exhibited reasonable resistance to fluorine and hydro-
gen fluoride but poor resistance in oxygen. On the other hand,
borides exhibited good resistance to oxygen but fair resistance
to fluorine. The carbide composites--TaC-C, which forms a low
melting oxide (~3300°F), and HfC-C, which forms a high melting
oxide (~5000°F)--exhibited reasonable resistance to fluorine
and hydrogen fluoride.

As previously stated, the primary objective of the
corrosion tests was to compare the resistance of materials to
fluorine-oxygen and hydrogen fluoride-oxygen atmospheres at tem-
peratures ranging from 3000°F to individual melting points. The
number of selected materials and atmospheres precluded in-depth
study of oxidation-corrosion mechanisms. Hopefully, however,
insight into fundamental oxidation-corrosion behavior would be
obtained. Such insight would permit prediction of corrosion be-
havior in atmospheres different from those used in this program
and thereby provide a basis of estimating nozzle throat reces-
sion rates in actual rocket engines.

a.   Tungsten

The surface recession rates for tungsten in flowing
argon containing 3.25, 4.0, and 5.4 v/o oxygen at 3000°-5000°F
are summarized in Table V and plotted in Figure 5. Previously
obtained recession rates of tungsten in 6.5 v/o fluorine are in-
cluded in Figure 5 for comparison. A greater number of tests in

TABLE V

CORROSION BEHAVIOR OF TUNGSTEN IN FLOWING OXYGEN[a]

Exposure Temp., °F	Oxygen Concentration, v/o	Weight Loss, g	Specific Weight Loss, mg/cm²/min	Surface Recession Rate, mils/min
3000	3.25	0.718	53.2	1.08
3000	3.25	0.710	52.5	1.07
3500	3.25	1.255	94.8	1.92
4000	3.25	1.777	129.7	2.62
4000	3.25	0.898	114.5	2.32
4500	3.25	0.871	102.0	2.07
5000	3.25	0.951	113.8	2.30
5000	3.25	1.292	105.0	2.15
3000	4.0	0.798	57.4	1.16
3500	4.0	0.909	105.4	2.15
3500	4.0	1.377	166.2	2.18
4000	4.0	1.083	131.0	2.66
4500	4.0	1.092	131.8	2.68
4500	4.0	1.131	133.8	2.72
5000	4.0	1.103	130.0	2.64
5000	4.0	1.832	128.1	2.60
5000	4.0	1.767	133.0	2.71
3000	5.4	0.992	70.5	1.43
3500	5.4	0.853	121.0	2.46
4000	5.4	1.187	154.0	3.13
4500	5.4	1.397	164.2	3.32
4500	5.4	1.281	191.0	3.88
5000	5.4	1.520	181.0	3.68
5000	5.4	1.342	186.0	3.80

[a]Total flow rate - 10 cfh (400 fps).

20
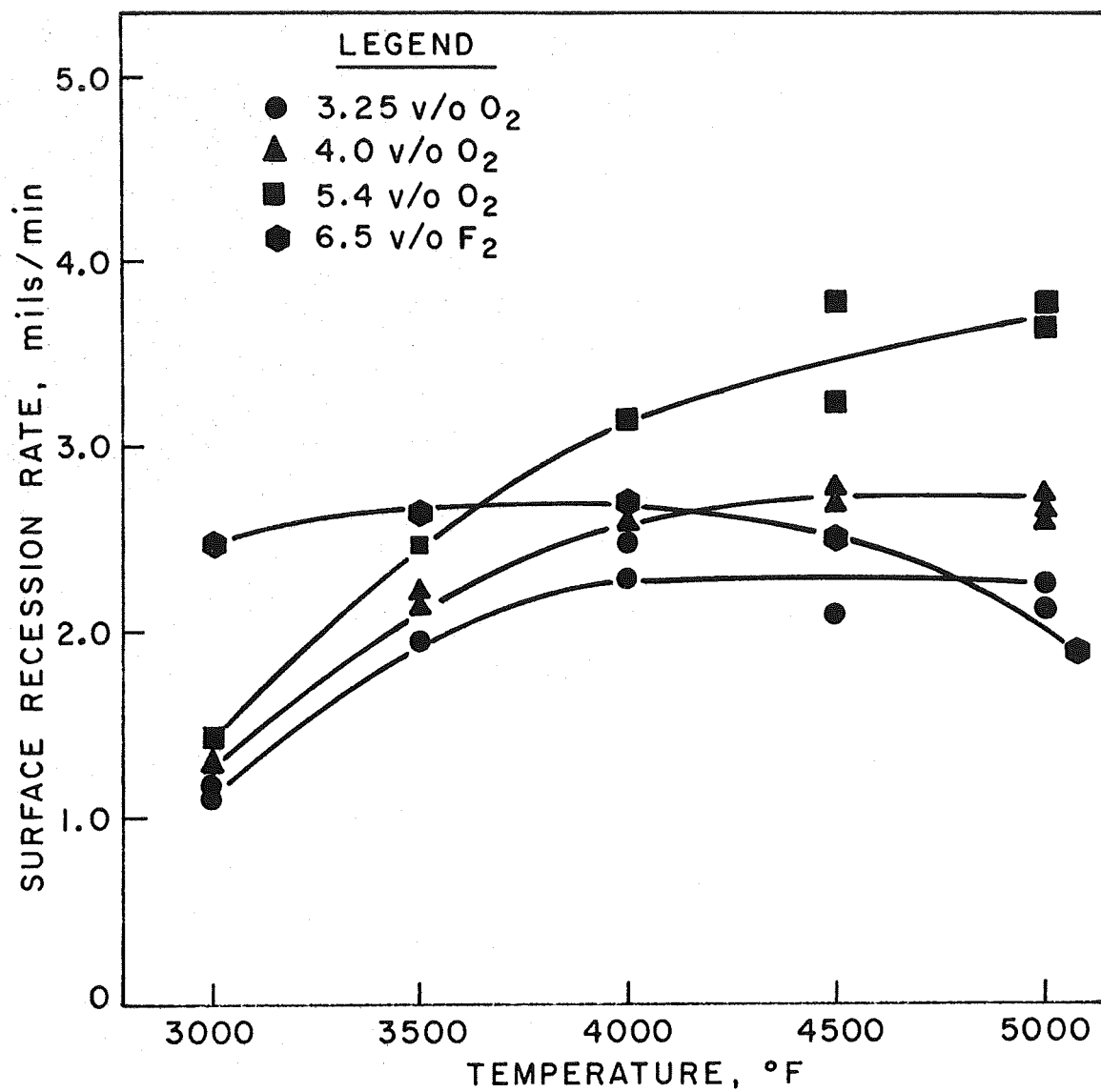
Fig. 5 - Surface Recession Rate of Tungsten in Flowing
Fluorine and Oxygen.

21

oxygen were conducted on tungsten and ATJ graphite since these materials are the reference material for corrosion tests and because of the data scatter for both materials. The recession rates at all three oxygen levels indicate that while the oxidation rate at 4000°F is nearly double that at 3000°F, there is little change in the range of 4000°-5000°F. Furthermore, at 4500°-5000°F the recession rate of tungsten in 3.25 v/o oxygen is about equal to that in 6.5 v/o fluorine. This could be due to the stoichiometry of the reaction products formed since the probable reaction products in oxygen and fluorine are WO_3 and WF_6, respectively. Thus, for a constant recession rate, the flow rate of fluorine should be about twice that of oxygen if stoichiometrically controlled steady-state equilibrium exists in the gas stream. This may well be the case since it was shown previously that corrosion rate in fluorine was a linear function of the flow rate.[2] The data in 3.25 to 5.4 v/o oxygen indicate that a similar flow rate dependence exists in oxygen above 4000°F.

The corrosion behavior of tungsten in 6.5 v/o fluorine, 6.5 v/o fluorine-4.0 v/o oxygen, and 6.5 v/o fluorine-5.4 v/o oxygen in the range of 3000°-5500°F is summarized in Table VI and plotted in Figure 6. Data in 3.25 v/o fluorine-2.0 v/o oxygen are included, along with previously obtained corrosion data in 6.5 v/o fluorine to 5100°F and current data in fluorine to 5500°F. The new data in 6.5 v/o fluorine illustrate that the corrosion rate continues to decrease at temperatures above 5100°F. This effect is due to thermal decomposition of WF_6.[2] In contrast, no decrease in the recession rate occurs in the combined environment; both the 4.0 and 5.4 v/o oxygen atmospheres show positive slopes to 5500°F. As a result, the recession rate in 6.5 v/o fluorine-5.4 v/o oxygen reaches nearly 6 mils/min at 5500°F. The corrosion mechanism is, therefore, not controlled by the observed decrease in stability of fluorides above 5000°F in fluorine. This could mean that oxyfluorides are formed in the combined environments which offset the effect observed in fluorine.

22

TABLE VI

CORROSION BEHAVIOR OF TUNGSTEN
IN FLOWING FLUORINE AND FLUORINE-OXYGEN[a]

Exposure Temp., °F	Fluorine Concentration, v/o	Oxygen Concentration, v/o	Weight Loss, g	Specific Weight Loss, mg/cm²/min	Surface Recession Rate, mils/min
3000	6.5	--	1.713	121.5	2.48
3500	6.5	--	1.718	126.4	2.58
4000	6.5	--	1.787	128.8	2.62
4580	6.5	--	1.747	124.8	2.54
5100	6.5	--	1.214	92.0	1.88
5500	6.5	--	0.460	55.2	1.13
5800	6.5	--	0.252	30.6	0.62
3500	3.2	2.0	1.011	73.5	1.49
4000	3.2	2.0	1.304	93.6	1.91
4500	3.2	2.0	1.270	108.1	2.12
5000	3.2	2.0	1.072	123.0	2.50
3000	6.5	4.0	1.694	209.9	4.26
3000	6.5	4.0	2.507	222.8	4.50
4000	6.5	4.0	1.785	215.0	4.38
5000	6.5	4.0	1.934	238.0	4.80
5500	6.5	4.0	1.759	228.0	4.65
3000	6.5	5.4	2.409	260.2	5.30
4000	6.5	5.4	2.277	276.0	5.62
5000	6.5	5.4	2.306	289.0	5.80
5500	6.5	5.4	2.124	278.0	5.65

[a]Total flow rate - 10 cfh (400 fps).
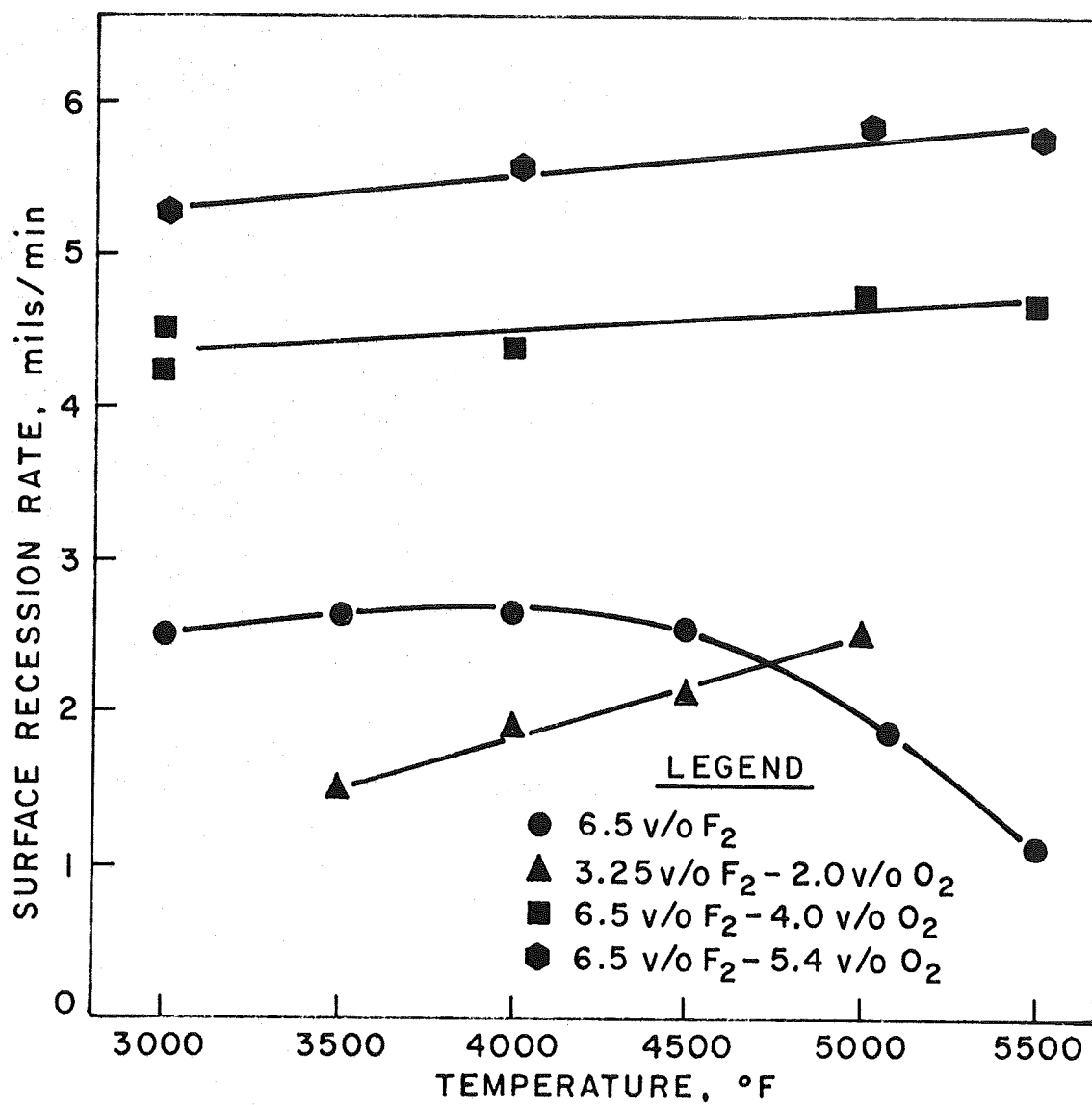
Fig. 6 - Surface Recession Rate of Tungsten in Flowing Fluorine and Fluorine-Oxygen.

It is interesting to compare the oxidation-corrosion rate in 6.5 v/o fluorine-4.0 v/o oxygen with an atmosphere of the same fluorine-oxygen ratio but one-half the total flow rate. Although the data in 3.25 v/o fluorine-2.0 v/o oxygen are limited, the corrosion curves at the lower concentration of corrodent gases indicate a greater positive slope. Thus, the corrosion rate in the $3.25F_2$-$2.0O_2$ atmosphere approaches one-half that in 6.5 v/o F_2-4.0 v/o O_2 only above 4500°F. This may be a consequence of the effect at lower oxygen levels shown in Figure 4. In any case, a reasonable correspondence with total flow rate exists above 4500°F.

The corrosion rate of tungsten in hydrogen fluoride and hydrogen fluoride-oxygen is summarized in Table VII and plotted in Figure 7. Previous studies of corrosion demonstrated that the corrosion rate of most materials in hydrogen fluoride was an order of magnitude less than in fluorine.[2] This is due to the stability of the HF molecule even at very high temperatures. The shape of the corrosion curves for hydrogen fluoride-oxygen is similar to that of oxygen (Figure 5). Above 4000°F, there is little change, especially in 10 v/o HF-0.56 v/o O_2. The findings in the combined hydrogen fluoride-oxygen atmosphere do suggest that most of the surface recession is due to oxygen, although some complex reactions may occur. The corrosion rate in hydrogen fluoride-oxygen appear to be higher than would be expected from the oxidation data in Figure 5. Thus, complex interactions between hydrogen fluoride and oxygen may occur in the gas stream to effectively increase the volume fraction of corrodent species.

A simple method of estimating whether significant synergistic effects occur in the combined atmospheres is to compare the experimental recession rates with the sum of the recession rates in the individual environments. This technique assumes that the individual recession rates are additive and that the reaction can be written as:

$$W + F_2 + O_2 \rightarrow W_xF_y + W_xO_y.$$
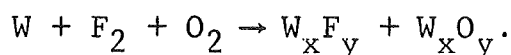
or, in terms of recession:

$$R_{total} = R_{F_2} + R_{O_2}$$

TABLE VII

CORROSION BEHAVIOR OF TUNGSTEN
IN HYDROGEN FLUORIDE AND HYDROGEN FLUORIDE-OXYGEN[a]

Exposure Temp., °F	Hydrogen Fluoride Concentration, v/o	Oxygen Concentration, v/o	Weight Loss, g	Specific Weight Loss, mg/cm²/min	Surface Recession Rate, mils/min
3500	10	--	0.044	3.09	0.06
4000	10	--	0.064	4.48	0.09
4500	10	--	0.052	5.22	0.12
5000	10	--	0.094	7.05	0.14
5800	10	--	0.057	7.22	0.15
3000	10	0.56	0.243	18.0	0.37
3500	10	0.56	0.393	28.0	0.59
4000	10	0.56	0.248	30.8	0.62
5000	10	0.56	0.277	35.0	0.71
3000	10	2.3	0.403	36.2	0.74
4000	10	2.3	0.899	66.2	1.35
5000	10	2.3	1.017	94.0	1.92

[a]Total flow rate - 10 cfh (400 fps).
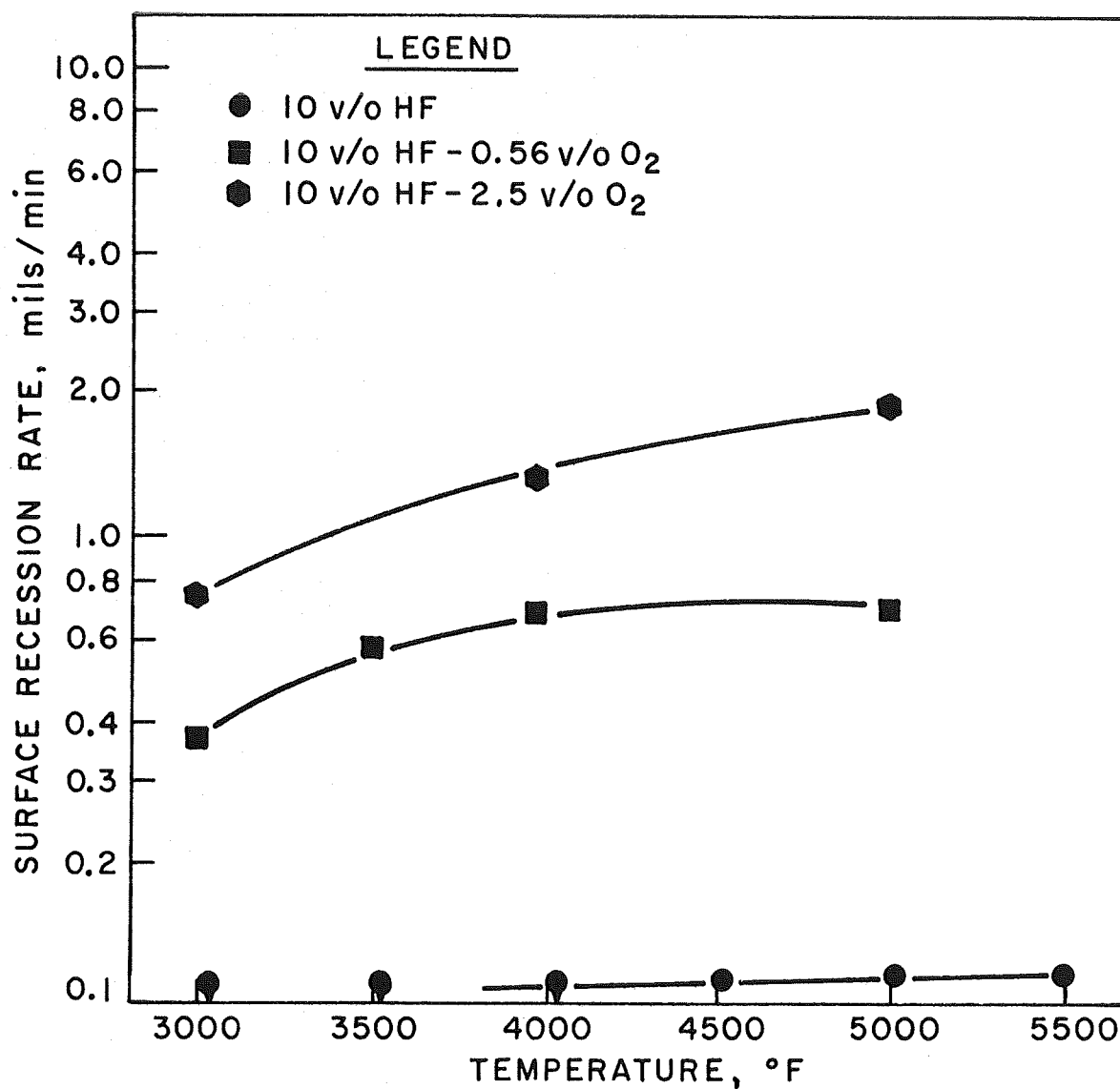
Fig. 7 - Surface Recession Rate of Tungsten in Flowing
Hydrogen Fluoride and Hydrogen Fluoride-Oxygen.

This will not occur if (1) a different corrosion product is formed in the combined environment, (2) interactions in the gas stream change the concentration of corrosive gaseous species, or (3) corrosion products are unstable and/or other than gaseous species. Obviously, the comparison of the experimental and calculated rates will not define which of these synergistic effects is operative since each could either increase or decrease the corrosion rate. However, it will define whether any appreciable combined effects can be expected.

The experimental and calculated corrosion rates at 3000, 4000, and 5000°F are compared in Figure 8. Since data in 0.56 and 2.3 v/o oxygen were not available, these rates were obtained by linear interpolation of data at 3.25, 4.0, and 5.4 v/o oxygen. The experimental results in both fluorine-oxygen and hydrogen fluoride-oxygen are quite similar to the calculated rates, except for the recession rate in fluorine-oxygen at 3000°F (Figure 8a). Here the experimental rates are greater than the calculated rates. This could be due to the formation of oxyfluorides which are not formed at higher temperatures. A converse effect is indicated at 4000°F, but it appears to be caused by a single data point at 3.25 v/o oxygen. This point may be high because of data scatter.

Calculated surface recession rates in hydrogen fluoride-oxygen (Figure 8b) tend to be slightly lower than the measured rates. In this environment, it is possible that interactions could occur in the gas stream which increases the effective concentration of corrodent gases. One such reaction, neglecting thermodynamic considerations, can be written:

$$2HF + O_2 \rightarrow H_2O + F_2 + \tfrac{1}{2}O_2$$
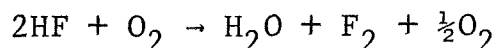
This reaction could provide a higher corrosion rate in that fluorine is released at a greater rate than can be obtained by thermal decomposition of the stable hydrogen fluoride molecule. However, the reaction should not increase the corrosion rate significantly because of the stoichiometry of the fluoride reaction
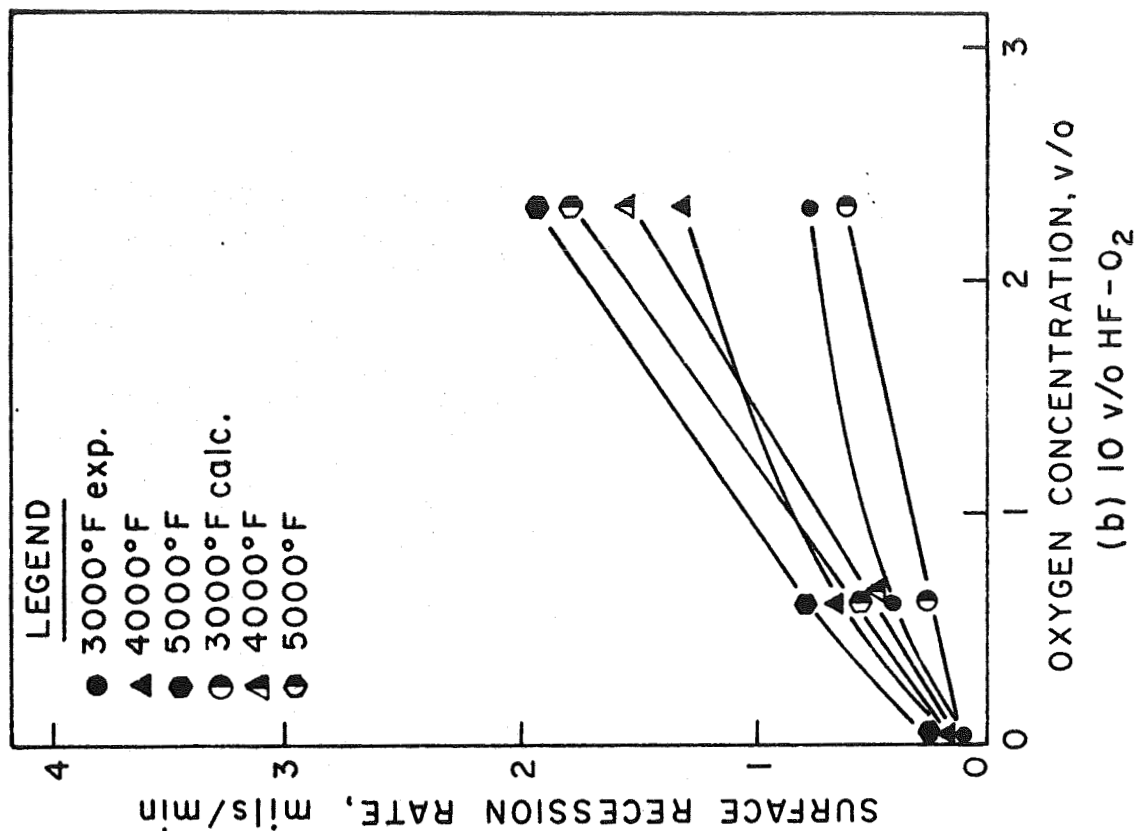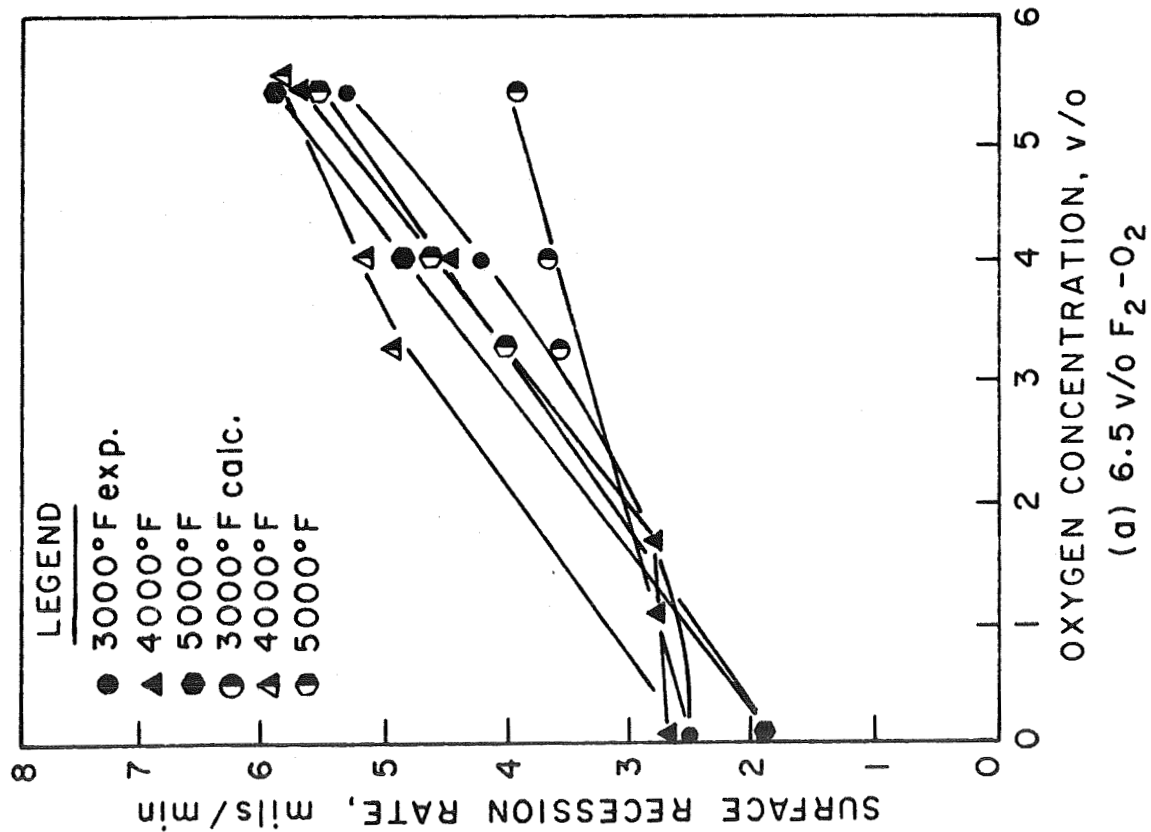
Fig. 8 - Comparison of Calculated and Experimental Corrosion Rates of Tungsten in Flowing Fluorine-Oxygen and Hydrogen Fluoride-Oxygen.

product discussed previously. In effect, the corrosive potential of an atmosphere obtained by the above reaction is about equivalent to that of the initial oxygen concentration. Any increase in corrosion rate over that of hydrogen fluoride and oxygen should, therefore, be controlled by the reaction rate with water vapor and/or hydrogen. Figure 8b does indicate that no appreciable synergistic effects exist for tungsten in hydrogen fluoride-oxygen. It appears that surface recession in the combined atmosphere is due to oxidation.

b.   Iridium

Iridium samples were prepared by cold pressing at 48 tsi and sintering at 3300°F in a vacuum resulting in a density of about 90%. The corrosion rate of iridium in oxygen, fluorine, and fluorine-oxygen is summarized in Table VIII. Surface recession data in fluorine and fluorine-oxygen are plotted in Figure 9. As expected, the surface recession rates of iridium in 2.3 and 5.4 v/o oxygen were much less than most of the other materials in the program. Weight losses were often in the range of 1-2 mg.

Oxidation tests were conducted in 10 v/o oxygen and for exposure times of up to 10 min in order to obtain higher weight losses. Very small weight losses were also obtained in hydrogen fluoride-oxygen because of the low oxygen levels used for these tests. As a result, calculated surface recession rates for iridium do not always indicate clear temperature and/or environmental trends. They do, however, demonstrate the excellent resistance of iridium to oxygen, hydrogen fluoride, and at higher temperatures, fluorine-oxygen.

The surface recession of iridium in fluorine and fluorine-oxygen illustrated in Figure 9 indicates a decreasing rate with increasing temperature as reported previously for fluorine.[2] The current results demonstrate that iridium shows a similar behavior in fluorine-oxygen. This can be expected since the corrosion rate of iridium in oxygen is much lower than in

TABLE VIII

CORROSION BEHAVIOR OF IRIDIUM
IN FLOWING OXYGEN, FLUORINE, AND FLUORINE-OXYGEN[a]

Exposure Temp., °F	Fluorine Concentration, v/o	Oxygen Concentration, v/o	Weight Loss, g	Specific Weight Loss, mg/cm^2/min	Surface Recession Rate, mils/min
3000[b]	--	2.3	0.001	0.09	0.002
4000[b]	--	2.3	0.002	0.19	0.003
4400[b]	--	2.3	0.005	0.38	0.007
3000	--	5.4	0.001	0.07	0.002
3500	--	5.4	0.002	0.27	0.005
3500[b]	--	5.4	0.007	0.27	0.005
4000	--	5.4	0.014	1.06	0.019
4400	--	5.4	0.006	1.55	0.027
3000	--	10	0.004	0.31	0.005
3500	--	10	0.005	0.45	0.008
4000	--	10	0.022	1.80	0.032
4400	--	10	0.032	2.18	0.038
2550	6.5	--	1.452	131.0	2.29
2730	6.5	--	1.287	105.0	1.84
3000	6.5	--	0.791	78.0	1.36
3000	6.5	--	0.776	68.0	1.19
3000	6.5	--	0.702	65.5	1.15
3500	6.5	--	0.472	29.4	0.51
3500	6.5	--	0.220	18.7	0.33
4000	6.5	--	0.173	15.3	0.27
4400	6.5	--	0.180	10.2	0.18
3000	6.5	4.0	0.765	60.2	1.05
3500	6.5	4.0	0.385	31.7	0.56
4000	6.5	4.0	0.221	19.0	0.33
3000	6.5	5.4	0.666	75.5	1.32
3500	6.5	5.4	0.136	22.2	0.39
4000	6.5	5.4	0.139	19.0	0.33
4000	6.5	5.4	0.095	15.7	0.28
4400	6.5	5.4	0.112	16.4	0.29

[a] Total flow rate - 10 cfh (400 fps).

[b] Ten minute runs.
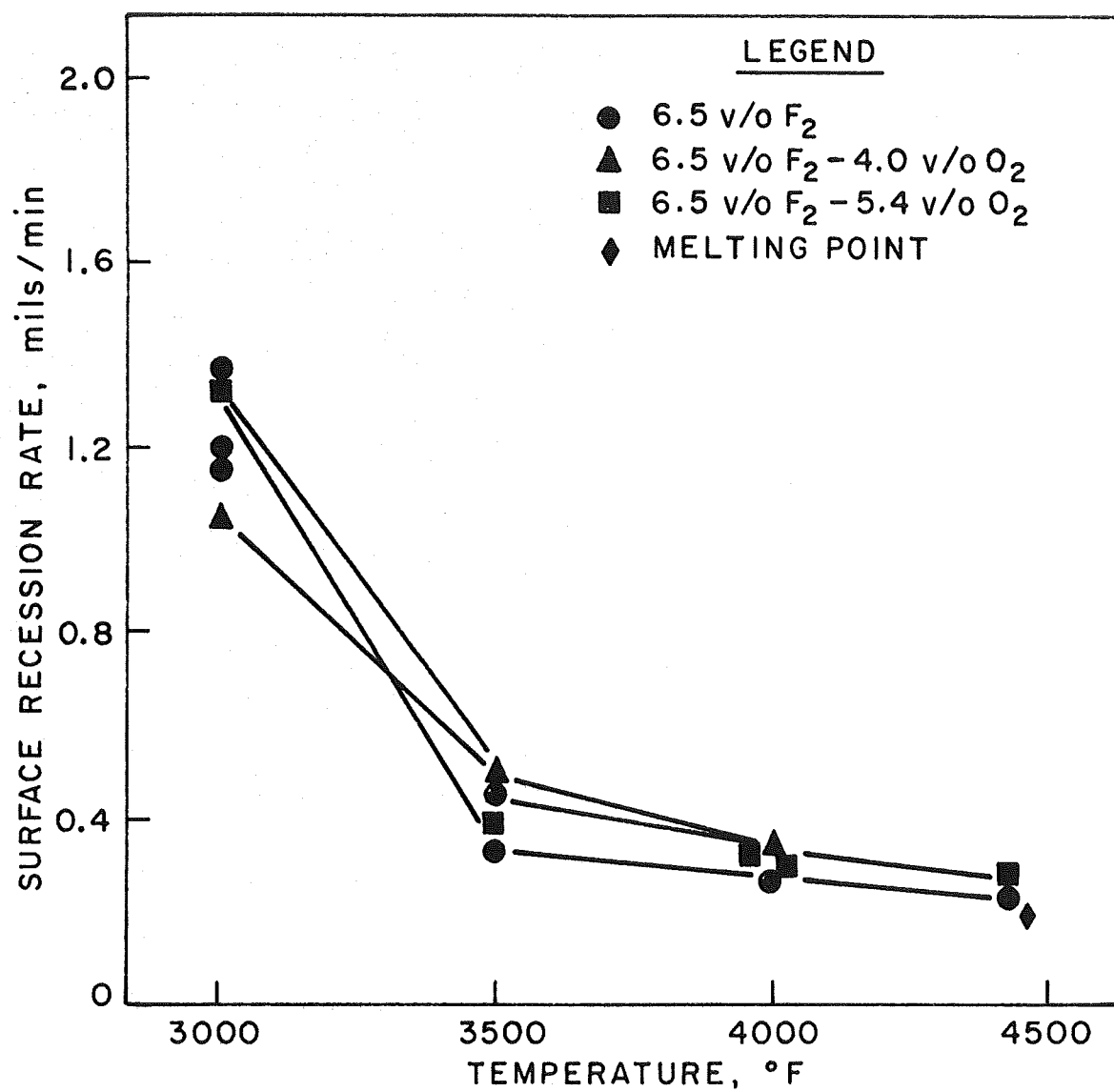
Fig. 9 - Surface Recession Rate of Iridium in Flowing
Fluorine and Fluorine-Oxygen.

fluorine at 3800° to 4400°F. As a result, the recession rates in the combined environments are very close to the rates in 6.5 v/o fluorine.

The corrosion behavior of iridium in hydrogen fluoride and hydrogen fluoride-oxygen are summarized in Table IX. The recession rate in hydrogen fluoride is plotted along with data for oxygen atmospheres (Table VIII) in Figure 10. Oxygen data are presented with hydrogen fluoride recession rates because of the similarity of the measured rates. It is apparent that iridium is essentially unreactive in 10 v/o hydrogen fluoride to the melting point (4450°F). Similarly, additions of up to 2.3 v/o oxygen do not result in any appreciable change in corrosion behavior.

Figure 10 indicates that the oxidation rate in oxygen does increase appreciably in the range of 3500° to 4400°F at all oxygen levels. However, the surface recession rate is only about 0.040 mils/min at 4400°F in 10 v/o oxygen. With the exception of Ir-33Re, this is lower by an order of magnitude than the other materials tested in the program in 5.4 v/o oxygen.

The very low surface recession rates in oxygen and hydrogen fluoride precludes comparison of the measured and calculated recession rates. In any case, because of higher recession rates in fluorine, it is apparent that calculated rates must be comparable to the experimental fluorine rates. Recession rates in oxygen and hydrogen fluoride-oxygen are too low to provide an accurate comparison. It is evident, however, that no synergistic corrosion effects occur in the combined atmospheres.

c.   <u>Iridium-33 w/o Rhenium</u>

The corrosion behavior of iridium-33 w/o rhenium in flowing oxygen, fluorine, and fluorine-oxygen is summarized in Table X, and plotted in Figure 11. Test samples were prepared both by cold pressing and sintering and by arc-melting without appreciable difference in measured corrosion behavior. As with iridium, test samples were used for multiple exposures with surface preparation after each run. This is important in the case

TABLE IX

CORROSION BEHAVIOR OF IRIDIUM IN FLOWING HYDROGEN FLUORIDE AND HYDROGEN FLUORIDE-OXYGEN[a]

Exposure Temp., °F	Hydrogen Fluoride Concentration, v/o	Oxygen Concentration, v/o	Weight Loss, g	Specific Weight Loss, mg/cm²/min	Surface Recession Rate, mils/min
3000	10	--	0.001	0.12	0.002
3000	10	--	0.001	0.05	0.001
3500	10	--	0.001	0.06	0.001
4000[b]	10	--	0.004	0.36	0.006
4000	10	--	0.004	0.32	0.006
3000	10	0.56	0.001	0.04	0.001
3500	10	0.56	0.001	0.10	0.002
3500[b]	10	0.56	0.002	0.07	0.001
3000	10	2.3	0.001	0.06	0.001
3500	10	2.3	0.001	0.04	0.001
3500[b]	10	2.3	0.003	0.13	0.002
4000	10	2.3	0.001	0.05	0.001

[a]Total flow rate - 10 cfh (400 fps).

[b]Ten minute exposure time.
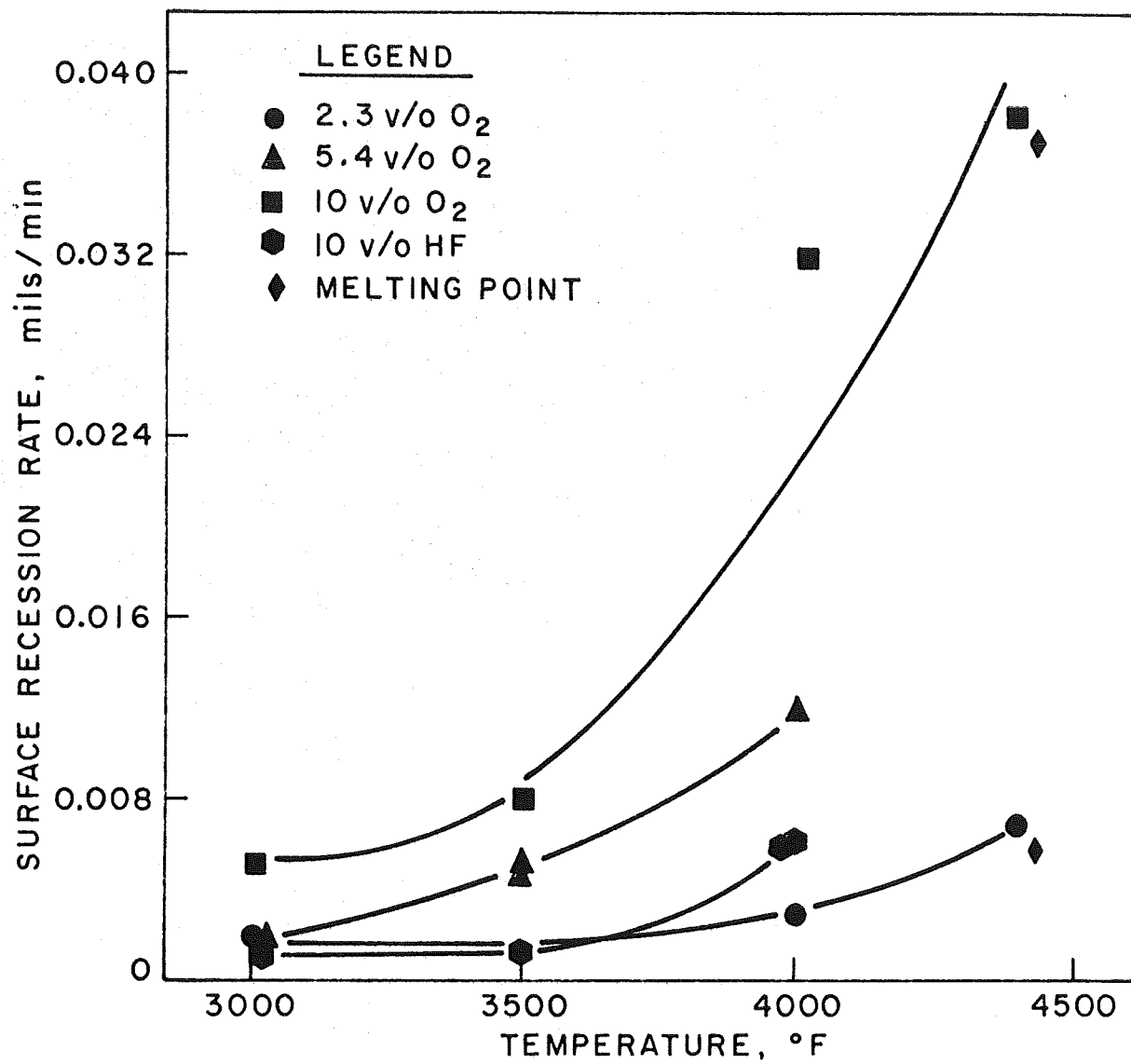
Fig. 10 - Surface Recession Rate of Iridium in Flowing Oxygen and Hydrogen Fluoride.

TABLE X

CORROSION BEHAVIOR OF IRIDIUM-33 w/o RHENIUM
IN FLOWING OXYGEN, FLUORINE, AND FLUORINE-OXYGEN[a]

Exposure Temp., °F	Fluorine Concentration, v/o	Oxygen Concentration, v/o	Weight Loss, g	Specific Weight Loss, mg/cm²/min	Surface Recession Rate, mils/min
3000	--	2.3	0.028	1.6	0.03
4000	--	2.3	0.102	5.7	0.10
4500	--	2.3	0.273	15.1	0.27
3000	--	5.4	0.027	1.9	0.04
3000	--	5.4	0.061	3.4	0.06
3500	--	5.4	0.280	7.1	0.11
4000	--	5.4	0.138	10.5	0.19
4000	--	5.4	0.078	5.2	0.09
4500	--	5.4	0.399	30.0	0.54
4500	--	5.4	0.338	22.8	0.41
2680	6.5	--	1.269	105.6	1.89
3060	6.5	--	0.872	70.6	1.27
3500	6.5	--	0.558	43.0	0.77
3500	6.5	--	0.592	46.0	0.82
4000	6.5	--	0.250	18.9	0.34
4000	6.5	--	0.404	29.3	0.53
4420	6.5	--	0.161	16.0	0.29
4500	6.5	--	0.207	13.3	0.24
4700	6.5	--	0.157	13.2	0.28
4730	6.5	--	Melted		
3000	6.5	4.0	1.273	75.4	1.35
4000	6.5	4.0	0.439	45.1	0.81
4500	6.5	4.0	0.225	27.9	0.50
3000	6.5	5.4	0.526	72.8	1.31
3500	6.5	5.4	0.400	48.2	0.87
4000	6.5	5.4	0.335	36.8	0.66
4500	6.5	5.4	0.214	28.9	0.53

[a] Total flow rate - 10 cfh (400 fps).

36
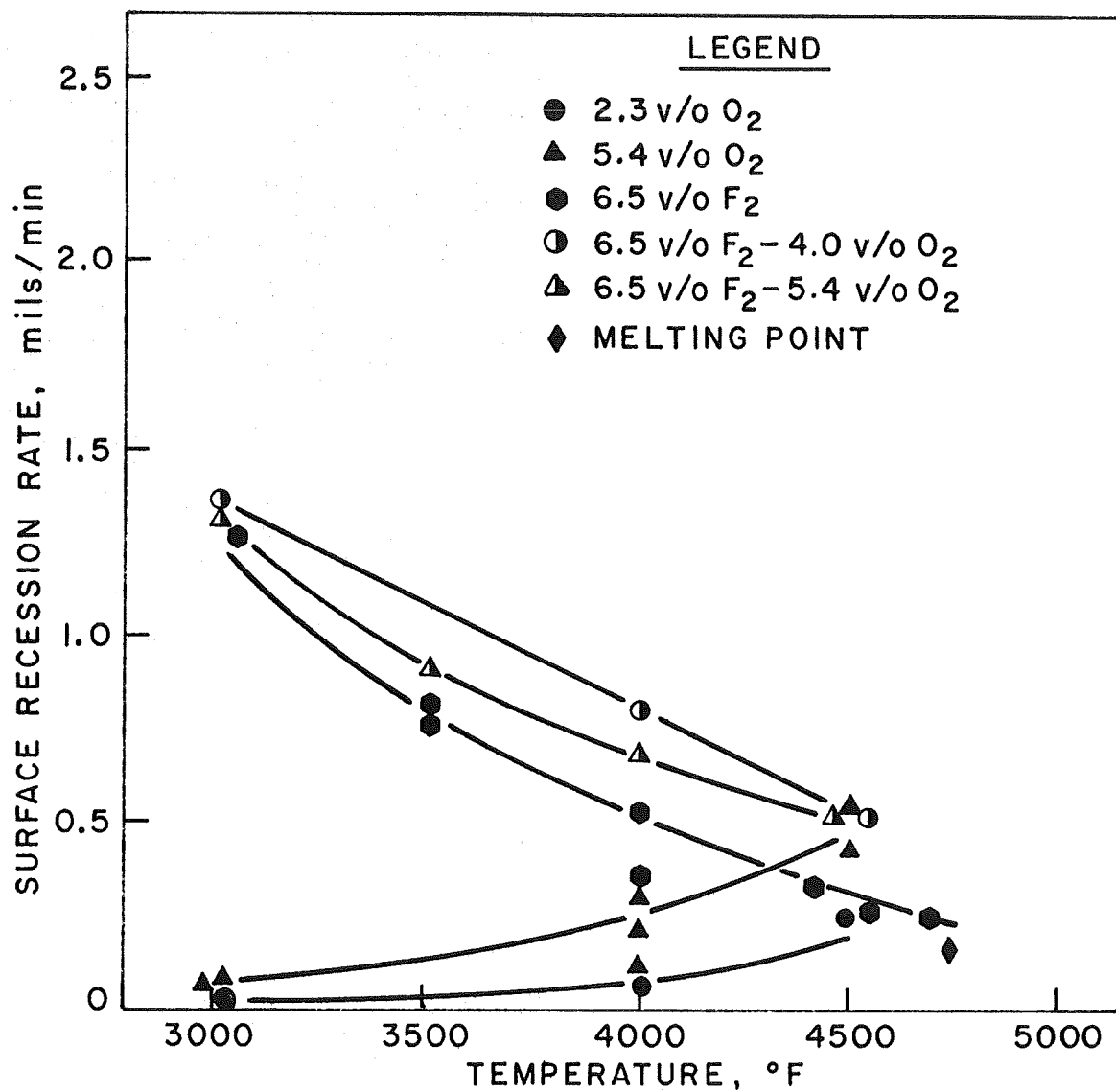
Fig. 11 - Surface Recession Rate of Ir-33Re in Flowing
Oxygen, Fluorine, and Fluorine-Oxygen.

of Ir-33Re because of the considerable difference in oxidation-corrosion rates of iridium and rhenium. It is for this reason also that the corrosion rates of Ir-Re alloys are probably not linearly time dependent, as will be discussed subsequently.

As shown previously for unalloyed iridium, Ir-33Re in fluorine exhibits decreasing corrosion rate with increasing temperature. Figure 11 shows that a similar behavior occurs in 6.5 v/o F_2-4.0 v/o O_2 and 6.5 v/o F_2-5.4 v/o O_2, although the recession rates in fluorine-oxygen are slightly higher than in fluorine alone. Although Figure 11 indicates a higher recession rate in 4.0 v/o O_2 than in 5.4 v/o O_2 in the combined environment, this is probably a result of data scatter caused by the relative low contribution of oxygen below 4000°F.

The oxidation rate at both 2.3 and 5.4 v/o oxygen tends to increase above 4000°F, as measured previously for unalloyed iridium. It is interesting to notice that at 4000°F, the surface recession rate in fluorine-oxygen is about equivalent to that of 5.4 v/o oxygen. At this temperature, it is apparent the relative contribution of fluorine and oxygen to metal removal is about equal. At 4500°F, the recession rates in 6.5 v/o F_2-5.4 v/o O_2 is still only about 0.5 mils/min, which is about an order of magnitude less than all of the other materials in the program except iridium.

The corrosion behavior of Ir-33Re in hydrogen fluoride and hydrogen fluoride-oxygen is summarized in Table XI and plotted in Figure 12. Calculated recession rates in these environments are very low, although somewhat higher than that of iridium. Considering the iridium and rhenium oxidation-corrosion data, it is likely that a major portion of the weight loss is due to selective reaction with rhenium in the surface layer. Although study of the time dependence of the corrosion rate was not conducted, a linear time dependence does not likely exist in this system. Thus, linear recession rates calculated from 5 min exposures may be conservative. Since the weight of rhenium within

TABLE XI

CORROSION BEHAVIOR OF IRIDIUM-33 w/o RHENIUM IN
FLOWING HYDROGEN FLUORIDE AND HYDROGEN FLUORIDE-OXYGEN[a]

Exposure Temp., °F	Hydrogen Fluoride Concentration, v/o	Oxygen Concentration, v/o	Weight Loss, g	Specific Weight Loss, mg/cm²/min	Surface Recession Rate, mils/min
3000	10	--	0.001	0.03	0.001
4000	10	--	0.002	0.18	0.003
4500	10	--	0.006	0.51	0.009
3000	10	0.56	0.013	0.9	0.02
4000	10	0.56	0.031	2.3	0.04
4500	10	0.56	0.028	4.4	0.08
3000	10	2.3	0.017	1.0	0.02
3000	10	2.3	0.028	2.4	0.04
4000	10	2.3	0.058	4.3	0.08
4500	10	2.3	0.083	13.4	0.24

[a]Total flow rate - 10 cfh (400 fps).
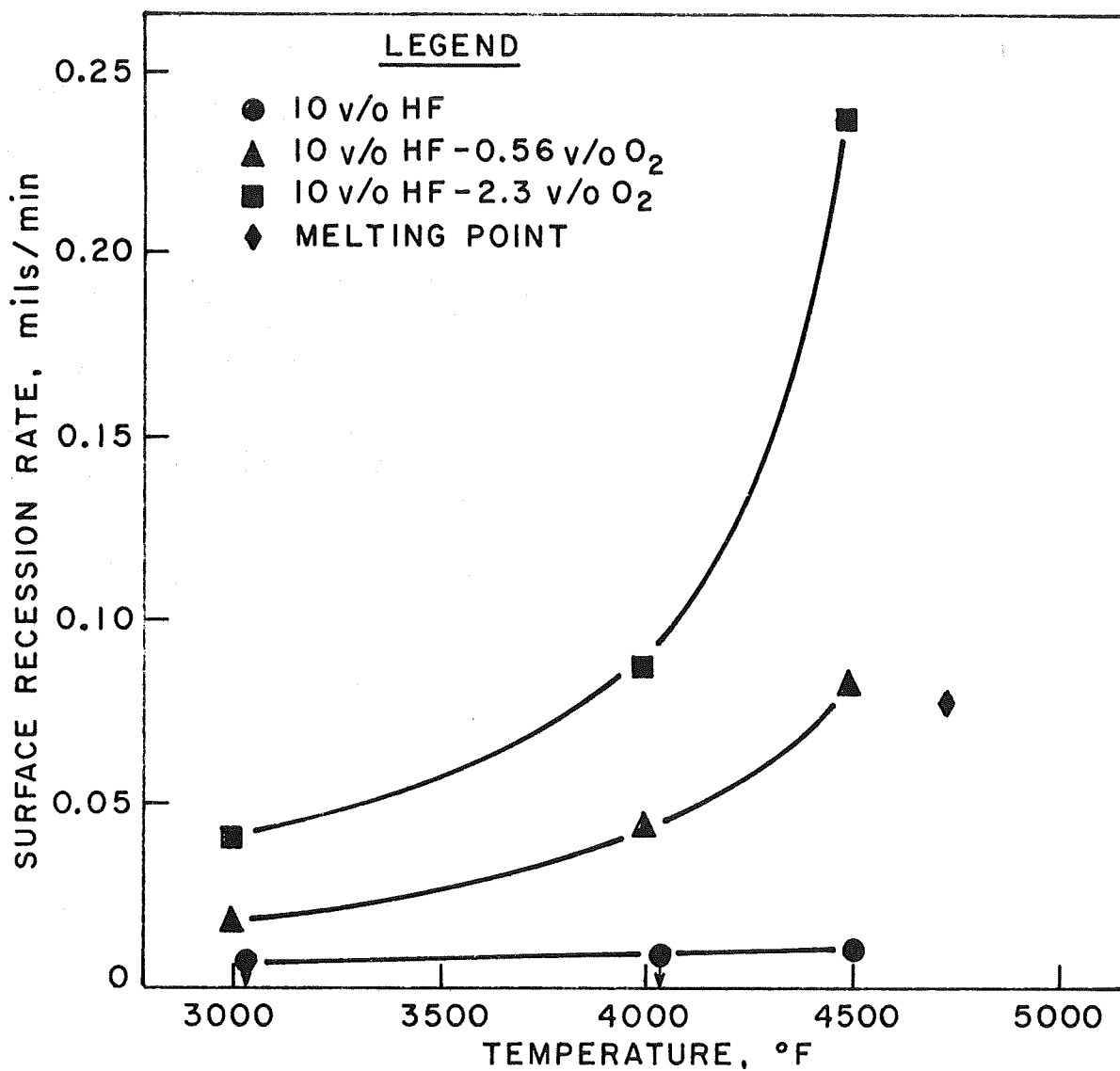
Fig. 12 - Surface Recession Rate of Ir-33Re in Flowing
Hydrogen Fluoride and Hydrogen Fluoride-Oxygen.

the sample surface is constant, an expected increase in recession rate due to a higher volume of corrosion gases may not be measured. Additional detailed oxidation-corrosion study is required to define this effect further.

Because of the low recession rates and nonlinear time dependence, comparison of the measured and calculated recession rates is not appropriate for Ir-33Re. However, it is apparent from the data that a reasonable correlation of both rates exists for 5 min exposure times.

d.   Rhenium

Rhenium samples were prepared by cold pressing at 48 psi and sintering at 3300-3500°F in a vacuum for two to four hours. This resulted in a sintered density of about 90% of theoretical. Arc-melted buttons were also used, but did not cause significant difference in oxidation-corrosion rate.

The corrosion behavior of rhenium in oxygen, fluorine, and fluorine-oxygen at 3000-5200°F is summarized in Table XII and plotted in Figure 13. Data obtained previously on rhenium in fluorine indicated that the corrosion rate, like that of iridium and Ir-33Re, decreased with increasing temperatures above 3500°F. During the current program, data was obtained on rhenium in fluorine at 5200°F. This additional data correlated with previous results. The recession rate in 6.5 v/o fluorine at 5200°F is about 0.5 mils/min, or about one-fourth that at 3500°F.

The recession rate of rhenium in both 2.3 and 5.4 v/o oxygen does not demonstrate significant temperature dependence in the range of 3500-5200°F. Surface recession rates in these atmospheres are about 1.2 and 2.5 mils/min, respectively, which are about one-half that of tungsten in these atmospheres.

In the combined fluorine-oxygen environments, the recession rate decreases with increasing temperature reaching about 3.8 mils/min. At 3500°F, the recession rate is about 5 mils/min and remains the same when the oxygen concentration is increased from

TABLE XII

CORROSION BEHAVIOR OF RHENIUM
IN FLOWING OXYGEN, FLUORINE, AND FLUORINE-OXYGEN[a]

Exposure Temp., °F	Fluorine Concentration, v/o	Oxygen Concentration, v/o	Weight Loss, g	Specific Weight Loss, mg/cm²/min	Surface Recession Rate, mils/min
3500	--	2.3	0.409	56.4	1.05
4500	--	2.3	0.550	73.4	1.37
5200	--	2.3	0.471	64.5	1.20
5200	--	2.3	0.432	61.0	1.13
3500	--	5.4	0.875	121.2	2.30
4500	--	5.4	0.971	136.0	2.55
5200	--	5.4	1.013	142.0	2.65
2500	6.5	--	1.330	119.0	2.24
2500	6.5	--	1.405	119.5	2.24
3000	6.5	--	1.412	119.0	2.22
3500	6.5	--	1.431	123.0	2.30
4000	6.5	--	1.292	87.6	1.64
4000	6.5	--	0.091	73.2	1.37
4500	6.5	--	0.678	61.9	1.16
4500	6.5	--	0.465	45.2	0.85
5000	6.5	--	0.352	23.0	0.43
5000	6.5	--	0.200	18.0	0.33
5200	6.5	--	0.200	28.3	0.53
4500	6.5	2.3	1.398	210.0	3.93
3500	6.5	4.0	2.387	245.0	4.22
4500	6.5	4.0	1.615	232.9	4.37
5200	6.5	4.0	1.213	181.0	3.39
3500	6.5	5.4	1.754	235.0	4.40
3500	6.5	5.4	1.916	268.0	5.02
4500	6.5	5.4	1.660	234.0	4.38
5200	6.5	5.4	1.432	210.0	3.94

[a]Total flow rate - 10 cfh (400 fps).

42
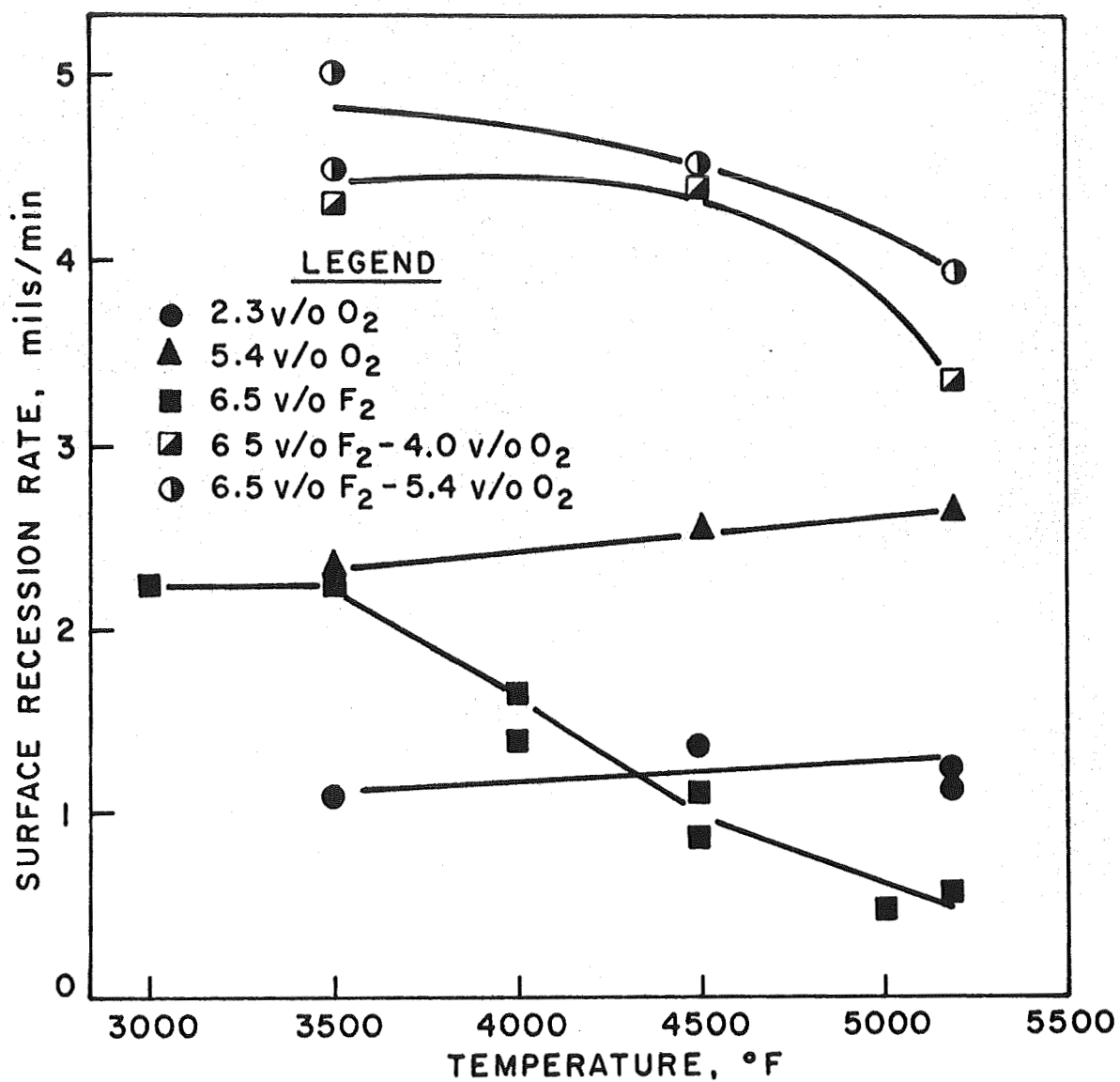
Fig. 13 - Surface Recession Rate of Rhenium in Flowing
Oxygen, Fluorine, and Fluorine-Oxygen.

4.0 to 5.4 v/o oxygen. A significant difference in the recession rate in these atmospheres was obtained only at 5200°F.

Oxidation-corrosion data for rhenium in hydrogen fluoride and hydrogen fluoride-oxygen is presented in Table XIII and plotted in Figure 14. Rhenium exhibits the very low corrosion rates in hydrogen fluoride which are typical of all refractory metals tested in the program. Additions of 0.56 and 2.3 v/o oxygen to the hydrogen fluoride result in a considerable increase in corrosion rates but not greater than can be expected based on oxygen data. An increase in the recession rate is shown at 4500°F in 10 v/o HF-2.3 v/o O_2, and perhaps in 10 v/o HF-0.56 v/o O_2. This may be associated with the reduction in the recession rate in fluorine above 4000°F. The oxidation-corrosion rates in 10 v/o HF-2.3 v/o O_2 are comparable to those in 2.3 v/o oxygen.

A comparison of the measured and calculated recession rates are presented in Figure 15. Like tungsten at 3000°F, rhenium exhibits higher experimental rates than calculated rates in fluorine-oxygen. Unlike tungsten, however, rhenium exhibits this synergistic effect over the total range 3500°-5200°F, and particularly at 4500°F. Although data are insufficient to accurately define the slopes of the calculated curves over the whole range, it appears that synergistic corrosion effects are greatest at intermediate oxygen levels of about 2-3 v/o. This may be due to the formation of oxyfluorides whose stoichiometry is such that a constant gas flow rate results in greater metal removal. Additional corrosion tests are required to define this effect further.

Comparison of the HF-O_2 recession rates indicate a similar behavior in this atmosphere. With one exception, the calculated rates are slightly greater than the measured rates; only in 2.3 v/o oxygen at 5200°F is the calculated rate considerably greater than the measured rate. This could be due to HF-O_2 gas stream interactions described previously for tungsten or to experimental data scatter.

TABLE XIII

CORROSION BEHAVIOR OF RHENIUM IN FLOWING
HYDROGEN FLUORIDE AND HYDROGEN FLUORIDE-OXYGEN[a]

Exposure Temp., °F	Hydrogen Fluoride Concentration, v/o	Oxygen Concentration, v/o	Weight Loss, g	Specific Weight Loss, mg/cm^2/min	Surface Recession Rate, mils/min
3000	10	--	0.001	0.045	0.001
4000	10	--	0.004	0.49	0.009
4500	10	--	0.021	2.20	0.041
5200	10	--	0.032	5.05	0.094
3500	10	0.56	0.090	8.2	0.15
4500	10	0.56	0.093	12.3	0.23
5200	10	0.56	0.056	7.9	0.15
3500	10	2.3	0.420	46.6	0.88
4500	10	2.3	0.532	75.6	1.42
4500	10	2.3	0.929	77.9	1.46
5000	10	2.3	0.362	58.4	1.09
5200	10	2.3	0.374	51.8	0.97

[a]Total flow rate - 10 cfh (400 fps).
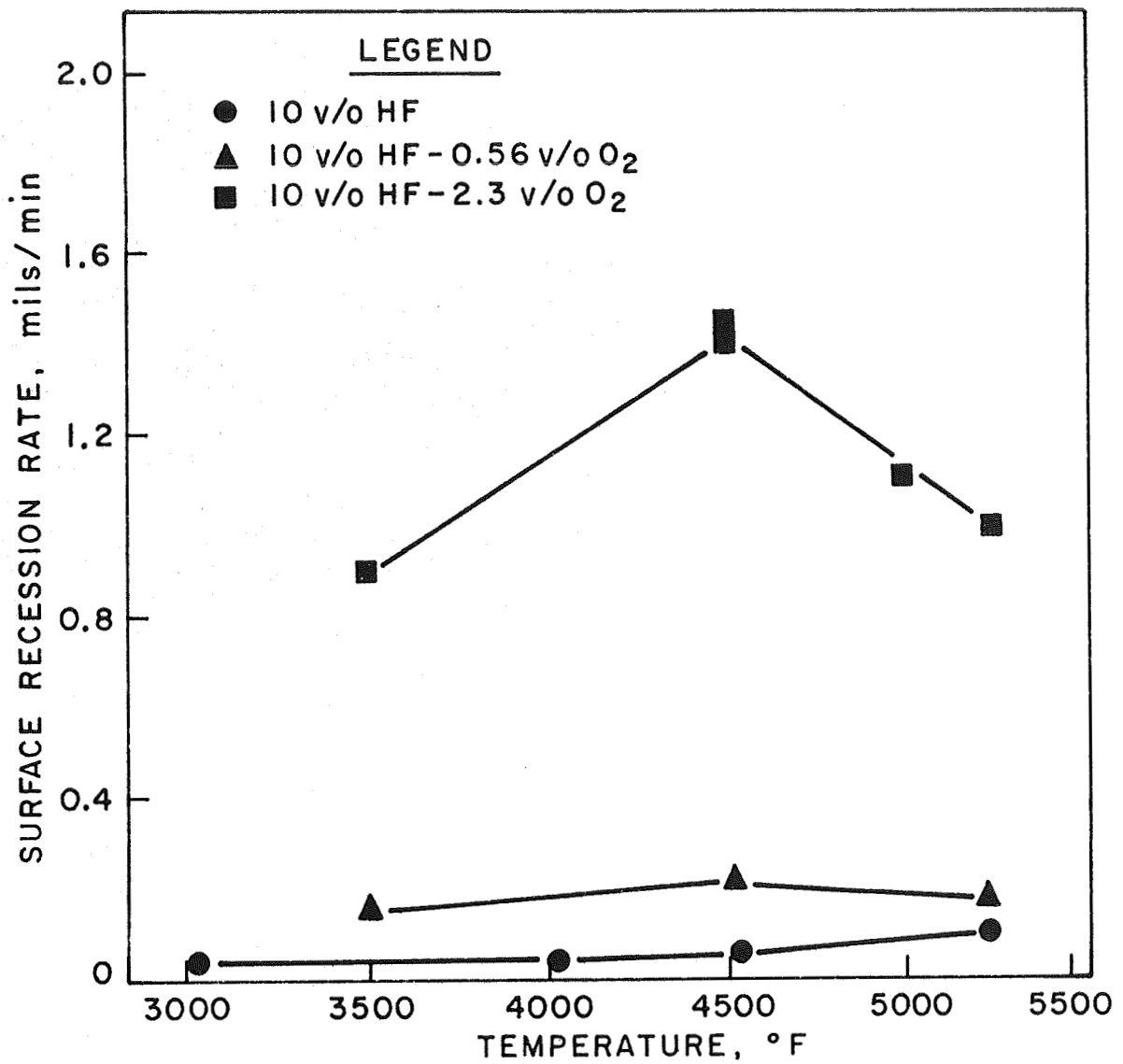
Fig. 14 - Surface Recession Rate of Rhenium in Flowing Hydrogen
Fluoride and Hydrogen Fluoride-Oxygen.
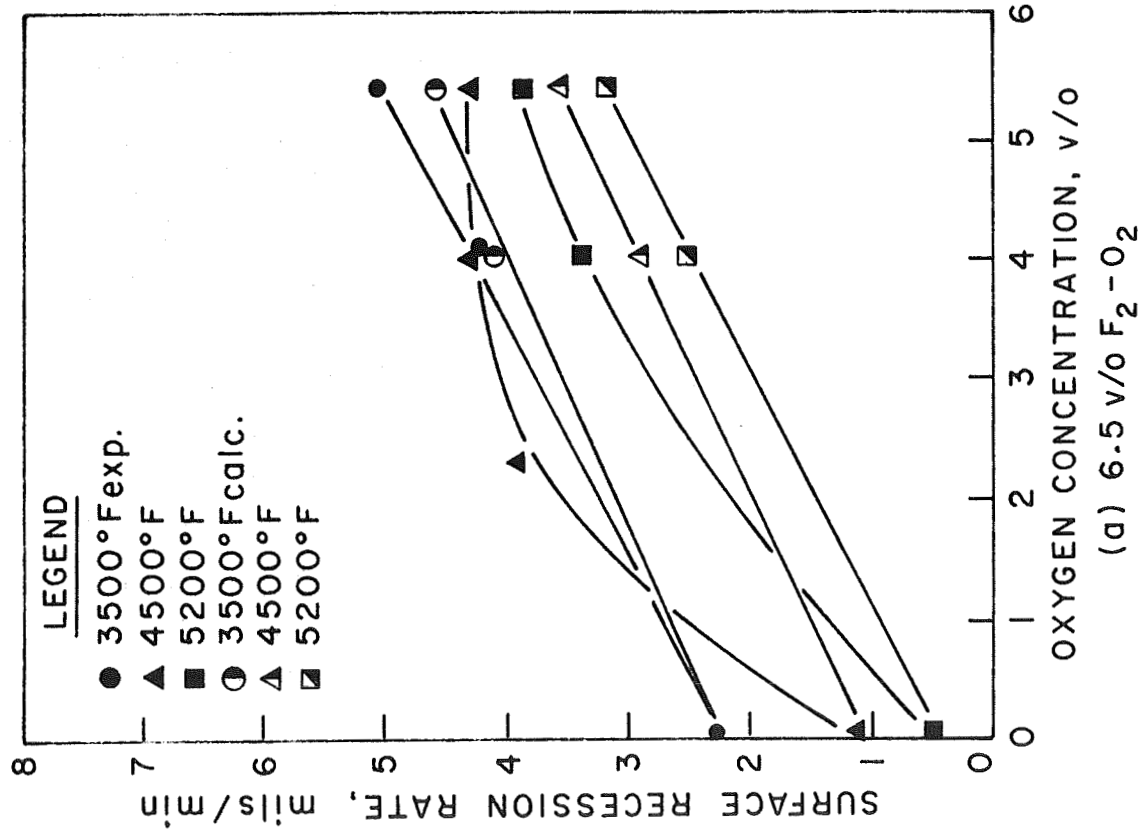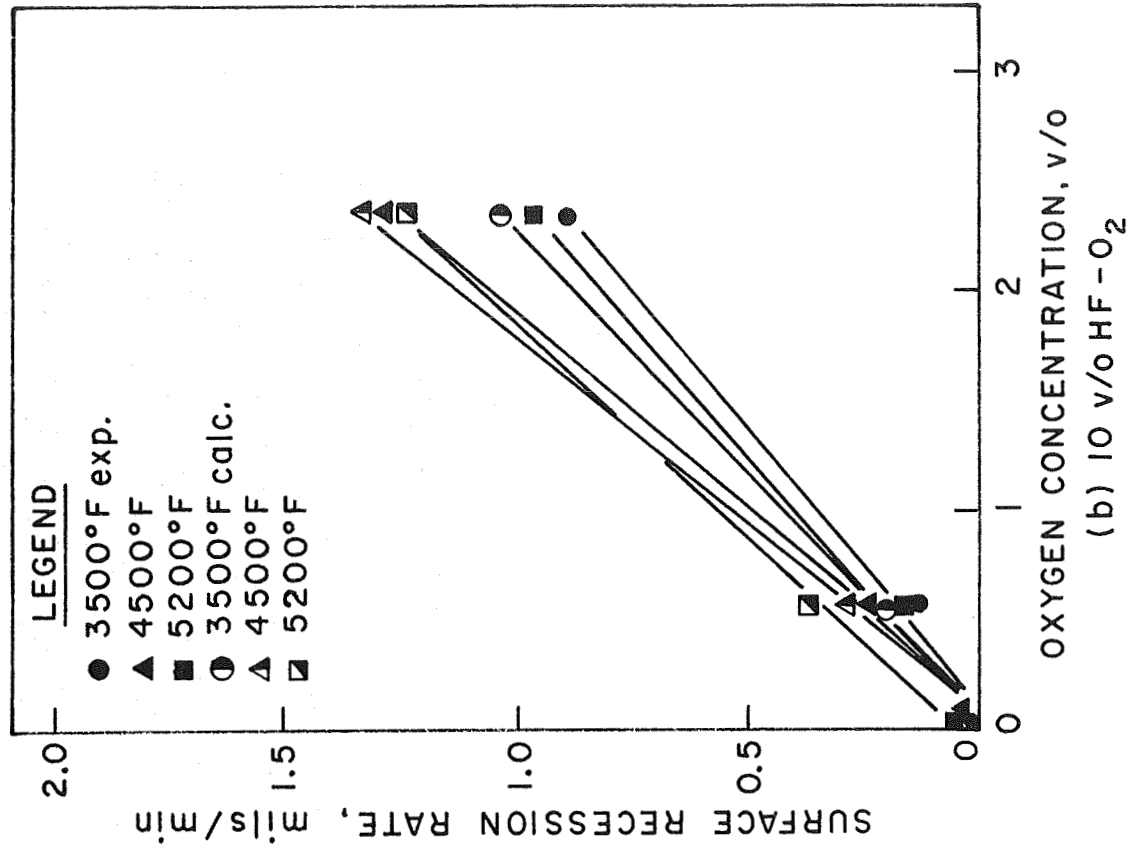
Fig. 15 - Comparison of Measured and Calculated Surface Recession Rate of Rhenium in Flowing Fluorine-Oxygen and Hydrogen Fluoride-Oxygen.

47

e.   ATJ Graphite

Samples for corrosion tests of ATJ graphite were sectioned from bulk material. In general, no attempt was made to test the influence of orientation of the material. Although low recession rates measured in hydrogen fluoride may have been slightly influenced by orientation effects and/or mechanical erosion,[2] orientation of the test samples probably did not influence the recession data in this program. Depending upon the test atmosphere, the maximum exposure temperature obtainable with the ATJ graphite was 4800°-4900°F.

A summary of oxidation tests in 4.0 and 5.4 v/o oxygen at 3000°-4800°F is presented in Table XIV and plotted with fluorine and fluorine-oxygen data in Figure 16. Corrosion data on ATJ graphite in fluorine and fluorine-oxygen are summarized in Table XV. Surface recession rates in oxygen are plotted in Figure 16, and demonstrate considerable scatter and only minor temperature dependence. In fact, the recession rate data tend to show a minimum in oxygen atmosphere at about 4000°F.

A similar effect exists for ATJ graphite in 6.5 v/o fluorine. Previous data in fluorine were obtained only to 4000°F because of input power limitations of the induction unit described in Section II-A-1. Current data in fluorine to 5000°F demonstrate that a minimum exists in the recession rate at 4000°F; the recession rate increases with increasing temperature in the range of 4000°-4900°F. Thus, a minimum appears to exist in the recession rate in both oxygen and fluorine, which may also be reflected in the corrosion data in fluorine-oxygen atmospheres. Again, additional corrosion studies are required to define the effect further.

ATJ graphite test samples exposed in fluorine-oxygen atmospheres normally had a thin film of loose, white reaction product after exposure. No corrosion residue was found in any other atmosphere, including the HF-O_2 environments. It appeared,

TABLE XIV

CORROSION BEHAVIOR OF ATJ GRAPHITE IN FLOWING OXYGEN[a]

Exposure Temp., °F	Oxygen Concentration, v/o	Weight Loss, g	Specific Weight Loss, mg/cm²/min	Surface Recession Rate, mils/min
3500	1.1	0.047	3.4	0.74
3000	4.0	0.137	17.2	3.76
3000	4.0	0.163	11.7	3.14
3500	4.0	0.143	17.8	3.90
3500	4.0	0.177	16.3	3.50
4000	4.0	0.142	15.6	3.46
4000	4.0	0.131	15.4	3.37
4000	4.0	0.122	14.3	3.14
4500	4.0	0.150	17.2	3.77
4500	4.0	0.117	15.3	3.34
4800	4.0	0.130	15.7	3.42
4930	4.0	0.110	15.3	3.35
2500	5.4	0.151	18.6	4.07
3000	5.4	0.180	23.5	5.14
3000	5.4	0.176	22.6	4.95
3500	5.4	0.208	25.0	5.46
3500	5.4	0.212	25.1	5.48
4000	5.4	0.196	23.7	5.20
4500	5.4	0.207	25.2	5.51
4500	5.4	0.232	26.8	5.85
4800	5.4	0.203	26.2	5.82

[a] Total flow rate - 10 cfh (400 fps).
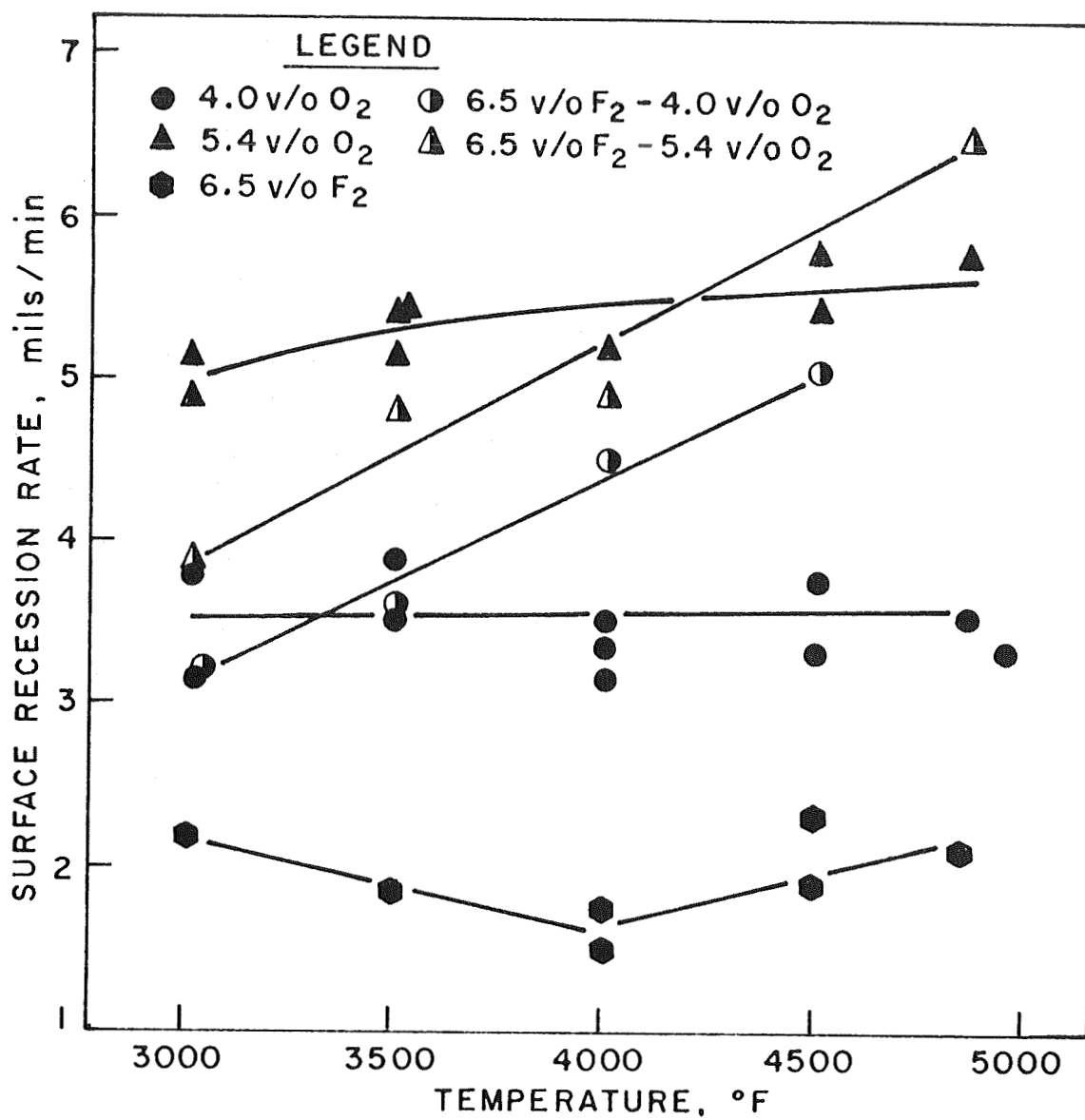
Fig. 16 - Surface Recession Rate of ATJ Graphite in Flowing Oxygen, Fluorine, and Fluorine-Oxygen.

TABLE XV

CORROSION BEHAVIOR OF ATJ GRAPHITE
IN FLOWING FLUORINE AND FLUORINE-OXYGEN[a]

Exposure Temp., °F	Fluorine Concentration, v/o	Oxygen Concentration, v/o	Weight Loss, g	Specific Weight Loss, mg/cm^2/min	Surface Recession Rate, mils/min
2400	6.5	--	0.159	11.3	2.46
3000	6.5	--	0.135	10.0	2.20
3500	6.5	--	0.116	8.28	1.79
4000	6.5	--	0.093	6.53	1.43
4000	6.5	--	0.068	7.40	1.62
4500	6.5	--	0.070	8.70	1.90
4500	6.5	--	0.086	10.9	2.39
4800	6.5	--	0.078	9.20	2.13
3000	6.5	4.0	0.117	14.4	3.14
3500	6.5	4.0	0.177	16.3	3.50
4000	6.5	4.0	0.163	20.8	4.50
4500	6.5	4.0	0.193	23.3	5.10
4800	6.5	4.0	0.153	21.7	4.73
3000	6.5	5.4	0.140	17.4	3.78
3500	6.5	5.4	0.168	21.8	4.78
4000	6.5	5.4	0.173	22.1	4.82
4800	6.5	5.4	0.255	30.2	6.60

[a] Total flow rate - 10 cfh (400 fps).

51

therefore, that a different corrosion mechanism may have been operative during fluorine-oxygen tests.

Oxidation-corrosion behavior of ATJ graphite in hydrogen fluoride and hydrogen fluoride-oxygen atmospheres is presented in Table XVI and plotted in Figure 17. As previously discussed, surface recession data in hydrogen fluoride may have been affected by sample orientation and/or gas erosion. It was found that the lower recession rates were obtained when samples were rerun and/or heated in argon prior to testing. In any case, the reaction rate of graphite in 10 v/o hydrogen fluoride is quite slow; the recession rate is about 0.15 mil/min at 4000°F.

Addition of 0.56 and 2.3 v/o oxygen increases the surface recession rate, as expected from the oxygen results. Figure 17 indicates that the recession rates at both oxygen levels are not strongly temperature dependent although both curves indicate a positive slope. The reaction rate of ATJ graphite in hydrogen fluoride-oxygen is 2.6 mils/min in 10 v/o HF-2.3 v/o O_2 at 4900°F, the highest of any material tested in the program. This is apparently due to high recession rates of graphite in oxygen atmospheres.

A comparison of the calculated and measured recession rates of ATJ graphite in fluorine-oxygen and hydrogen fluoride-oxygen at 3000°, 4000°, and 4900°F is presented in Figure 18. As previously, recession rates in 0.56 and 2.3 v/o oxygen were obtained by linear interpolation of data in 4.0 and 5.4 v/o oxygen. Figure 18a shows that ATJ graphite in fluorine-oxygen exhibits converse behavior from that of tungsten and rhenium; the measured recession rates are lower than the calculated rates. This effect is greatest at 3000°F but is appreciable at all three temperatures. The calculated recession rate at 3300°F is about twice that of the measured rate in 6.5 v/o F_2-5.4 v/o oxygen. This could be due to the formation of oxyfluorides as evidenced by the presence of a thin, white reaction product not found in fluorine or oxygen. In spite of this effect, which is least significant at 4900°F, the surface recession rates of graphite in fluorine-oxygen were the highest measured in the program.

52

TABLE XVI

CORROSION BEHAVIOR OF ATJ GRAPHITE IN FLOWING
HYDROGEN FLUORIDE AND HYDROGEN FLUORIDE-OXYGEN[a]

Exposure Temp., °F	Hydrogen Fluoride Concentration, v/o	Oxygen Concentration, v/o	Weight Loss, g	Specific Weight Loss, mg/cm²/min	Surface Recession Rate, mils/min
3000	10	--	0.007	0.49	0.11
3000	10	--	0.009	0.64	0.14
3000	10	--	0.007	0.52	0.11
3000	10[b]	--	0.004	0.29	0.06
3000	10[b]	--	0.004	0.30	0.07
3500	10	--	0.009	0.62	0.14
3500	10[b]	--	0.005	0.37	0.08
3500	10[b]	--	0.004	0.37	0.07
3820	10[b]	--	0.004	0.30	0.06
4000	10[b]	--	0.005	0.29	0.08
4000	10	--	0.006	0.68	0.15
4800	10	--	0.018	0.40	0.53
3000	10	0.56	0.037	2.8	0.62
3500	10	0.56	0.042	3.2	0.70
4000	10	0.56	0.046	3.7	0.80
4500	10	0.56	0.043	3.5	0.77
4930	10	0.56	0.055	6.5	1.42
3000	10	2.3	0.134	10.0	2.18
3500	10	2.3	0.141	10.6	2.30
4000	10	2.3	0.108	13.2	2.86
4500	10	2.3	0.164	12.2	2.67
4900	10	2.3	0.090	11.8	2.57

[a] Total flow rate - 10 cfh (400 fps).

[b] Rerun samples.
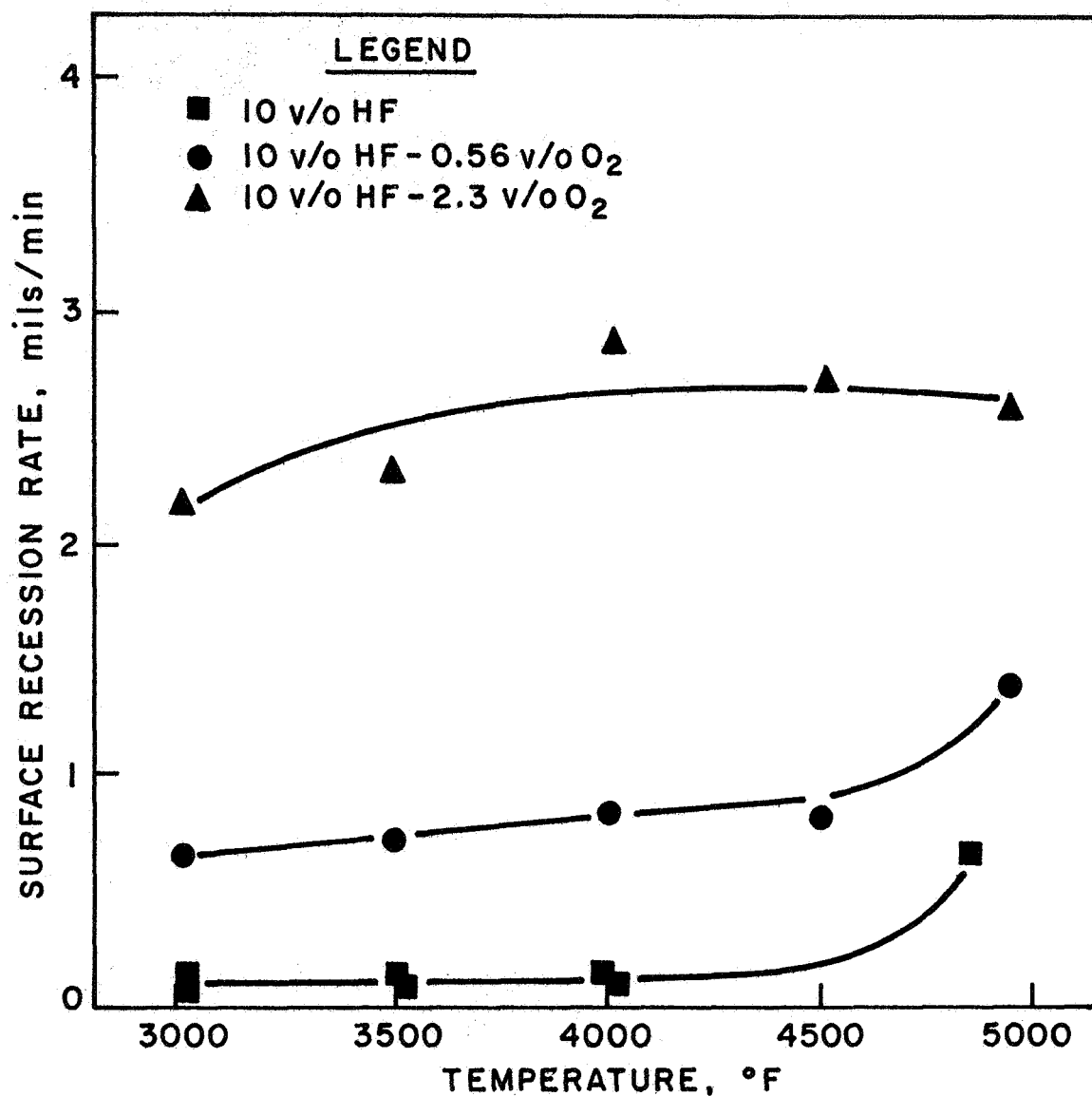
Fig. 17 - Surface Recession Rate of ATJ Graphite in Flowing
Hydrogen Fluoride and Hydrogen Fluoride-Oxygen.
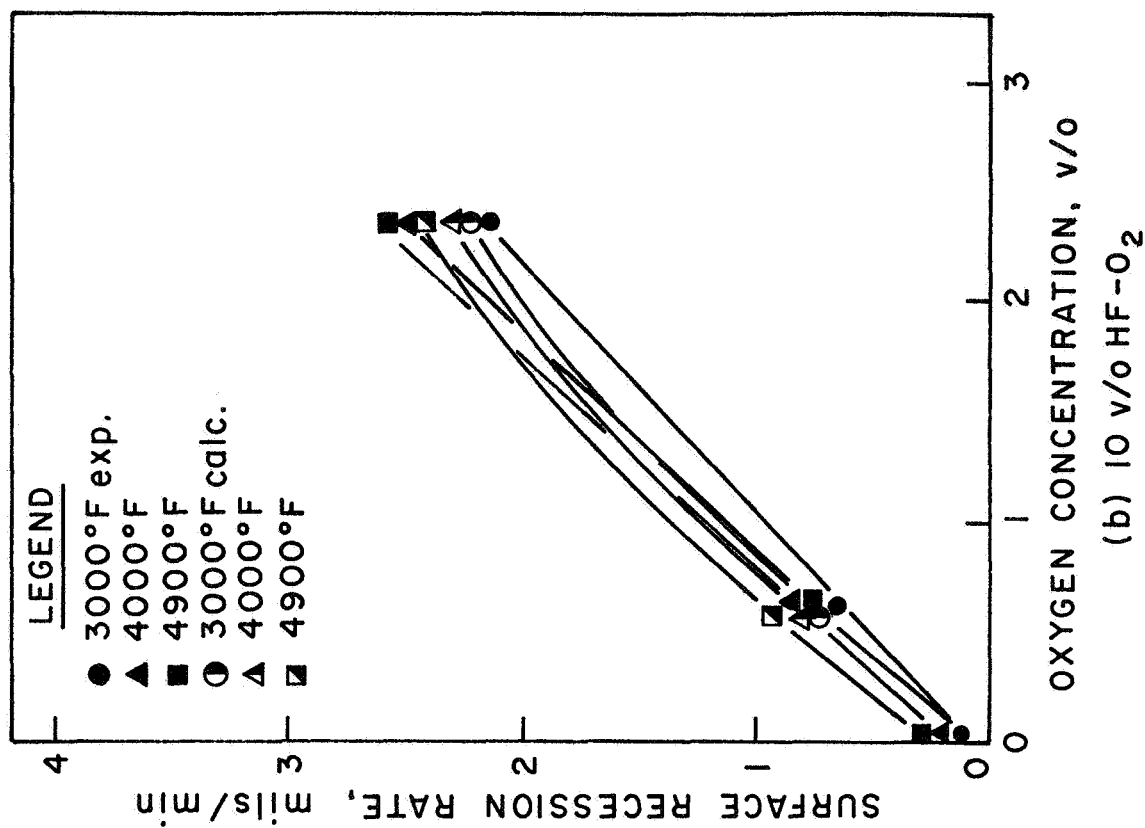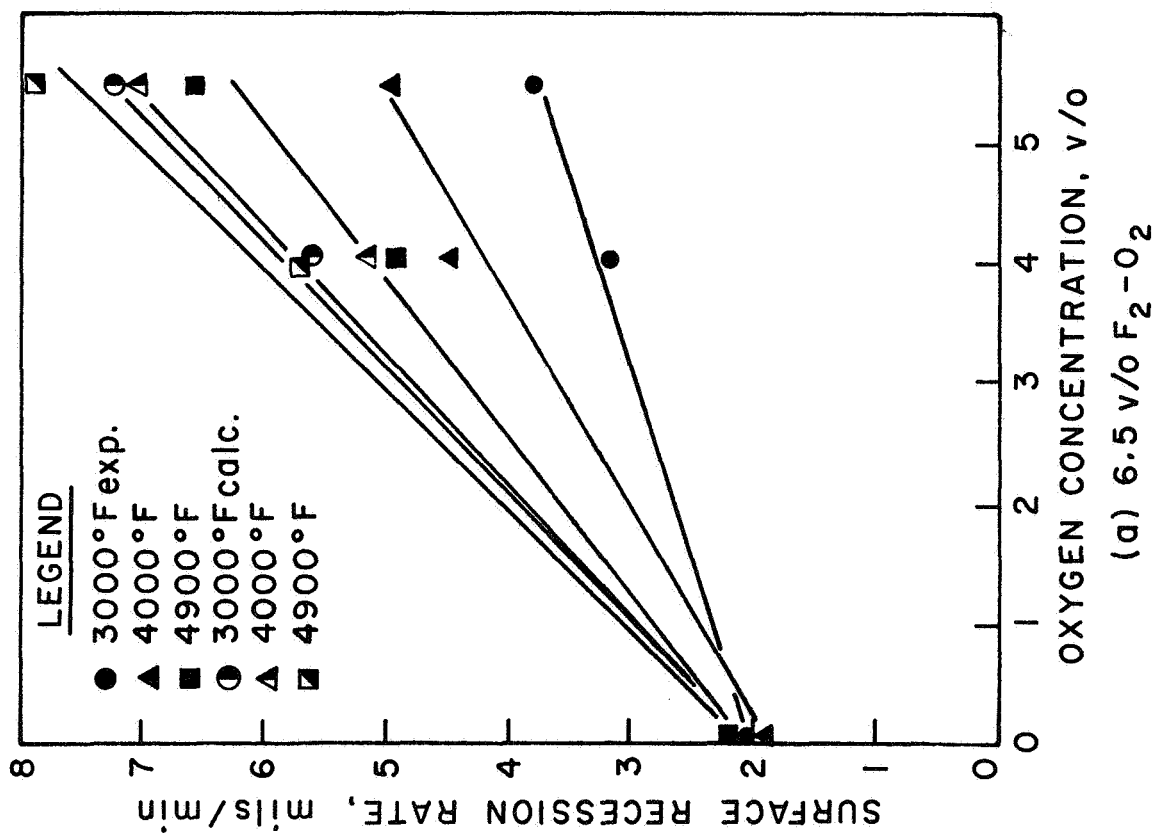
Fig. 18 - Comparison of Measured and Calculated Surface Recession Rates of ATJ Graphite in Flowing Fluorine-Oxygen and Hydrogen Fluoride-Oxygen.

In hydrogen fluoride-oxygen atmospheres (Figure 18b), no comparable effect is indicated. The calculated and measured recession rates are similar, despite the fact that graphite could conceivably behave differently than metals. Interactions between hydrogen fluoride and oxygen releasing hydrogen could increase the surface recession rate since graphite reacts with hydrogen to form hydrocarbons at high temperatures. The simplified overall reaction can be written as:

$$C_{(g)} + HF_{(g)} + O_{2(g)} \rightleftarrows C_xH_{y(g)} + C_xF_{y(g)} + C_xO_{y(g)}$$
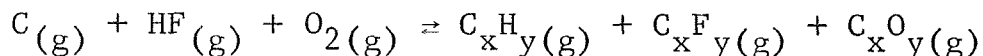
Thus, three reactive species could be present at the graphite surface. However, the plot in Figure 18b does not suggest that interactions of this type occurred. Rather, it demonstrates that, like tungsten and rhenium, surface recession is primarily due to oxidation.

f.   Carbide-Graphite Composites

The candidate carbide-graphite composites, developed under contract NASr-65-(09),[8] were HfC-33 v/o C and TaC-20 v/o C fabricated by hot-pressing and resulting in densities of 95-97%. Test samples of these materials were sectioned from bulk material and evaluated in fluorine and hydrogen fluoride to 4000°F in earlier work on this program.[2] The data were extended to 5000°F during the current year. As with ATJ graphite, no attempts were made to correlate the oxidation-corrosion behavior with any orientation derived in fabrication. However, it was previously found that the corrosion rate in hydrogen fluoride was dependent on the known sample orientation of HfC-C. Any orientation effects were negated in the current work by the higher reaction rates in the combined environments.

The corrosion mechanisms of carbide-graphite composites in the combined environments are different than that of metals and graphite. Both of the carbide materials form solid oxides within the testing range of this program, whereas all of the reaction products of metals and graphite are gaseous. However, the melting

points of the formed oxides are considerably different. Ta_2O_5 has a melting point of about 3400°F, whereas HfO_2 melts at about 5000°F. Consequently, the carbide composite materials included a material which exhibited a liquid oxide (TaC-C) and a solid oxide (HfC-C) throughout most of the 3000°-5000°F range of testing in the program. Since these materials do not develop solid films in either fluorine or hydrogen fluoride, it was expected that the above differences would influence the corrosion behavior in the combined environments.

Another factor in the oxidation-corrosion mechanism of carbide composites in oxygen-containing atmospheres is important because of the graphite phase that is present and the mechanism of reaction of the carbide. Oxidation of the M_xC_y phase to M_xO_y results in a weight gain. However, this is accompanied by weight losses due to the formation of gaseous CO and/or CO_2. The individual reactions in oxygen can be written as follows:

$$MC_{(s)} + O_{2(g)} \rightleftarrows M_xO_{y(s,l)} + C_xO_{y(g)}$$

$$C_{(s)} + O_{2(g)} \rightleftarrows C_xO_{y(g)}$$
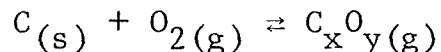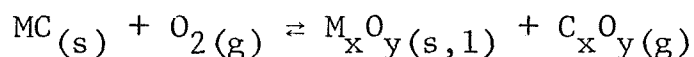
The overall reaction is therefore:

$$MC_{(s)} + C_{(s)} + O_{2(g)} \rightleftarrows M_xO_{y(s,l)} + C_xO_{y(g)}$$
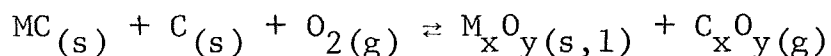
As previously discussed, M_xO_y is a solid (HfO_2) for hafnium carbide and a liquid (Ta_2O_5) for tantalum carbide. The weight change resulting from the overall reaction can be readily calculated from information on the composite composition. Assuming complete reaction and full density of the composite, oxidation results in weight gain of 2.5 $mg/cm^2/mil$ for TaC-20 v/o C and a weight loss of 0.3 $mg/cm^2/mil$ for HfC-33 v/o C. These calculations apply only for short exposure times because the development of the stable oxide layer results in nonlinear oxidation rates. If the formed oxide spalls from the surface, the weight losses are about 23 and 30 $mg/cm^2/mil$ for HfC-33 v/o C and TaC-20 v/o C,

respectively. This illustrates the overriding effect of spalling on the measured weight change of carbide composites exposed in oxygen.

In the combined environments, additional complexities of the reaction mechanism can occur. Depending upon the ratio of oxygen to fluorine or hydrogen fluoride, oxidation of the carbide phase could proceed preferentially. The simplified individual reactions for oxygen-fluorine can be written as follows:

$$MC_{(s)} + O_{2(g)} \rightleftarrows M_xO_{y(s,1)} + C_xO_y$$

$$M_xO_{y(s)} + F_{2(g)} \rightleftarrows M_xF_{y(g)} + O_xF_y$$
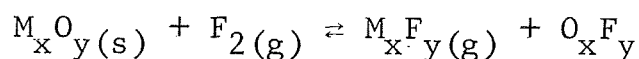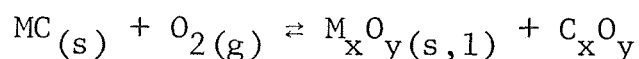
The overall reaction, in terms of gaseous surface recession only, can be written:

$$MC_{(s)} + O_{2(g)} + F_{2(g)} \rightleftarrows M_xF_{y(g)} + C_xO_{y(g)} + O_xF_{y(g)}$$
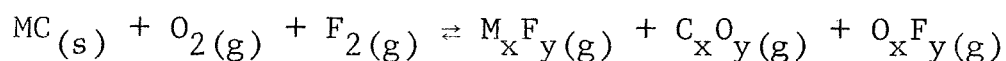
However, the possibility of interactions of fluorine with carbon and/or the formation of both metallic and carbonaceous oxyfluorides cannot be ignored. Including these possibilities and eliminating fluorine-oxygen compounds, the overall reaction can be written as:

$$MC_{(s)} + C_{(s)} + O_{2(g)} + F_{2(g)} \rightleftarrows M_xF_{y(g)} + C_xO_{y(g)} +$$

$$M_xF_yO_{z(g)} + C_xF_yO_{z(g)} +$$

$$C_xF_{y(g)} + M_xO_{y(s,1)}$$
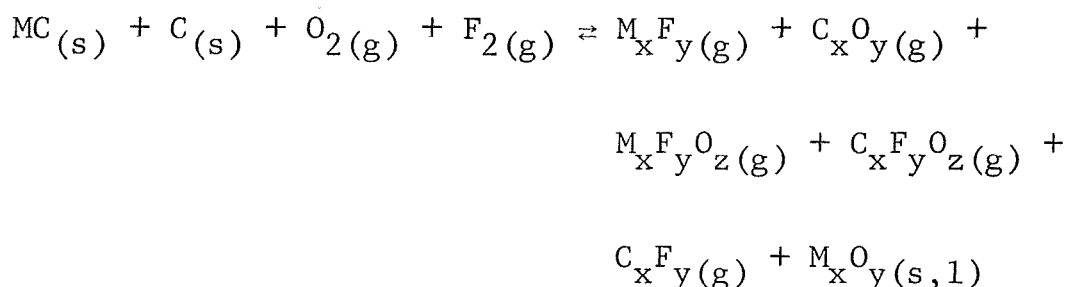
Thus, one solid or liquid and five general gaseous species are possible in the reaction. It is unlikely that all these products are formed. Rather, the measured surface recession was most likely controlled by the formation of two or three reaction products dependent upon the fluorine-oxygen ratio. It was found that both carbide and boride composites normally had some oxide

residue on the reaction surface after exposure. The above reaction does illustrate the very complex oxidation-corrosion mechanism of these materials.

The oxidation-corrosion behavior of HfC-33 v/o C in oxygen, fluorine, and fluorine-oxygen is summarized in Table XVII and plotted in Figure 19. Oxidation data are presented two ways in Table XVII. Because of the low weight change and possibility of oxide spalling associated with oxidation of carbide composites and borides, calculations of surface recession from weight losses are questionable. Accordingly, an alternate approach was used to obtain surface recession in oxygen for HfC-C, TaC-C, and ZrB_2-SiC-C. After exposure, the oxide present on the sample was mechanically removed, and the samples re-weighed for surface recession calculations. Removal of the oxide was not difficult for HfC-C composites exposed at 3000° and 4000°F since the uniform, white oxide developed was friable. Samples exposed at 5000°F above the melting point of HfO_2 (~4900°F) had a gray, glassy oxide, which was blown from the sample by the gas stream. Consequently, oxide removal was continuous during the run leaving a relatively thin oxide layer after exposure. Except for oxide clinging to the edges of the test sample, removal of the thin residual oxide was not necessary. Table XVII includes both methods of calculation, although the oxide removal method is probably more accurate. Both methods contain the errors introduced by assuming a linear time dependence for a system which should exhibit nonlinear oxidation rates.

The surface recession data in 6.5 v/o fluorine show a similar result to that of ATJ graphite in that a minimum exists at about 4500°F. It will be shown subsequently that TaC-C composites exhibit a similar behavior. In view of the minimum shown for ATJ graphite, some of the measured increase above 4500°F can be attributed to the graphite portion of the composite. However, the volume fraction of graphite in these materials is insufficient

59

TABLE XVII

CORROSION BEHAVIOR OF HfC-33 v/o C IN
FLOWING OXYGEN, FLUORINE, AND FLUORINE-OXYGEN[a]

Exposure Temp., °F	Fluorine Concentration, v/o	Oxygen Concentration, v/o	Weight Loss, g	Specific Weight Loss, mg/cm²/min	Surface Recession Rate, mils/min
3000	--	2.3	+0.005	+0.7	--
3000	--	2.3	0.095	13.7	0.60[c]
4000	--	2.3	0.002	0.3	0.20[b]
4000	--	2.3	0.152	20.8	0.90[c]
5000	--	2.3	0.429	49.2	2.10
5000	--	2.3	0.463	53.2	2.30[c]
3000	--	5.4	+0.006	+0.8	--
3000	--	5.4	0.245	34.7	1.50[c]
4000	--	5.4	0.001	0.1	0.05[b]
4000	--	5.4	0.200	25.9	1.10[c]
5000	--	5.4	0.768	81.5	3.50
5000	--	5.4	0.930	98.8	4.30[c]
3000	6.5	--	0.758	52.3	2.26
3500	6.5	--	0.678	47.0	2.03
4000	6.5	--	0.595	43.0	1.85
4500	6.5	--	0.209	22.3	0.96
4500	6.5	--	0.187	19.6	0.85
5000	6.5	--	0.432	52.5	2.26
5000	6.5	--	0.435	51.5	2.22
3000	6.5	4.0	0.885	95.5	4.12
4000	6.5	4.0	0.900	113.0	4.87
5000	6.5	4.0	1.302	138.8	5.96
3000	6.5	5.4	1.922	95.5	4.15
3500	6.5	5.4	1.106	132.2	5.59
3500	6.5	5.4	1.048	122.8	5.30
4000	6.5	5.4	1.110	116.1	5.01
4000	6.5	5.4	1.114	135.9	5.85
4750	6.5	5.4	1.225	141.0	6.10

[a] Total flow rate - 10 cfh (400 fps).

[b] Surface recession calculated from oxidation stoichiometry.

[c] Surface recession calculated from weight loss after oxide removal.
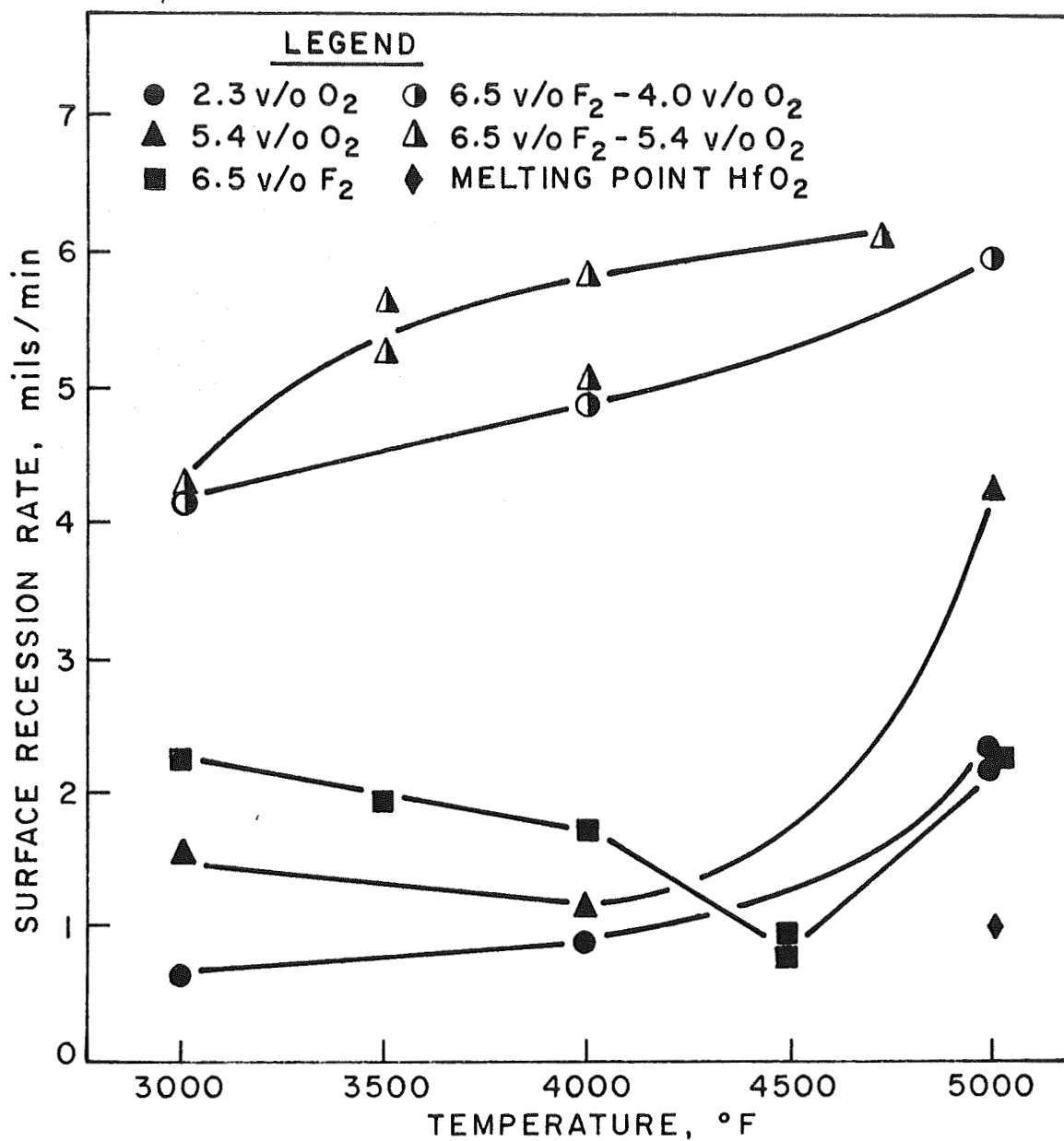
Fig. 19 - Surface Recession Rate of HfC-33 v/o C in Flowing
Oxygen, Fluorine, and Fluorine-Oxygen.

to provide all of the measured minimum. The increase in recession above 4500°F can be explained by the tendency of carbides to reject carbon at high temperatures resulting in metal-rich carbides. Metallic tantalum and hafnium had the highest reaction rates in fluorine measured in this program.[2] It is not surprising, therefore, that an increase in recession rate is obtained at 4500°-5000°F, since any tendency to produce a metal-rich phase should increase the recession rate.

The recession rates in 6.5 v/o F_2-5.4 v/o O_2 and 6.5 v/o F_2-4.0 v/o O_2 indicate a somewhat different corrosion behavior at higher oxygen levels; the temperature dependence of surface recession appears greater at 5.4 v/o O_2. The data point at 5000°F was run initially in 4.0 v/o O_2. Some flow of oxide developed on the sample. To eliminate this effect, the test temperature was lowered to 4750°F for 6.5 v/o F_2-5.4 v/o O_2. However, the results indicate little difference in measured recession rates, due to the complexity of the oxidation-corrosion reactions described previously.

Both environments demonstrate that the recession rates in oxygen-fluorine are probably accelerated by the combined environment. This should not be surprising in view of the poor resistance of oxides to fluorine and hydrogen fluoride.[10] As previously stated, all samples exposed in fluorine-oxygen had thin oxide films on the samples after exposure. Below 5000°F these oxides were white and powdery, but at 5000°F the oxide was slightly more continuous; in no case were thick oxides found on the reaction surface. However, glassy oxide globules were found on the edges of 5000°F samples, indicating some flow of oxide had occurred during exposure.

The corrosion behavior of HfC-33 v/o C in hydrogen fluoride and hydrogen fluoride-oxygen is presented in Table XVIII; surface recession data are plotted in Figure 20. Surface recession in 10 v/o HF is very low in the range of 3000°F-4500°F, but increases abruptly in the range of 4500°-5000°F, due to a loss of

TABLE XVIII

CORROSION BEHAVIOR OF HfC-33 v/o C IN FLOWING HYDROGEN FLUORIDE AND HYDROGEN FLUORIDE-OXYGEN[a]

Exposure Temp., °F	Hydrogen Fluoride Concentration, v/o	Oxygen Concentration, v/o	Weight Loss, g	Specific Weight Loss, mg/cm²/min	Surface Recession Rate, mils/min
3000	10	--	0.020	1.4	0.06
3000+	10	--	0.039	2.8	0.12
3500	10	--	0.026	1.7	0.07
3500	10	--	0.032	2.1	0.09
3500	10	--	0.027	1.8	0.08
3500+	10	--	0.061	4.2	0.18
4000	10	--	0.340	2.2	0.09
4000	10	--	0.041	2.7	0.12
4000+	10	--	0.070	4.7	0.20
4500	10	--	0.166	10.7	0.46
5000	10	--	0.490	35.7	1.54
3000	10	0.56	0.142	15.7	0.68
4000	10	0.56	0.117	12.1	0.52
4000	10	0.56	0.123	12.6	0.55
4500	10	0.56	0.133	17.4	0.75
5000	10	0.56	0.335	40.5	1.75
5000	10	0.56	0.720	50.2	2.17
3000	10	2.3	0.233	17.8	0.77
4000	10	2.3	1.013	68.2	2.94
5000	10	2.3	1.229	146.8	6.30

[a] Total flow rate - 10 cfh (400 fps).
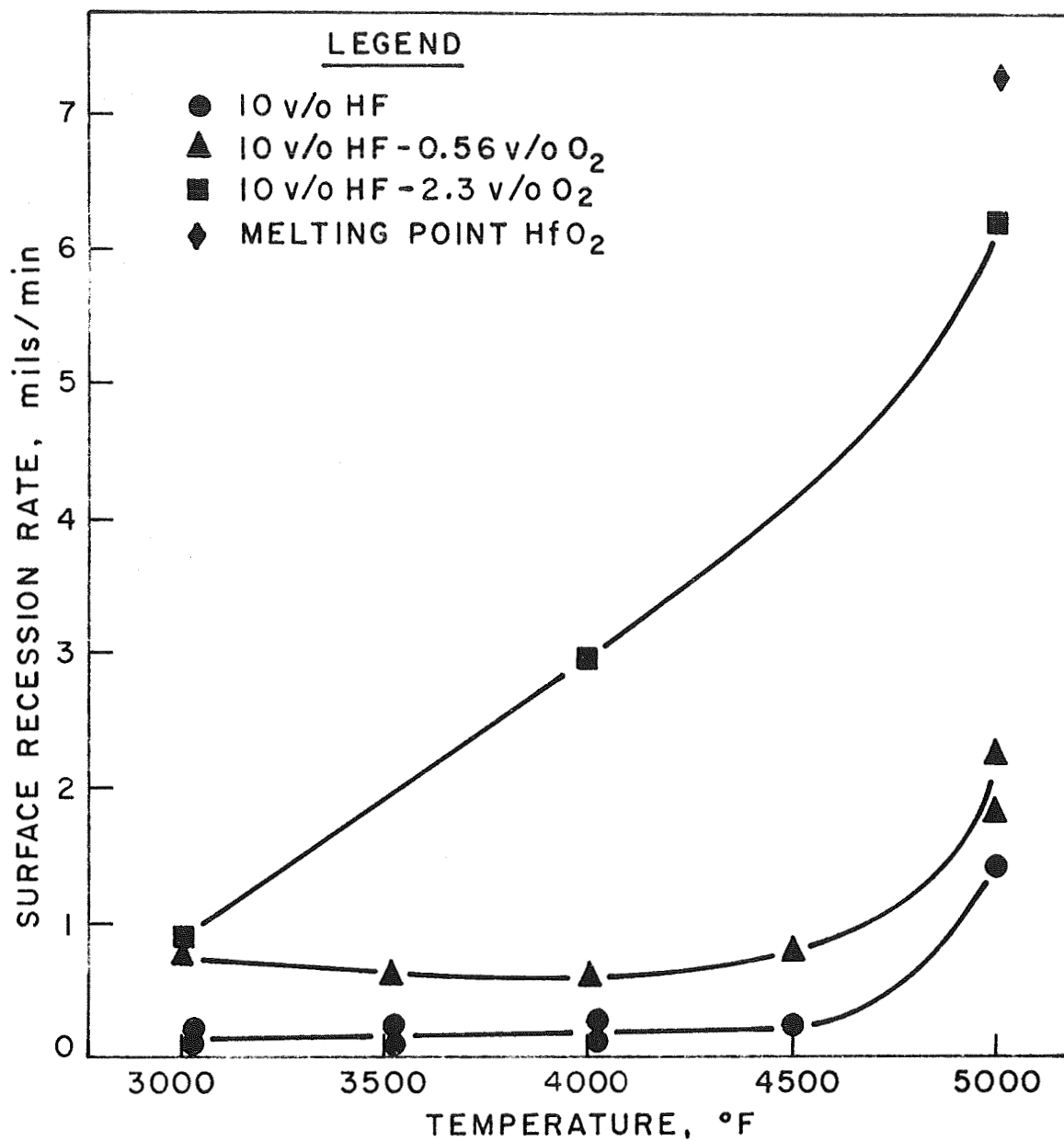
Fig. 20 - Surface Recession Rate of HfC-33 v/o C in Flowing
Hydrogen Fluoride and Hydrogen Fluoride-Oxygen.

carbon from the carbide phase previously shown in fluorine. Additions of 0.56 and 2.3 v/o oxygen increase the recession rate considerably, particularly at higher temperatures. At 5000°F, the recession rates in 10 v/o HF-0.56 v/o O_2 and 10 v/o HF-2.3 v/o O_2 are about 2.0 and 6.3 mils/min, respectively. A portion of the abrupt increase at 5000°F could be due to oxidation and melting of HfO_2, since some glassy materials was present as globules on the edges of the samples. These globules also contained a black phase which was apparently graphitic material eroded from the sample surface. All of these factors probably contributed to the very high recession rates measured in hydrogen fluoride-oxygen at 5000°F.

Oxidation-corrosion data for TaC-20 v/o C in oxygen, fluorine, and fluorine-oxygen are contained in Table XIX and plotted in Figure 21. As previously discussed, Ta_2O_5 melts at about 3400°F, and a liquid oxide is formed in oxygen atmospheres above this temperature. Under these conditions, surface recession calculations from weight loss are inappropriate, so alternate approaches for HfC-33 v/o C were used. Surface recession at 3000°F was calculated by the stoichiometric weight loss analysis described previously for TaC-C; i.e., a weight gain of approximately 2.5 mg/cm^2/mil for the formation of a solid oxide. At 4000°F, some ablation of the glassy transparent formed oxide occurred. Surface recession calculations at 4000°F were obtained from the weight loss after mechanical removal of the oxide layer. Extensive sample deterioration occurred at both 2.3 and 5.4 v/o at 5000°F. Test samples after exposure included a large globule of glassy oxide, although little ablation occurred as shown by the relatively low weight losses. For these tests, the surface recession was estimated from the dimensions of the unreacted portion of the sample after exposure. The surface recession rates at the various test conditions in oxygen (Table XIX) were obtained by both methods whenever possible. The surface recession calculated at 3000°F and 4000°F show reasonable correlation of the two methods. Furthermore, the recession

TABLE XIX

CORROSION BEHAVIOR OF TaC-20 v/o C IN
FLOWING OXYGEN, FLUORINE, AND FLUORINE-OXYGEN[a]

Exposure Temp., °F	Fluorine Concentration, v/o	Oxygen Concentration, v/o	Weight Loss, g	Specific Weight Loss, mg/cm²/min	Surface Recession Rate, mils/min
3000	--	2.3	+0.029	+4.0	1.60 [b]
3000	--	2.3	0.214	29.8	1.00 [c]
4000	--	2.3	0.053	6.3	0.20
4000	--	2.3	0.278	33.5	1.10 [c]
5000	--	2.3	0.125	19.4	13.00 [d]
3000	--	5.4	+0.044	+5.2	2.10 [b]
3000	--	5.4	0.401	45.3	1.50 [c]
4000	--	5.4	0.137	17.1	0.60
4000	--	5.4	0.487	60.3	2.00 [c]
5000	--	5.4	0.178	22.7	20.00 [d]
3000	6.5	--	0.933	65.7	2.19
3500	6.5	--	0.766	52.6	1.75
4000	6.5	--	0.562	40.8	1.36
4500	6.5	--	0.188	21.3	0.71
4500	6.5	--	0.253	17.8	0.59
5000	6.5	--	0.435	30.8	1.04
3000	6.5	4.0	2.400	166.0	5.49
4000	6.5	4.0	1.223	152.0	5.05
4000	6.5	4.0	1.437	161.0	5.35
5000	6.5	4.0	1.162	133.0	12.00 [d]
5000	6.5	4.0	1.218	145.0	15.00 [d]
3000	6.5	5.4	1.225	148.0	4.92
3500	6.5	5.4	1.081	144.5	4.80
4000	6.5	5.4	1.136	147.0	4.90
5000	6.5	5.4	1.238	145.0	20.00 [d]

[a] Total flow rate - 10 cfh (400fps).

[b] Surface recession based on oxidation stoichiometry.

[c] Surface recession calculated after oxide removal.

[d] Extensive oxidation of sample; surface recession estimated from final dimensions.
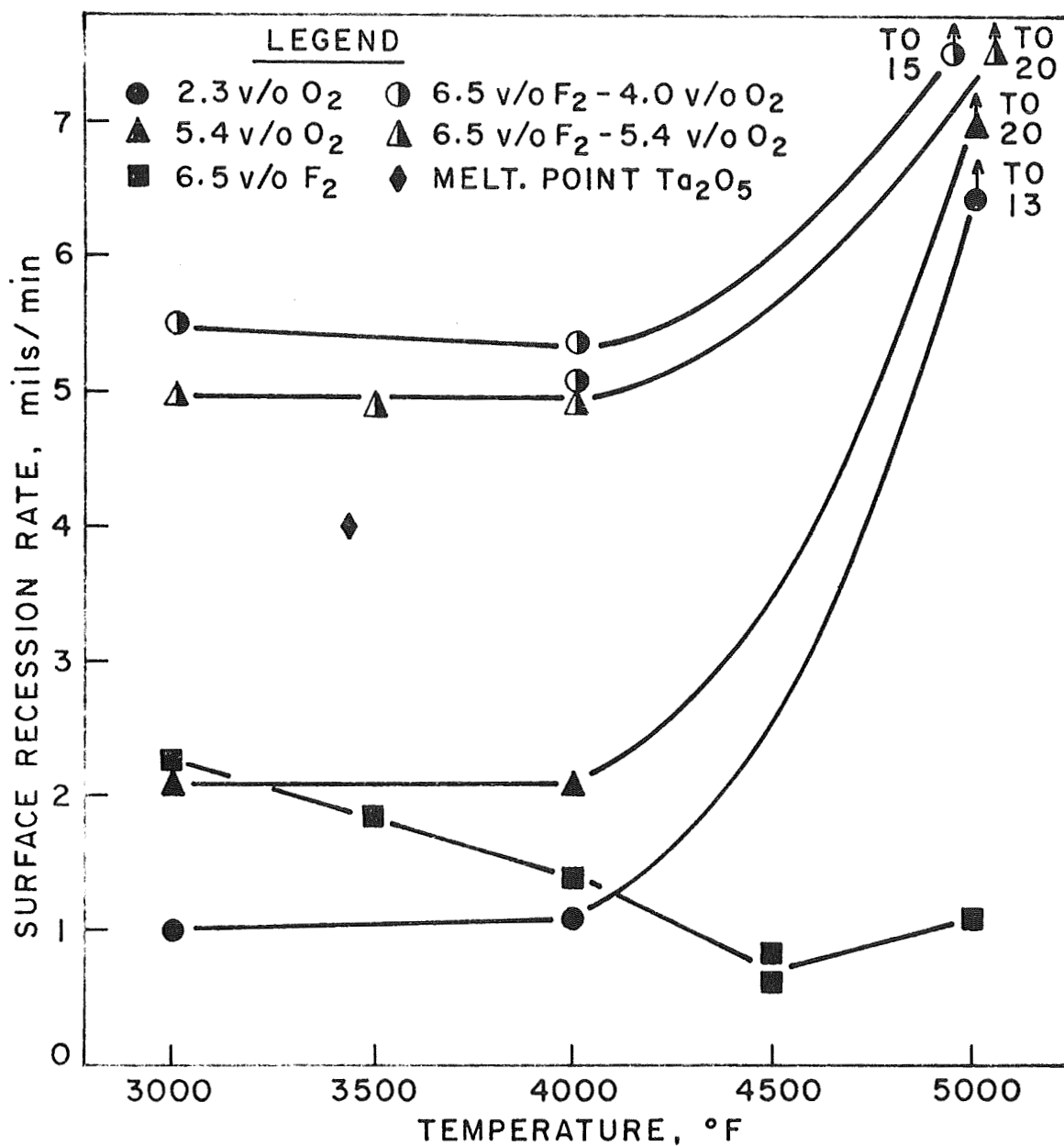
Fig. 21 - Surface Recession Rate of TaC-20 v/o C in Flowing Oxygen, Fluorine, and Fluorine-Oxygen.

rate at 4000°F is not much different than at 3000°F at both oxygen levels. The formation of a molten oxide did not cause catastrophic oxidation at 600°F above the melting point of Ta_2O_5, and thus, in contrast to HfC-C which exhibited ablation of molten oxide at about its melting point, TaC-C developed a high viscosity oxide which provided protection to at least 4000°F.

Figure 21 also shows that TaC-C, like ATJ graphite and HfC-C, exhibits a similar corrosion curve minimum in fluorine at 4500°F. The effect, however, is not as great for TaC-20 v/o C as for HfC-33 v/o C, partially due to the lower volume fraction of graphite in the TaC-20 v/o C composite. Surface recession in 6.5 v/o F_2 is about 1 mil/min at 5000°F.

Below 4000°F, the oxidation-corrosion rate in fluorine-oxygen changes little in 5.4 v/o oxygen, but decreases slightly with increasing temperature in 6.5 v/o F_2-4.0 v/o O_2. In fact, the measured increase rates are slightly higher at the lower oxygen level at 3000°F-4000°F. It is not known whether this is due to experimental error, or the controlling mechanism. However, the data is reasonably reproducible suggesting that the effect is due to the oxidation-corrosion mechanism. At 5000°F, extensive attack of the test samples occurred as described previously for oxygen tests. Surface recession for these conditions were also estimated from the final sample dimensions, although deterioration of the tests samples at 6.5 v/o F_2-4.0 v/o O_2 was somewhat less than in oxygen. Samples exposed at 5000°F in 6.5 v/o F_2-4.0 v/o O_2 exhibited extensive cratering after exposure rather than the general dimensional deterioration that occurred in 4.0 v/o oxygen.

Oxidation-corrosion data for TaC-20 v/o C in hydrogen fluoride and hydrogen fluoride-oxygen is summarized in Table XX and plotted in Figure 22. Here the results are somewhat surprising because of the very strong temperature dependence of the corrosion in 10 v/o HF-2.3 v/o O_2. A minor change in slope does exist in 10 v/o HF at about 4000°F, but does not appear to be

TABLE XX

CORROSION BEHAVIOR OF TaC-20 v/o C IN FLOWING
HYDROGEN FLUORIDE AND HYDROGEN FLUORIDE-OXYGEN[a]

Exposure Temp., °F	Hydrogen Fluoride Concentration, v/o	Oxygen Concentration, v/o	Weight Loss, g	Specific Weight Loss, mg/cm^2/min	Surface Recession Rate, mils/min
3000	10	--	0.069	4.87	0.14
3500	10	--	0.062	4.45	0.15
3500	10	--	0.068	4.82	0.16
4000	10	--	0.037	5.66	0.19
4000	10	--	0.087	6.24	0.21
4500	10	--	0.115	9.11	0.30
5000	10	--	0.174	12.60	0.42
3000	10	0.56	0.131	15.50	0.51
4000	10	0.56	0.197	24.10	0.80
5000	10	0.56	0.262	32.90	1.09
3000	10	2.3	0.198	21.30	0.71
3000	10	2.3	0.203	25.30	0.84
3500	10	2.3	0.429	54.00	1.79
4000	10	2.3	0.679	76.60	2.54
5000	10	2.3	0.790	88.50	5.00[b]

[a]Total flow rate - 10 cfh (400 fps).

[b]Estimated from sample dimensions after exposure.
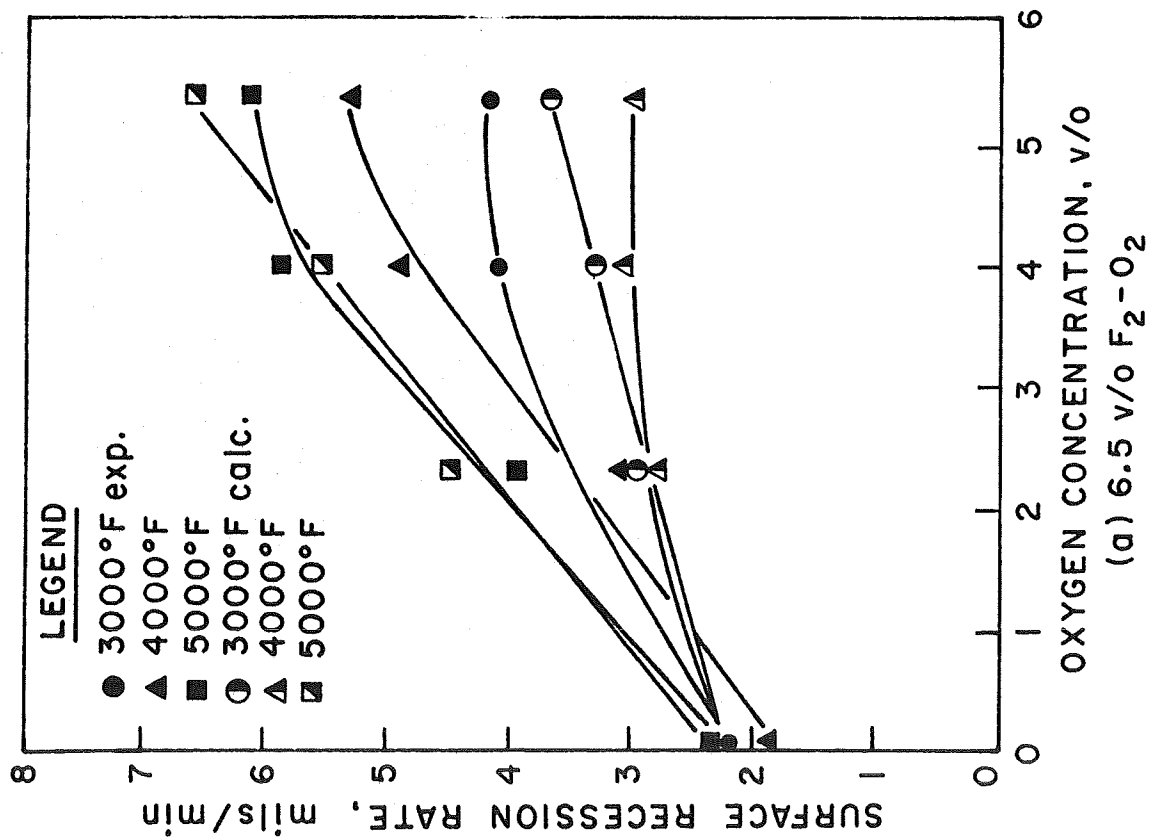
Fig. 22 – Comparison of Experimental and Calculated Surface Recession Rate of HfC-33 v/o C in Flowing Fluorine-Oxygen and Hydrogen Fluoride-Oxygen.

reflected in the data in 10 v/o HF-0.56 v/o O_2. The sample exposed in 10 v/o HF-2.3 v/o O_2 at 5000°F did not deteriorate to the same extent as the sample exposed in 2.3 v/o oxygen. However, the surface recession for this sample was also estimated from the final sample dimensions. Both fluorine-oxygen and hydrogen fluoride-oxygen atmospheres, therefore, tended to reduce the catastrophic oxidation obtained in oxygen.

Comparison of the experimental and calculated (summated) rates for HfC-C and TaC-C are presented in Figures 22 and 23, respectively. As previously, data for interim points in oxygen were obtained by interpolation of data in 2.3 and 5.4 v/o oxygen. For HfC-C fluorine-oxygen (Figure 22a), the calculated recession rates are considerably lower than the measured rates at 3000°F and 4000°F, whereas a close correlation is obtained at 5000°F due to the use of linearly calculated oxidation data. If the "instantaneous oxidation rate" were used, a closer correlation of the calculated and experimental rates could be expected. The "instantaneous oxidation rate" is that early portion of the particular weight gain vs. the linear time curve and is approximated at 5000°F by ablation of molten oxide. Thus, at 5000°F, the rate of oxidation-corrosion of HfC-C in fluorine-oxygen is generally controlled by the rate of oxidation.

In hydrogen fluoride-oxygen (Figure 22b) the conclusions are similar; the calculated rate is lower than the experimental rate at 3000°F and 4000°F, and a correlation of both rates is obtained at 5000°F. Thus, a similarity exists in the controlling mechanism in both fluorine-oxygen and hydrogen fluoride-oxygen.

Figure 23 illustrates that TaC-C exhibits a similar comparison of the calculated and measured rates. For TaC-C, catastrophic oxidation at 5000°F dominates the corrosion behavior in the combined environments. At 3000°F and 4000°F, the calculated rates are lower than the measured rates except at 3000°F in hydrogen fluoride-oxygen. Apparently, the oxidation-corrosion rate of TaC-C in the combined environments is controlled by the rate of reaction with oxygen.
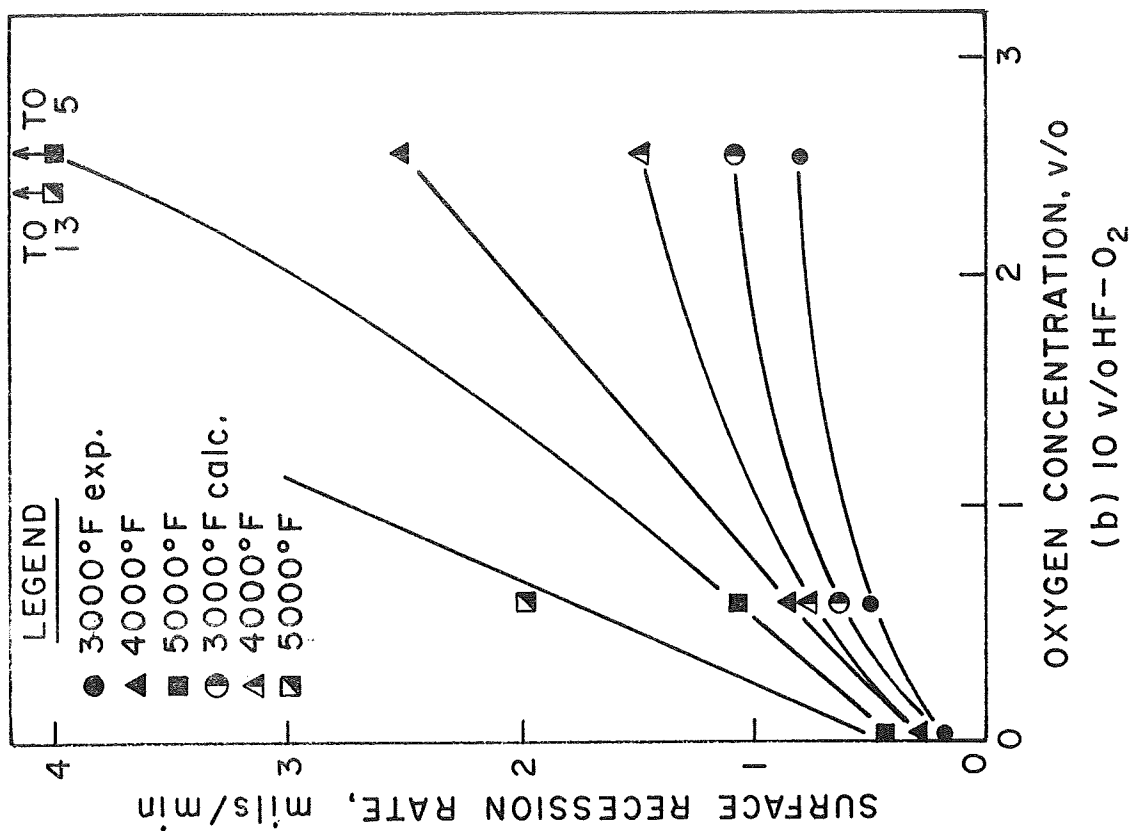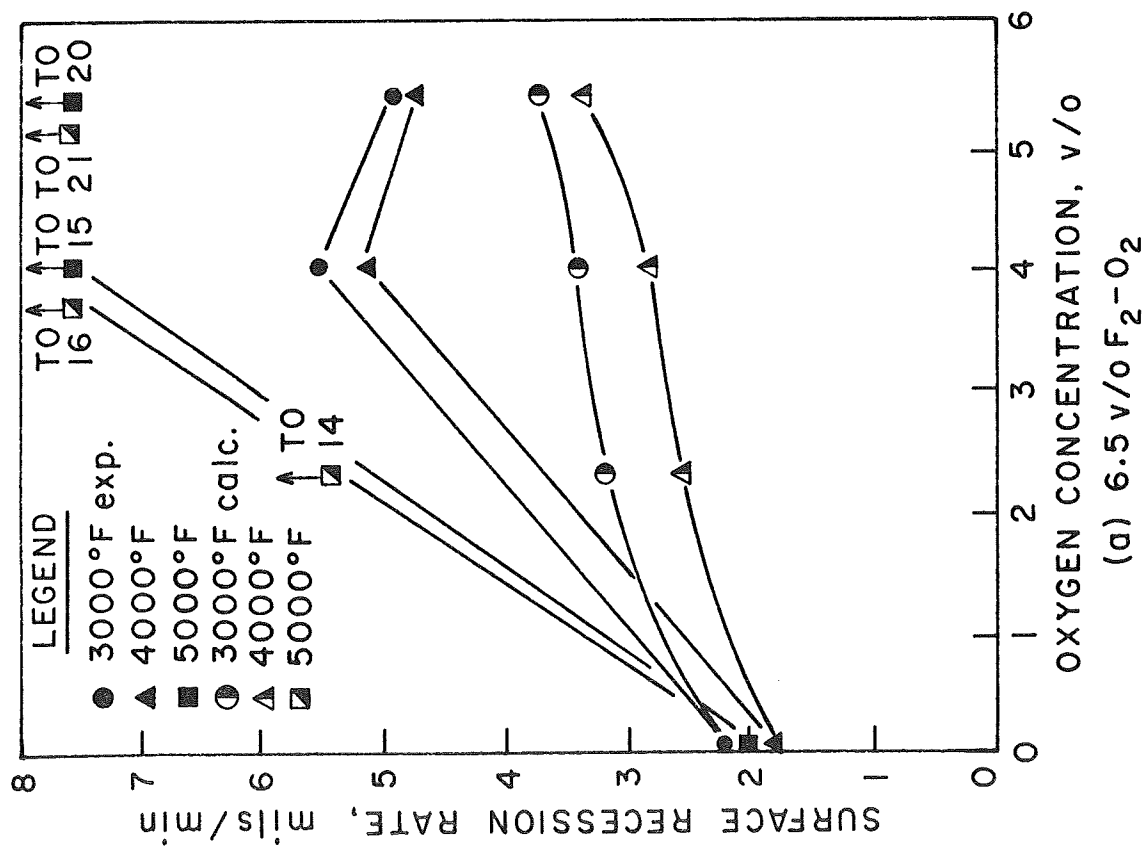
Fig. 23 – Comparison of Experimental and Calculated Surface Recession Rate of TaC-20 v/o C in Flowing Fluorine-Oxygen and Hydrogen Fluoride-Oxygen.

g.   <u>Boride Composite</u>

The candidate ZrB_2-SiC-C composite, an experimental material consisting of ZrB_2-14 v/o SiC-30 v/o C, was fabricated at ManLabs Inc. on Contract AF33(615)-3611.[9] The additions of the SiC and carbon are intended to improve oxidation and thermal shock resistance of the material. Machined test samples of the boride composite were supplied by ManLabs from lots VIII 07-2317L and VIII 07-00621K. The density used for surface recession calculations was 4.37 g/cc, which is within the normal range of hot pressed density for this material.

Since the boride material was experimental, no emittance data were available. An emittance of 0.85 was assumed because of the high volume fraction of carbon and silicon carbide, but was found to be too high during testing. As a result, the test temperatures described in the following data tables and figures are about 200°-400°F below the actual temperature but do not modify the resulting oxidation-corrosion information to any great extent. Oxidation-corrosion data of ZrB_2-SiC-C were limited to 4000°F because of melting of the composite at 4500°F. All 4000°F tests also resulted in slight edge melting. Assuming the corrected temperature of 4000°F to be the actual melting point of 4350°F, the resulting emittance is about 0.5.

The oxidation-corrosion behavior of ZrB_2-SiC-C in oxygen, fluorine, and fluorine-oxygen is summarized in Table XXI and plotted in Figure 24. A constant recession rate is exhibited in 6.5 v/o fluorine at 2.0 mils/min and a low rate exhibited in 4.0 and 5.4 v/o oxygen of about 1.0 mils/min over the range of 3000°-4000°F. Like the carbon composites, this material acts as a partial ablator because of the graphite phase. However, in oxygen the silicon carbide phase reacts to form CO or CO_2 and a silicon oxide. Above 3000°F, silicon oxides also vaporize, probably as SiO, adding to the weight loss. Thus, the ZrB_2-SiC-C composite in oxygen has a complex ablative mechanism producing C_xO_y and Si_xO_y (and perhaps B_xO_y) gaseous phases, and a solid oxide ZrO_2.

TABLE XXI

CORROSION BEHAVIOR OF ZrB_2-SiC-C IN FLOWING
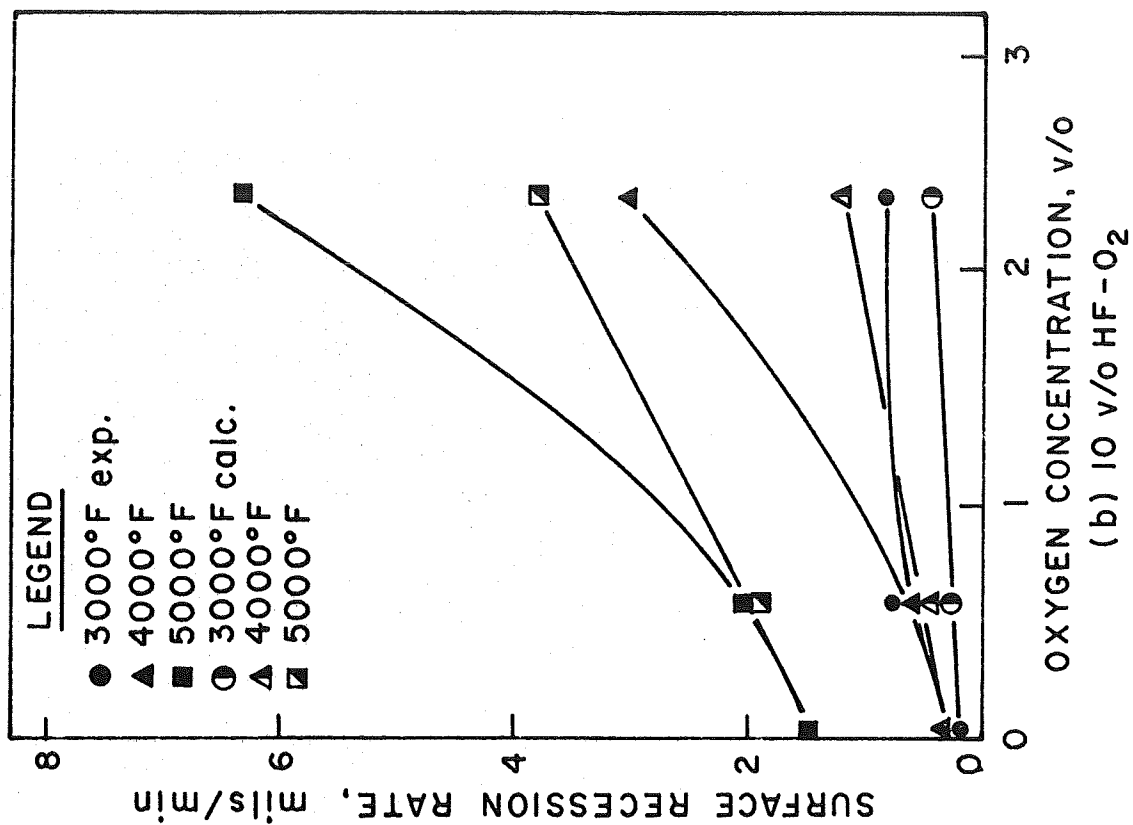
HYDROGEN FLUORIDE AND HYDROGEN FLUORIDE-OXYGEN[a]

Exposure Temp., °F	Hydrogen Fluoride Concentration, v/o	Oxygen Concentration, v/o	Weight Loss, g	Specific Weight Loss, mg/cm²/min	Surface Recession Rate, mils/min
3000	10	--	0.243	17.7	1.59
3000	10	--	0.210	15.3	1.38
3500	10	--	0.178	13.1	1.08
4000	10	--	0.162	11.8	1.06
3000	10	0.56	0.142	14.6	1.32
3000	10	0.56	0.249	16.2	1.46
3500	10	0.56	0.347	24.7	2.22
3500	10	0.56	0.243	28.6	2.58
4000	10	0.56	0.181	21.4	1.93
4000	10	0.56	0.163	17.7	1.59
4000	10	0.56	0.249	22.8	2.04
3000	10	2.3	0.222	26.4	2.38
3500	10	2.3	0.326	39.1	3.44
4000	10	2.3	0.374	45.0	4.05

[a]Total flow rate - 10 cfh (400 fps).

74
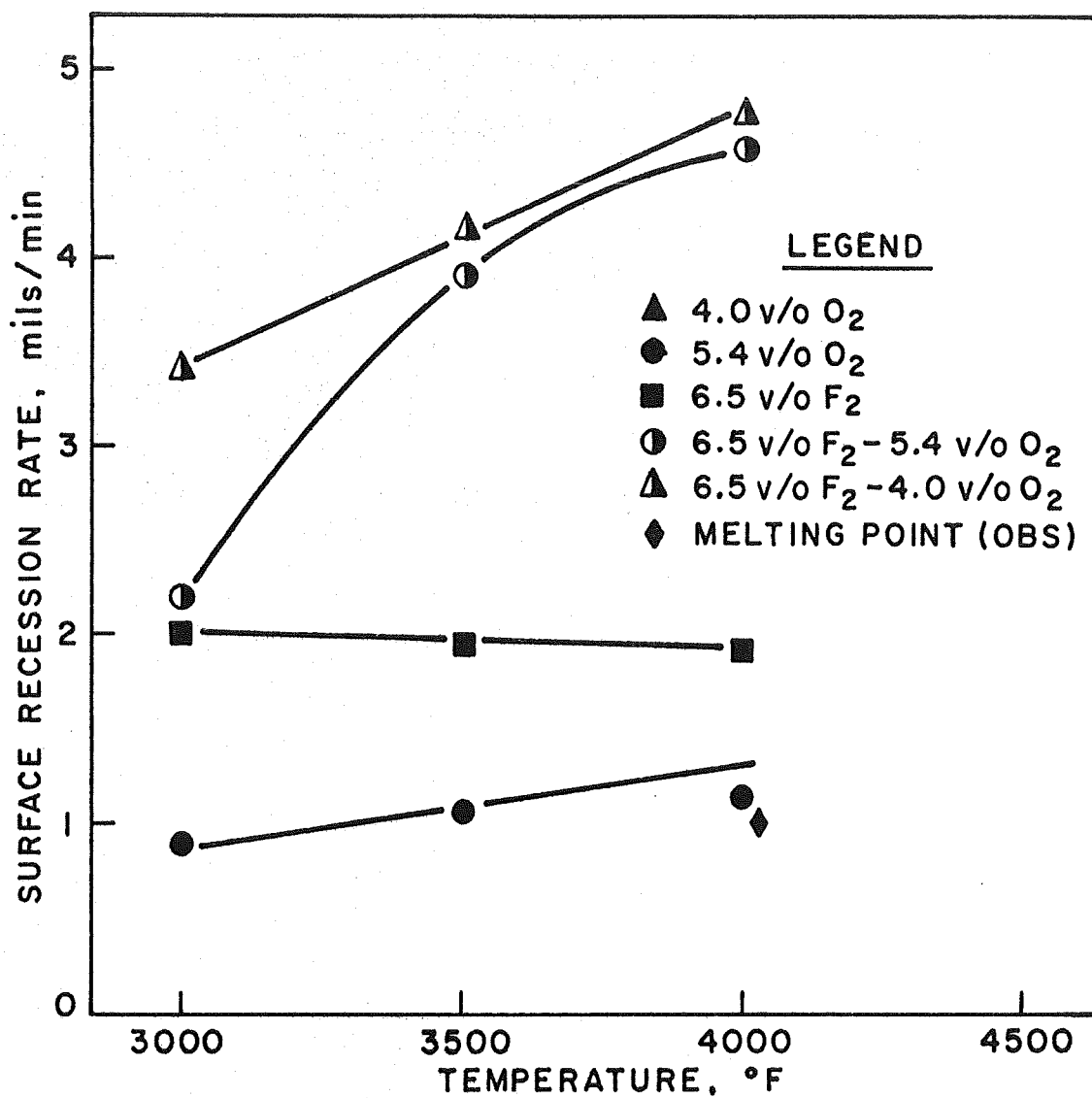
Fig. 24 - Surface Recession Rate of ZrB_2-SiC-C in Flowing
Oxygen, Fluorine, and Fluorine-Oxygen.

This normally results in a weight loss at all oxygen concentrations. Assuming evaporation of all but the ZrO_2 reaction product, the calculated weight loss resulting from stoichiometric oxidation is about 3 $mg/cm^2/mil$. Again, this must only apply for short exposure times because of the solid ZrO_2 which is formed.

Surface recession rates in oxygen obtained by both methods described previously for carbide composites are presented in Table XXII. These include calculation of recession from the measured weight loss assuming graphite evaporation of all products except ZrO_2. Surface recession was also calculated from weight loss after mechanical removal of the oxide. Complete removal of the oxide was not possible from samples exposed at 4000°F because of slight edge melting; these data are therefore slightly low. However, the rates shown at 4000°F are slightly low since the oxide formed at 4000°F was denser and, therefore, should have been more protective. Surface recession data in oxygen plotted in Figure 24 are those obtained by the oxide removal method.

In contrast to both oxygen and fluorine, Figure 24 shows a strong temperature dependence of the recession rate in both 6.5 v/o F_2-4.0 v/o O_2 and 6.5 v/o F_2-5.4 v/o O_2, and therefore, indicates that a synergistic effect of the combined environment is operative. The recession rate in fluorine-oxygen is about 4.7 mils/min at 4000°F. Boride composite samples tested in fluorine-oxygen had a thin, gray residual oxide, whereas those evaluated in oxygen had a thicker, white oxide.

Oxidation-corrosion data for ZrB_2-SiC-C in hydrogen fluoride and hydrogen fluoride-oxygen is presented in Table XXII and plotted in Figure 25. These results show corrosion behavior in hydrogen fluoride-oxygen similar to that of the carbide composites. A maximum in the recession rate curve exists at 3500°F in 0.56 v/o oxygen. In contrast, a strong temperature dependence is shown for 2.3 v/o oxygen; the recession rate nearly doubles at 4000°F compared to 3000°F. Thus, the measured corrosion rate appears to be dependent upon the hydrogen fluoride to oxygen ratio.

TABLE XXII

CORROSION BEHAVIOR OF ZrB_2-SiC-C IN FLOWING OXYGEN, FLUORINE, AND FLUORINE-OXYGEN[a]

Exposure Temp., °F	Fluorine Concentration, v/o	Oxygen Concentration, v/o	Weight Loss, g	Specific Weight Loss, mg/cm²/min	Surface Recession Rate, mils/min
3000	--	2.3	0.012	1.5	0.5[b]
3000	--	2.3	0.068	8.2	0.7[c]
4000	--	2.3	0.024	2.8	0.9[b]
4000	--	2.3	0.079	9.5	0.9[c]
5000	--	2.3	0.067	8.7	2.8[b]
5000	--	2.3	0.067	8.7	0.8[c]
3000	--	5.4	0.096	8.4	2.8[b]
3000	--	5.4	0.136	9.7	0.9[c]
3500	--	5.4	0.132	9.2	3.1[b]
3500	--	5.4	0.172	11.8	1.1[c]
4000	--	5.4	0.111	8.5	2.8[b]
4000	--	5.4	0.180	13.1	1.2[c]
3000	6.5	--	0.316	22.4	2.0
3500	6.5	--	0.308	21.9	2.0
4000	6.5	--	0.304	21.5	1.9
3000	6.5	4.0	0.531	38.6	3.5
3500	6.5	4.0	0.647	47.1	4.2
4000	6.5	4.0	0.732	53.3	4.8
3000	6.5	5.4	0.547	39.8	3.6
3500	6.5	5.4	0.372	43.8	3.9
4000	6.5	5.4	0.431	51.0	4.6

[a] Total flow rate - 10 cfh (400 fps).

[b] Calculated from oxidation stoichiometry.

[c] Calculated from weight loss after oxide removal.
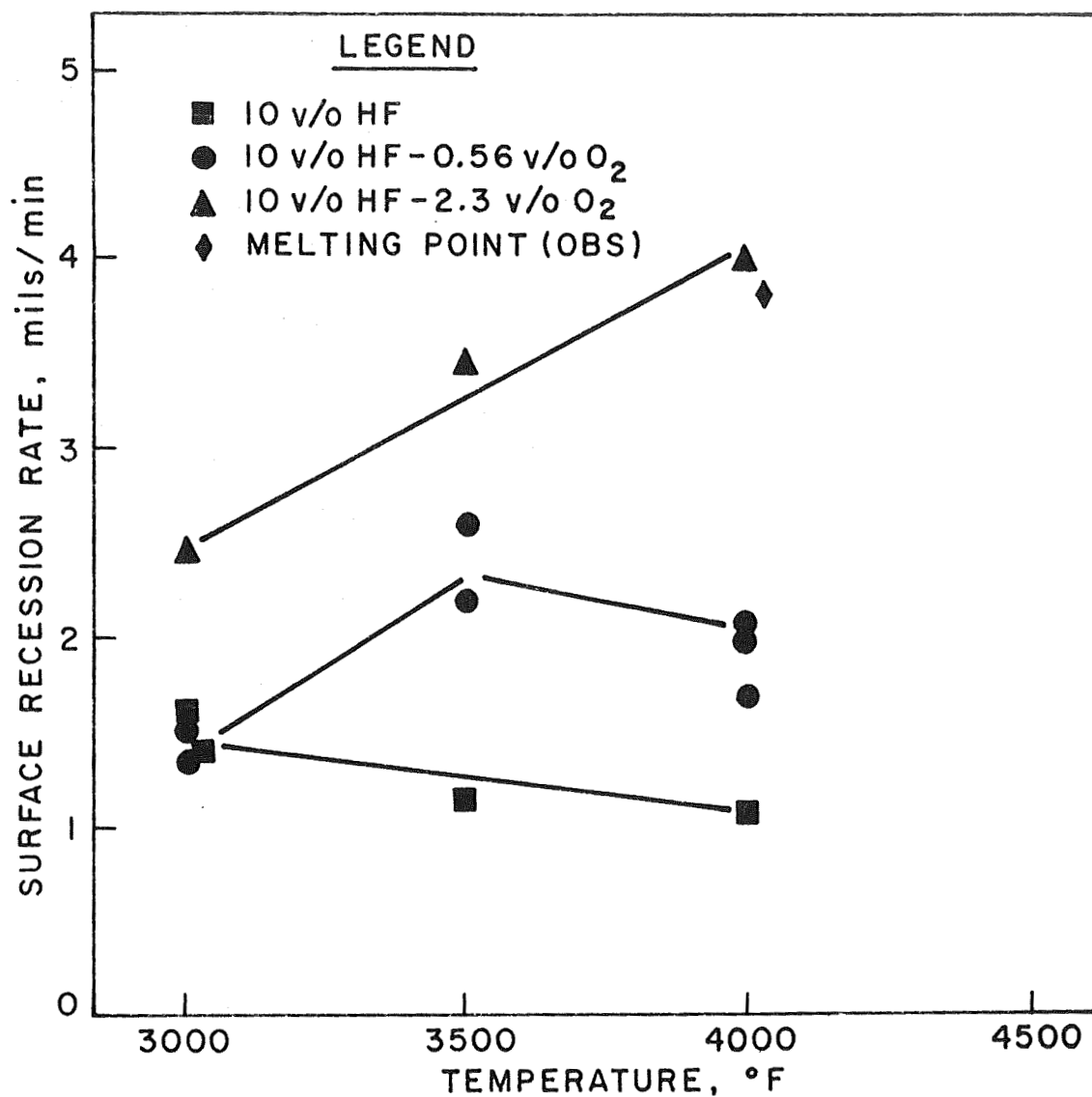
Fig. 25 - Surface Recession Rate of ZrB_2-SiC-C Composite in Flowing Hydrogen Fluoride and Hydrogen Fluoride-Oxygen.

Test samples evaluated in hydrogen fluoride-oxygen had a thin, continuous gray oxide after exposure, as did samples exposed in fluorine-oxygen. Apparently, a different mechanism was operative in the ZrB_2-SiC-C composite from that of the carbide composites in the combined atmospheres, although in both systems, a solid oxide was a possible reaction product.

A comparison of the experimental and calculated rates for ZrB_2-SiC-C in the combined environments is presented in Figure 26. Again, data at 0.56 and 2.3 v/o oxygen was obtained by linear interpolation of recession rates in 4.0 and 5.4 v/o oxygen. In both fluorine-oxygen and hydrogen fluoride-oxygen, the measured rates are considerably greater than the calculated rates, the effect being most significant in the latter. The plot in Figure 26 also indicates a tendency toward a maximum at 4.0 v/o oxygen in fluorine-oxygen. These effects can be explained in terms of retarded recession rate in oxygen due to the formation of a partially protective oxide film. In atmospheres containing either fluorine or hydrogen fluoride, the oxide film is not as stable, resulting in higher surface recession. Oxidation-corrosion of ZrB_2-SiC-C is therefore probably also controlled by the rate of interaction with oxygen.

The interactions by which a multicomponent material such as ZrB_2-SiC-C is attacked in the combined atmospheres is very complex. In fluorine-oxygen, the general reaction can be written:

$$ZrB_2 + SiC + C + F_2 + O_2 \rightleftharpoons Zr_xF_{y(g)} + B_xF_{y(g)} + Si_xF_{y(g)}$$
$$+ C_xF_{y(g)} + C_xO_{y(g)} + Si_xO_{y(s,g)}$$
$$+ Zr_xF_yO_{z(g)} + C_xF_yO_{z(g)}$$
$$+ Si_xF_yO_{z(g)} + ZrO_{2(s)} + B_xO_{y(l,g)}$$
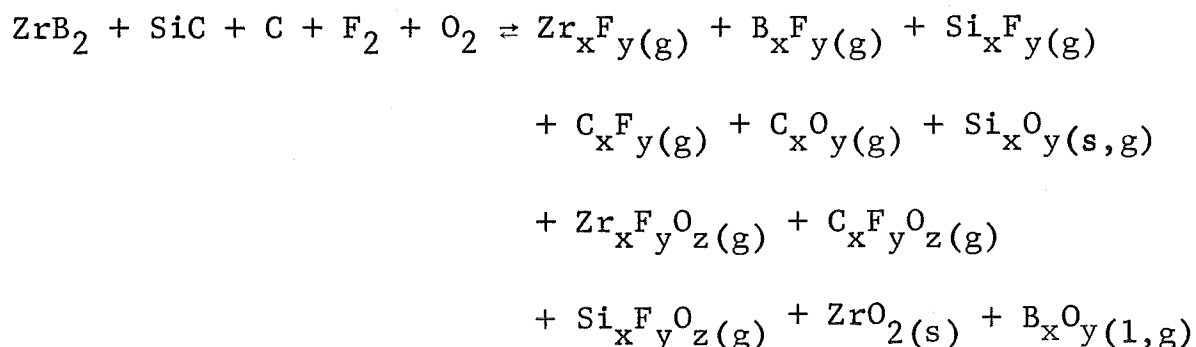
Thus, eight general gaseous fluorides, oxides, or oxyfluorides are possible in addition to three oxides, of which only ZrO_2 is a
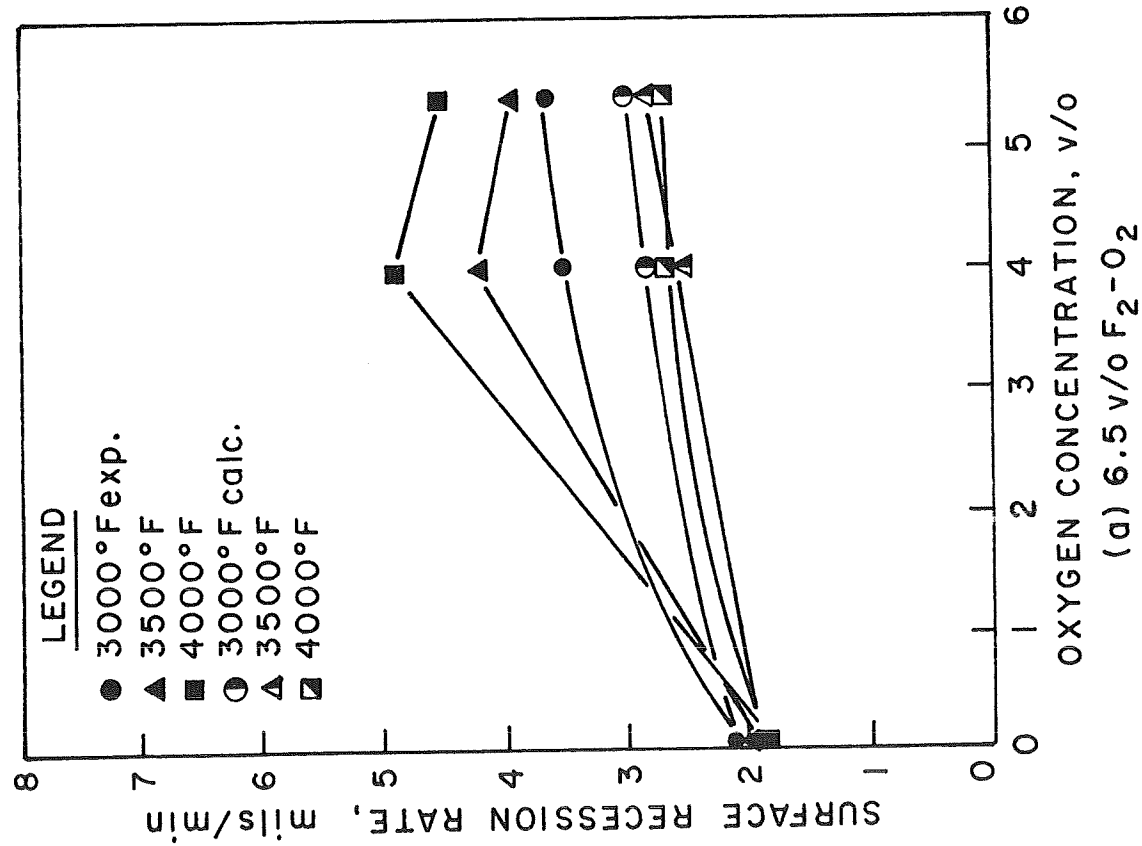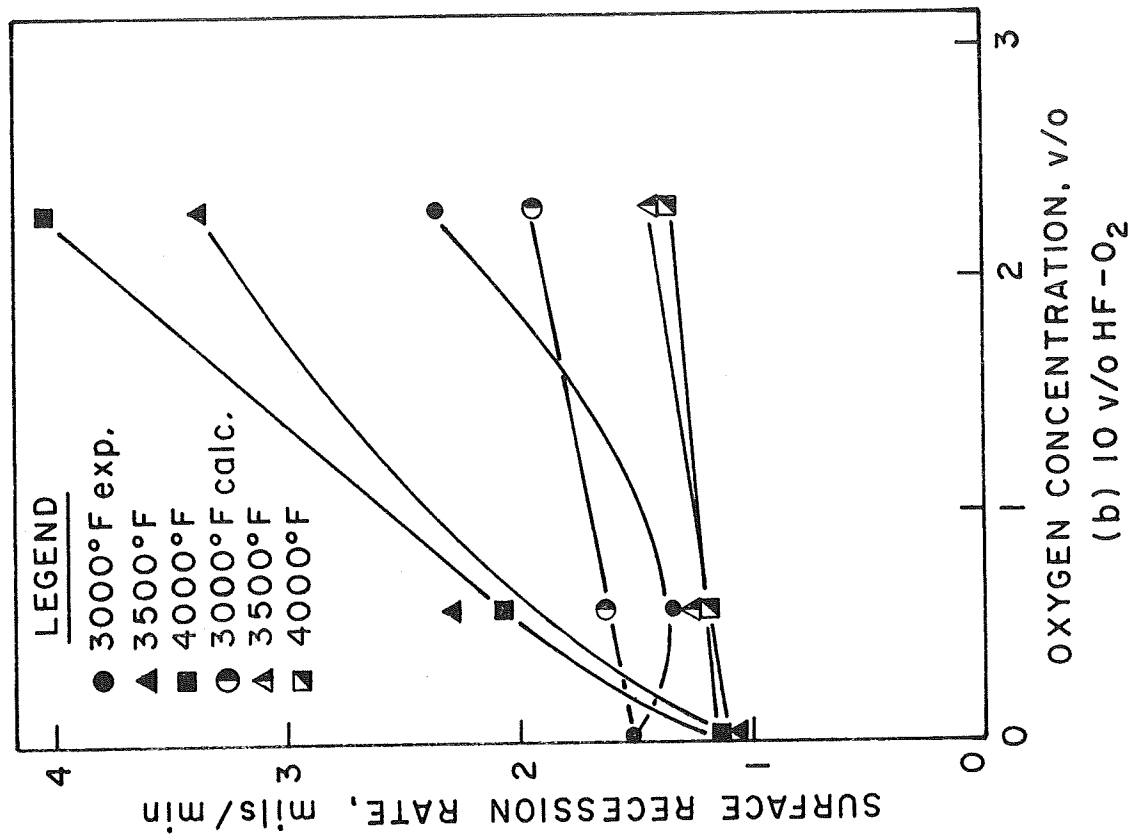
Fig. 26 - Comparison of Experimental and Calculated Recession Rates of ZrB_2-SiC-C in Flowing Fluorine-Oxygen and Hydrogen Fluoride-Oxygen.

solid phase. Above 3000°F, the Si_xO_y phase begins to evaporate as $SiO_{(g)}$ which may have influenced the recession data above 3000°F. In hydrogen fluoride-oxygen, further complications exist because of the possible formation of $C_xH_{y(g)}$ and $B_xH_{y(g)}$ as additional reaction products which suggest a reason for the greater acceleration of the recession rate in hydrogen fluoride-oxygen. The complexity of these reactions indicates the difficulty in analysis of the controlling reaction mechanism in surface recession of ZrB_2-SiC-C.

3.   <u>Summary and Discussion</u>

Summary plots of the surface recession rate of the eight materials evaluated in 6.5 v/o fluorine, 5.4 v/o oxygen, 10 v/o HF, 6.5 v/o F_2-5.4 v/o O_2, and 10 v/o HF-2.3 v/o O_2 are presented in Figures 27 through 31. A comparison of the recession of the rates at 4000°F and 5000°F in these environments is summarized in Tables XXIII and XXIV. These results demonstrate quite clearly the following conclusions:

a. Materials which form gaseous reaction products must be resistant to the individual environments in order to be resistant to the combined environments.

b. Materials which form solid oxides are not resistant to the combined environments, although they may be resistant to oxygen alone.

c. Iridium and iridium alloys are the most resistant materials to the combined environments up to their melting points.

d. The remaining materials, in decreasing order of oxidation-corrosion resistance in fluorine-oxygen at 4000°F are: Rhenium, ZrB_2-SiC-C, ATJ graphite, TaC-C, tungsten, and HfC-C. In hydrogen fluoride-oxygen, the ranking is similar, except that ZrB_2-SiC-C has the highest recession rate.

e. At 5000°F, rhenium has the lowest rate in both fluorine-oxygen and hydrogen fluoride-oxygen. The solid recession materials in decreasing order of oxidation-corrosion resistance are: tungsten, ATJ graphite, HfC-33 v/o C, and TaC-20 v/o C. Both HfC-C and TaC-C exhibit melting of oxide developed at oxygen concentrations above 2.3 v/o.
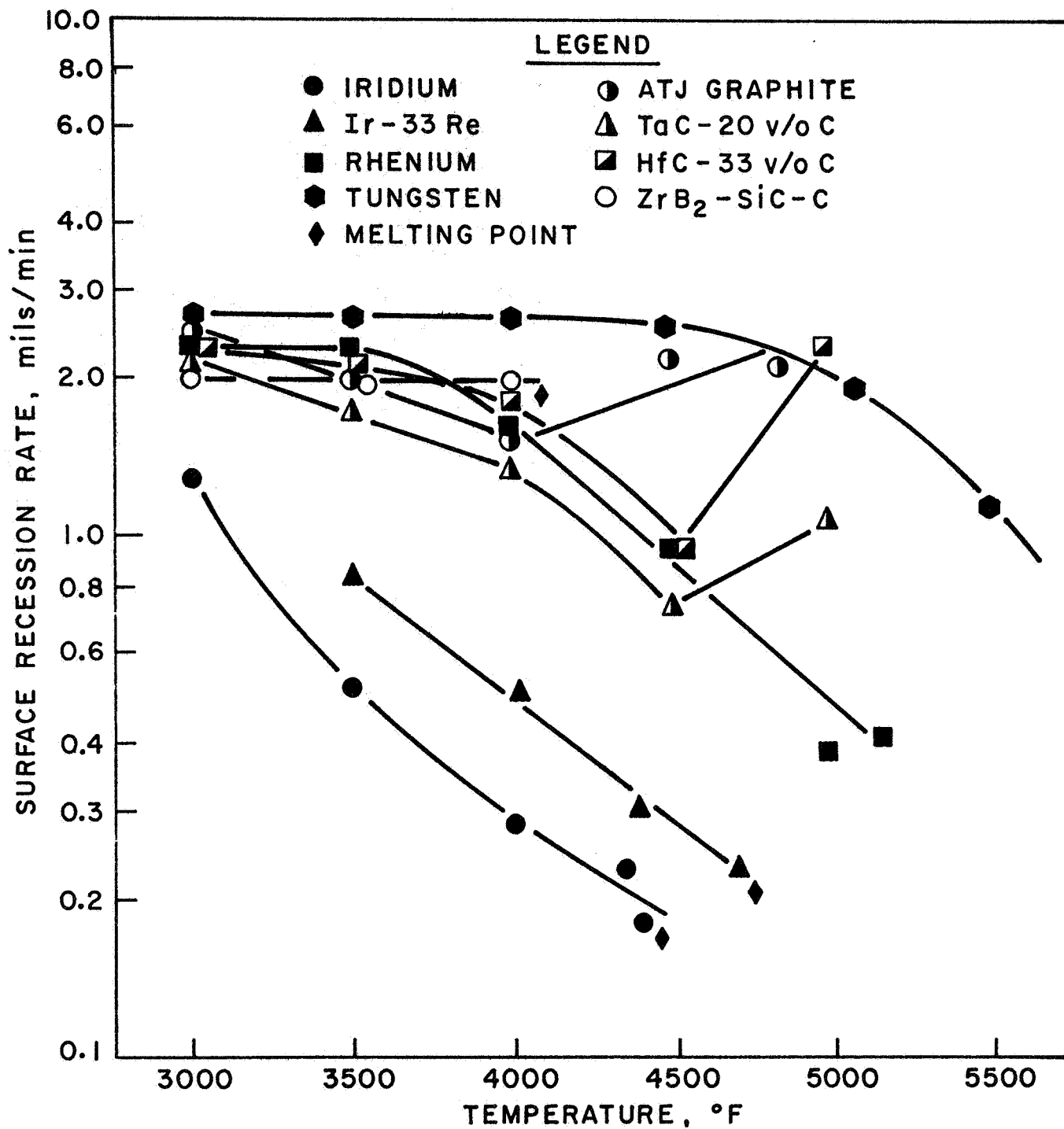
Fig. 27 - Surface Recession Rate of Refractory Materials
in Flowing 6.5 v/o Fluorine.
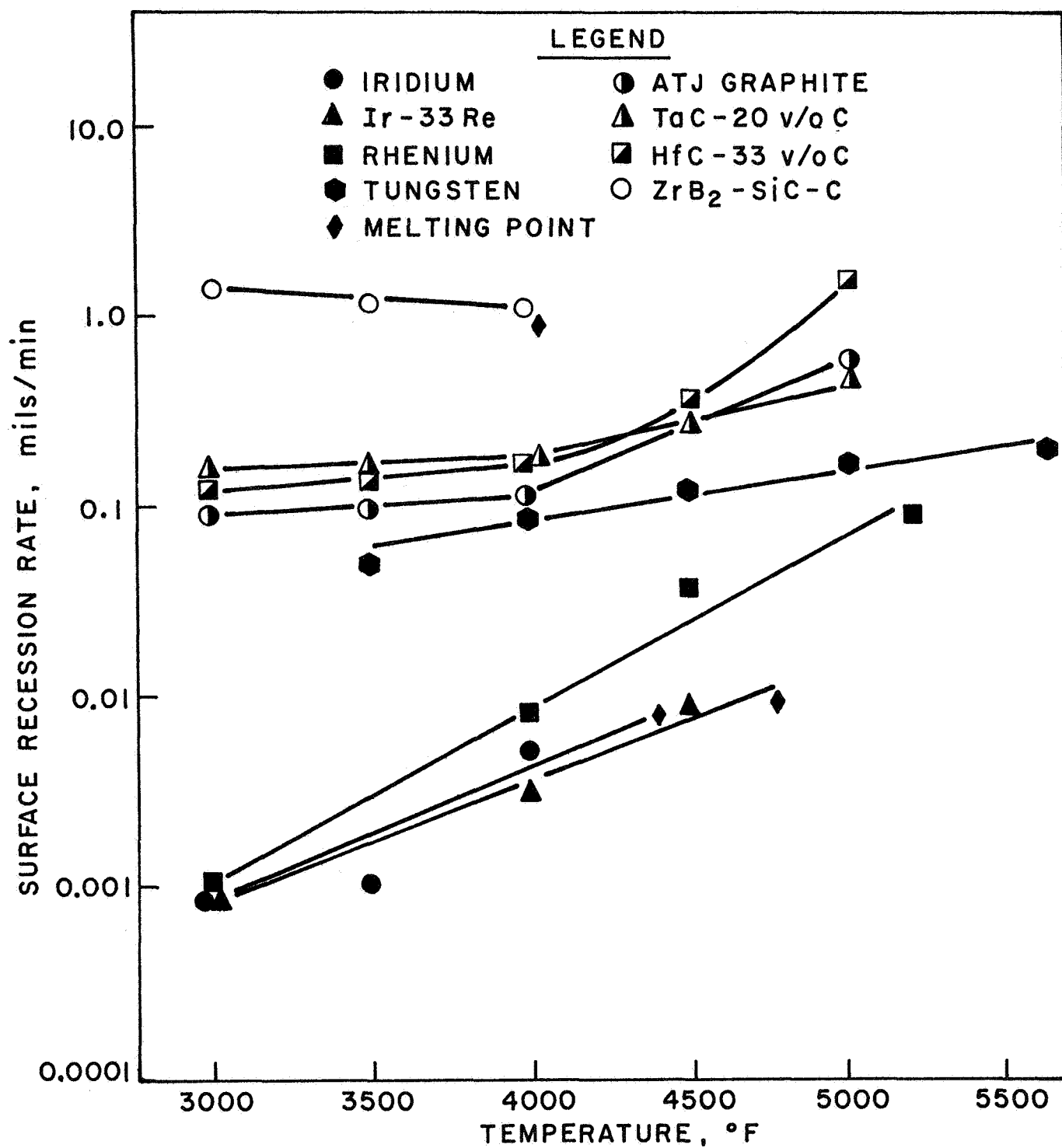
Fig. 28 - Surface Recession Rate of Refractory Materials
in Flowing 10 v/o Hydrogen Fluoride
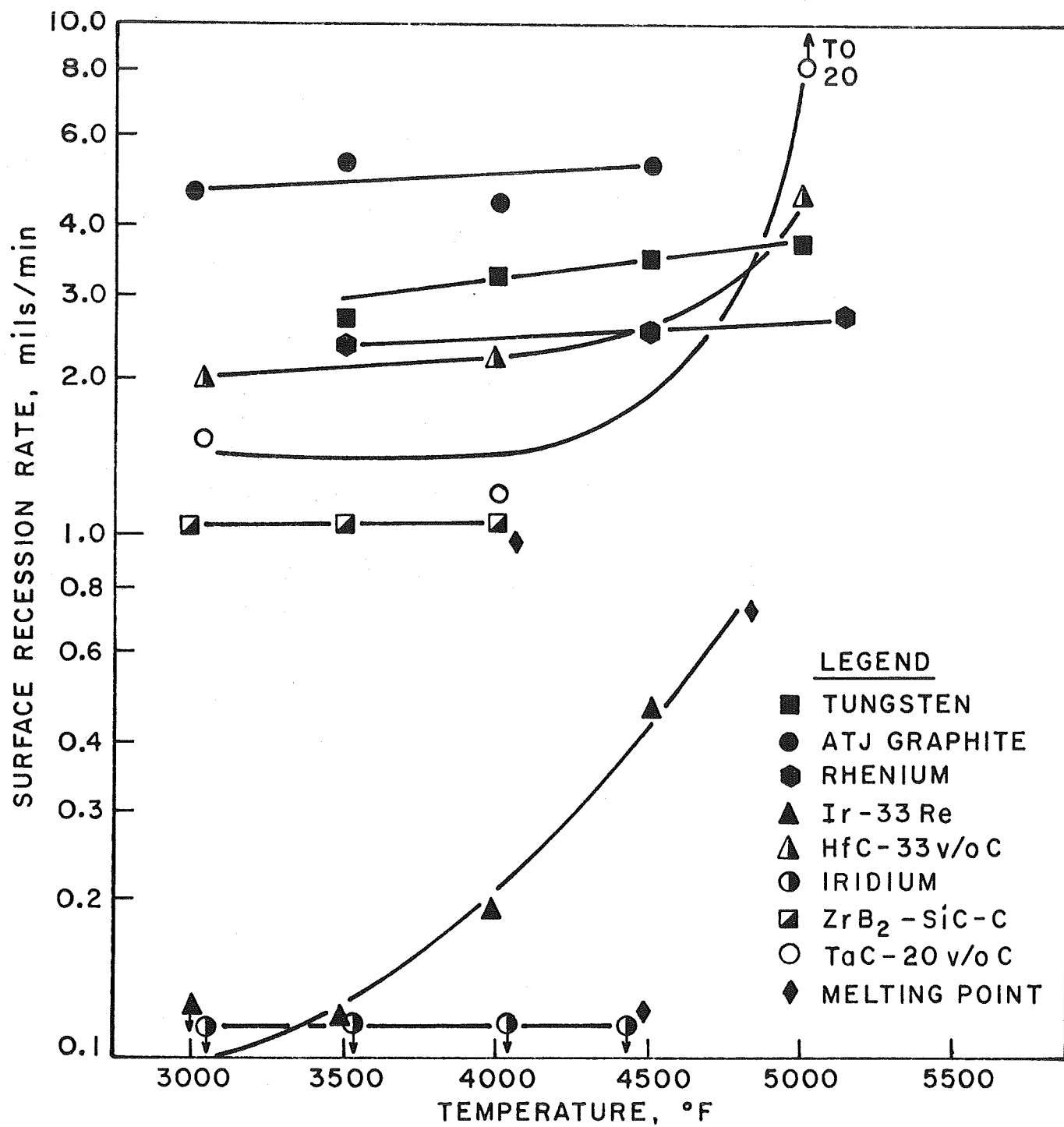
Fig. 29 - Surface Recession Rate of Refractory Materials in Flowing Argon-5.4 v/o Oxygen.
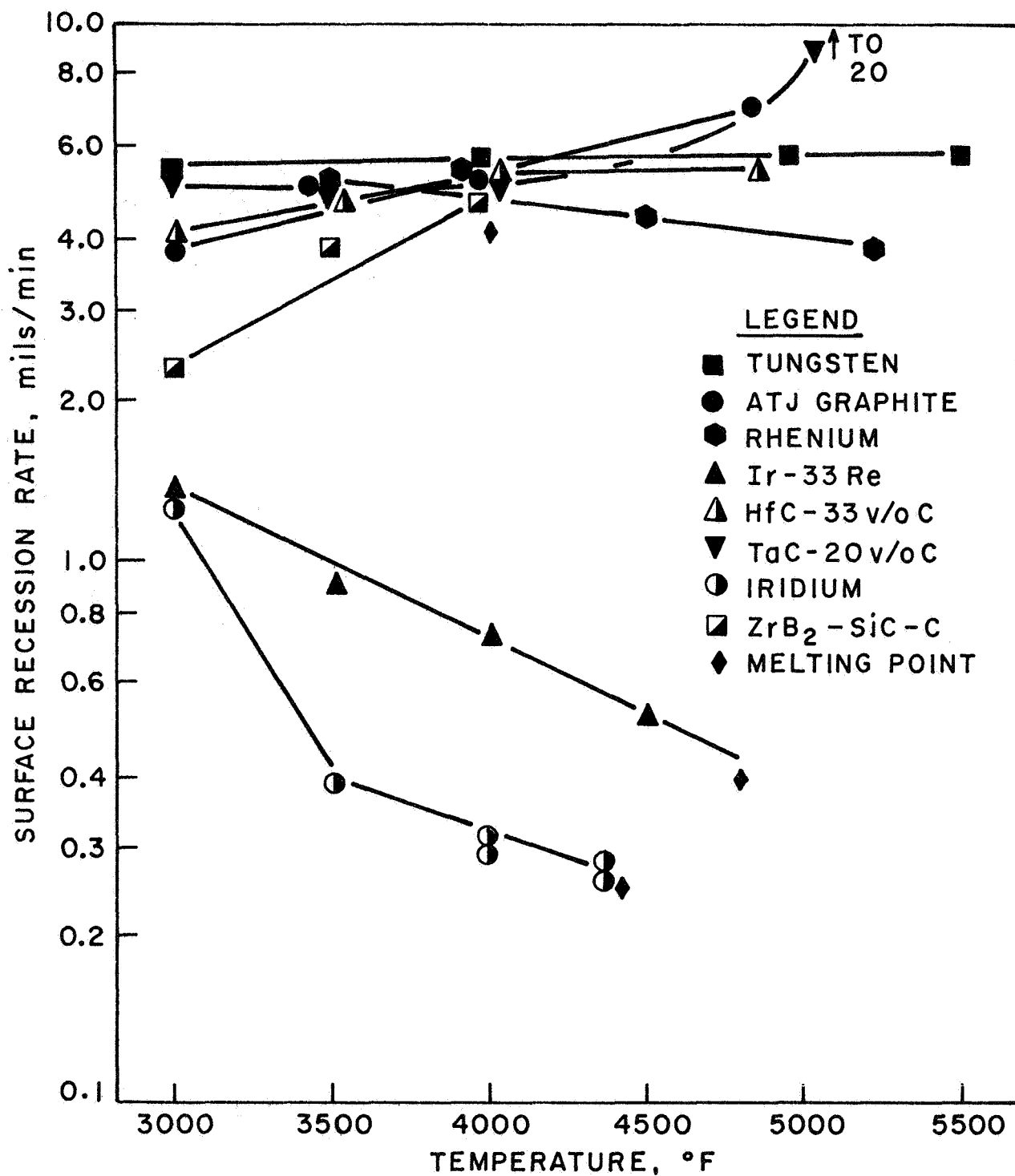
Fig. 30 - Surface Recession Rate of Refractory Materials in
Flowing Argon-6.5 v/o Fluorine-5.4 v/o Oxygen.
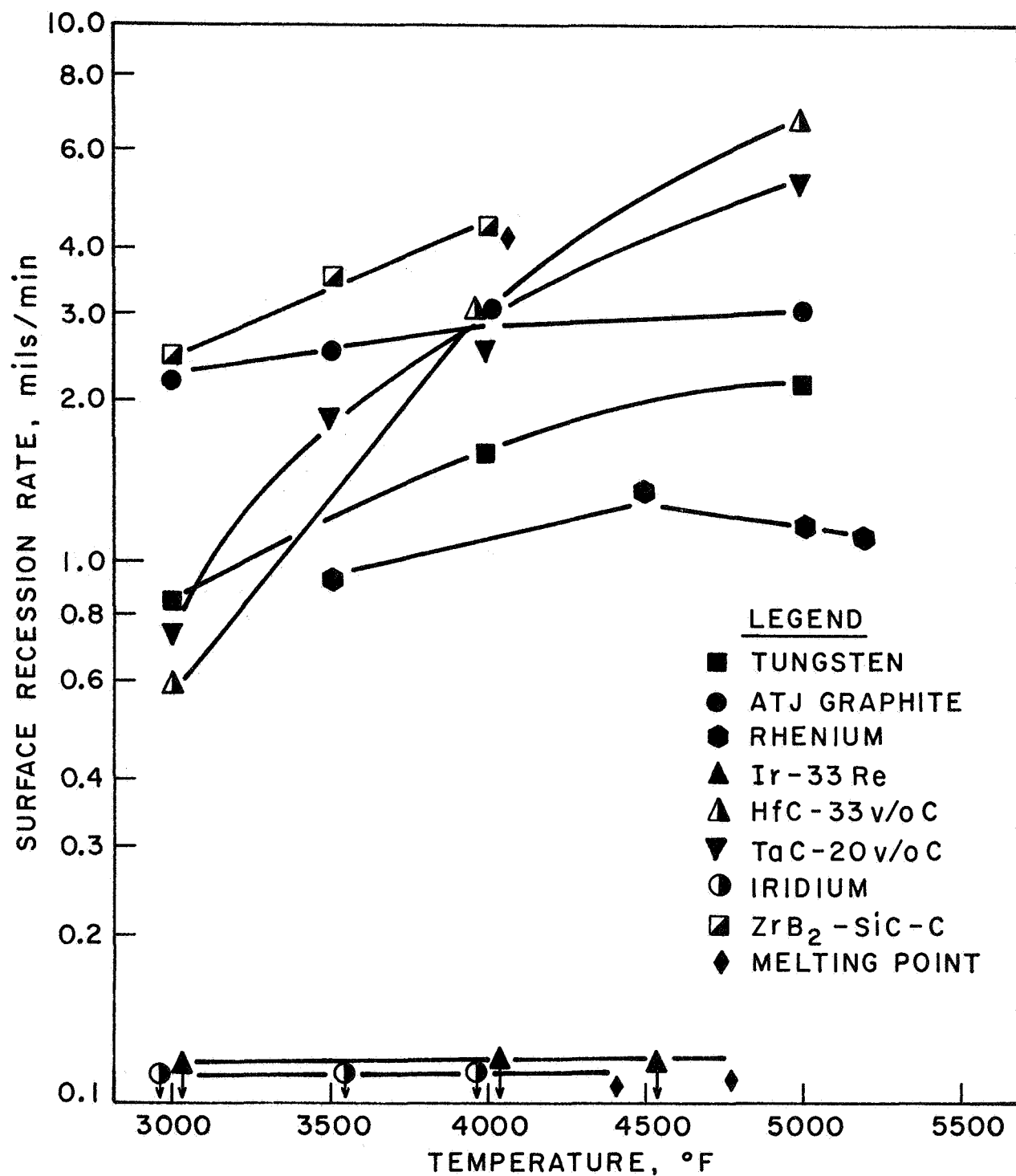
Fig. 31 - Surface Recession Rate of Refractory Materials
in Flowing Argon-10 v/o Hydrogen Fluoride-
2.3 v/o Oxygen.

TABLE XXIII

SURFACE RECESSION RATES OF REFRACTORY MATERIALS
IN FLOWING OXYGEN, FLUORINE, AND
HYDROGEN FLUORIDE ENVIRONMENTS AT 4000°F

| Material | Surface Recession Rate, mils/min | | | | |
	6.5 v/o F_2	10 v/o HF	5.4 v/o O_2	6.5 v/o F_2 - 5.4 v/o O_2	10 v/o HF - 2.3 v/o O_2
Tungsten	2.6	0.09	3.1	5.6	2.8
Iridium	0.3	0.006	0.01	0.3	0.001
Rhenium	1.5	0.009	2.5	4.4	1.1
Ir-33Re	0.8	0.004	0.06	0.8	0.08
ATJ Graphite	1.4	0.075	5.2	4.8	2.9
HfC-33 v/o C	1.8	0.12	0.006[a]	5.8	2.6
TaC-20 v/o C	1.4	0.20	2.0[b]	4.9	2.5
ZrB_2-SiC-C	1.9	1.1	0.77[a]	4.6	4.0

[a] Solid protective oxide formed.

[b] Oxide melts.

TABLE XXIV

SURFACE RECESSION RATES OF REFRACTORY MATERIALS
IN FLOWING OXYGEN, FLUORINE, AND
HYDROGEN FLUORIDE ENVIRONMENTS AT 5000°F

Material	6.5 v/o F_2	10 v/o HF	5.4 v/o O_2	6.5v/oF_2- 5.4v/oO_2	10v/oHF- 2.3v/oO_2
Tungsten	1.9	0.15	3.7	5.8	1.9
Iridium	Melts at 4450°F				
Rhenium	0.5	0.1	2.7	4.0	1.0
Ir-33Re	Melts at ∼4750°F				
ATJ Graphite[a]	2.2	0.5	5.8	6.6	2.7
HfC-33v/oC	2.2	1.5	3.5[b]	5.8[b]	6.3[b]
TaC-20v/oC	1.04	1.1	20.0[b]	20.0[b]	5.0[b]
ZrB$_2$-SiC-C	Melts at ∼4350°F				

[a] 4800-4900°F.

[b] Oxide melts.

The above conclusions apply not only to the individual materials that were evaluated in this program but also to the various classes of materials that they represent. For example, the results obtained for ATJ graphite should represent other graphite materials with only minor deviations. Furthermore, development of oxidation-corrosion protection by the development of oxide surface coatings does not appear to be a fruitful method of materials development for fluorine-oxygen or hydrogen fluoride-oxygen containing exhaust products.

The preceding information suggests that the problem of fluorine-oxygen or hydrogen fluoride-oxygen corrosion can be solved with iridium and iridium-base alloys or coatings. However, iridium has several disadvantages including very high cost, limited availability, difficulties in working, and a relatively low melting point (4450°F). As shown previously, however, alloying with 33 w/o rhenium will increase the melting point without sacrificing oxidation-corrosion resistance. This also lowers the alloy cost, since rhenium is about one-fifth the price of iridium.

Because of the above limitations, iridium has been employed only as a coating for graphite, tungsten, and tantalum to date. Iridium-base coatings have been produced by slurry deposition,[2,3] fused salt electrolysis,[11] vapor deposition,[11] and arc-plasma spraying.[12] All of this work, except slurry deposition, was concerned with graphite substrates. Iridium coatings produced by all of these techniques are envelope-type coatings; i.e., little or no interdiffusion occurs during the coating process. As a result, the coatings must have a zero defect density in order to be protective for long periods at high temperatures. The normal mode of failure of these coatings occurs as a result of substrate pitting through localized surface cracks or pinholes in the coating. Thus, the efficiency of iridium as a coating for high temperatures is generally related to the reproducibility of the coating process. An improvement in coating performance could be obtained if a secondary mode of protection of the substrate were operative in iridium-base coating systems.

89

Such a protective system could be obtained by the use of iridium as an alloying element in tungsten-base alloys. The test method used in this program did not consider the time dependence of the corrosion rate; recession rates were assumed to be linear. This is a reasonable assumption for (1) materials which have gaseous reaction products and (2) multicomponent materials in which the various components have similar recession rates in the oxidation-corrosion environment. The latter condition does not exist for tungsten and iridium since the recession rates are different by an order of magnitude. Therefore, selective removal of tungsten should occur, resulting in the development of a protective iridium-rich layer. As pointed out in the discussion of data for Ir-33Re, the recession rate cannot be linearly time-dependent in a system of this type.

Continued exposure of tungsten-rich alloys above 4400°F will result in liquation since the melting points of iridium (4450°F) and the tungsten-iridium eutectic (4200°F) are below the melting point of tungsten-rich alloys. However, melting and flow of the reaction layer will be an integral part of the surface recession mechanism. The overall recession rate could be reasonably slow in this system. In any case, the relatively high recession rates of the other materials in this program and the potential uniqueness of the tungsten-iridium system suggest that this system should be evaluated further.

B.   Coating Development

Development of coating systems during the current year was based on preceding phases in this program. Two coating systems were investigated: (1) the Ir-Re/Re duplex slurry coating for tungsten and tantalum, and (2) a (Hf-10Ta)C slurry coating for tantalum-base alloys. Investigation of the Ir-Re/Re duplex coating was based on Ir and Ir/Re slurry coatings developed previously in this program. This system was selected for study because of excellent resistance to fluorine, hydrogen fluoride, and oxygen.

90

Alloying of iridium with 33 w/o rhenium also provides a potential increase in operating temperature from about 4450° to about 4750°F.

The carbide coating system was hopefully a higher melting, lower cost alternative to iridium coatings for tantalum-base alloys, although the recession rates in fluorine and hydrogen fluoride were known to be higher than those of iridium. This system was selected for further study prior to measurement of the recession rate of carbide composites in combined fluorine-oxygen environments. As shown in the previous section, carbide composites are not resistant to combined environments although they have reasonable resistance to both fluorine and oxygen individually. Thus, the carbide coatings could have application for rocket nozzles in which either fluorine or oxygen are present singly, but not in combination.

The carbide coatings all had the basic composition (Hf-10Ta)C since it was thought that a small percentage of tantalum oxide, as in Hf-Ta alloys, would improve the adherence and protectiveness of the oxide layer. Obviously, this was shown to have no advantage in combined fluorine-oxygen atmospheres; the recession rates of the oxides of both hafnium and tantalum appear to be similar. However, the results of oxidation exposure of TaC-C composites suggest that addition of TaC in HfC-C composites should be effective in oxygen environments.

1. Iridium-Base Coatings

In previous work during this program, iridium coatings produced by slurry techniques were developed for tungsten- and tantalum-base alloys. The initial coatings were unalloyed iridium used only for tungsten because of the relatively low melting point of the Ir-Ta eutectic (~3350°F).[1] In the W-Ir system, the eutectic is at about 4200°F, which is within the range of the melting point of unalloyed iridium (4450°F). Introduction of a rhenium reaction barrier on both tungsten and tantalum-base alloys increases the maximum operating temperature to the melting point of

iridium. Accordingly, the Ir-Re duplex slurry coating was developed during the second year on this program.[2] Finally, alloying of iridium with rhenium permits operation to about 4750°F at the maximum solubility of 33 w/o Re for the iridium-rich solid solution.[4] Effort during the current year was intended to develop a duplex Ir-Re/Re coating based on the slurry techniques used for the previous iridium-base coating systems. Iridium coatings have also been developed by fused salt electrolysis,[11] vapor deposition,[11] and arc plasma spraying.[12] However, no other techniques for developing duplex Ir-Re/Re coatings have been reported.

The slurry technique used for Ir-Re coatings differs from that of most slurry coatings, such as the carbide slurry process described in the subsequent section. Previous reports on this program[1,2] have described the slurry process in detail. Briefly, the process consists of sintering a slurry consisting of iridium powder and powders of a metallic vehicle suspended in an organic vehicle. The organic vehicle employed in this program was a mixture of collodion and a nitrocellulose lacquer, which was evaporated during the initial stages of sintering. The metallic vehicle is intended to provide a liquid phase medium for nucleation and growth of the iridium coating and is also evaporated by vacuum treatment during the latter stages of the sintering cycle. Finally, a high-temperature treatment is performed which is intended to maximize the coating density and insure bonding to the substrate by solid-state diffusion. All of the iridium, rhenium, and Ir-Re slurry coatings produced in this program employed this general method. Copper was used for the metallic vehicle in iridium-base coatings and Cu-Al for rhenium coatings.

Liquid-phase sintering is obviously the most critical part of the slurry coating process consisting of several steps in both argon and vacuum. A typical sintering cycle for iridium, rhenium, and Ir-Re coatings used in this program is as follows:

1. 2300°-2450°F in argon for 2-4 hr.
2. 2050°F in vacuum for 1 hr.
3. 2300°F in vacuum for 2 hr.
4. 2400°F in vacuum for 1 hr.
5. 3000°-3300°F in vacuum for 2 hr.

Step 1 provides collapse and densification through melting of the metallic vehicle of the slurry and the initial nucleation of the iridium coating on the substrate. The lower temperatures were used for iridium and the higher temperatures for rhenium. If the temperature or time of Step 1 is too short, nonuniform coating thickness results since portions of the coating tend to segregate into areas of low liquid concentration. (An example of this effect will be shown subsequently.) Evaporation of metallic vehicle is minimal during this step.

Metallic evaporation occurs primarily during steps 2-4. The temperature of the initial vacuum treatment is lowered to reduce the evaporation rate from the high-copper liquid. If the copper is evaporated at 2300°F, blisters and bubbles are formed which cannot be removed by subsequent treatment. This causes non-uniform coating thickness and discontinuities in the sintered coatings. Removal of copper is completed in vacuum by increasing the temperature as the copper content of the slurry is decreased by evaporation. Normally, all of the copper in the slurry can be removed by evaporation from coatings in the range of 3 mils within the detection limits of gravimetric analysis.

One other effect is observed in the latter stage if copper removal is performed too rapidly. Since copper has essentially a zero contact angle on iridium, the residual copper tends to be located at the grain boundaries at low copper concentration. Removal of this copper results in delineation of the grain boundaries due to the localized shrinkage. Grain-boundary delineation occurs in unalloyed iridium coatings, but iridium-rhenium slurry coatings tend to be more prone to this effect. The effect is similar to what is observed after high-temperature oxidation of iridium. If it is severe, it can lead to grain boundary weakness

93

causing "craze cracking" of the coating. For this reason, the latter stages of copper removal are as important as the initial stages. To minimize this effect, an interim vacuum treatment at 2700°F for 1 hr was sometimes used before the final solid-state sintering. "Craze cracking" is easier to control on small test coupons than on rocket nozzles where the rate of copper removal is less controllable because of temperature gradients in the nozzles.

Finally, the high-temperature vacuum treatment is intended to provide maximum density and bonding to the substrate by solid-state diffusion. It was found that 3000°F is adequate for unalloyed iridium, but that 3300°F is required for Ir-Re coatings due to the relatively high oxygen content of rhenium powders (~1 w/o) and the relatively slow diffusion rates in the iridium-rhenium system.[13]

All slurry coatings in this program were applied by brushing in order to conserve iridium and rhenium powder. The applied slurry compositions for iridium coatings were Ir-25 to 30 w/o Cu and Re-15 w/o (75Cu-25Al) for rhenium coatings. It was found during the current work that 30 w/o copper was optimum for Ir-20 w/o Re coatings using the sintering cycle described previously. However, this composition may not be optimum under different sintering conditions since it was not possible to conduct a wide variation of composition-temperature sintering studies within the scope of this program.

A series of sintering studies was conducted on Ir-20Re and Ir-30Re coatings using 25-40 w/o Cu and Cu-Al as the metallic vehicle. All sintering studies were intended to develop a 3 mil coating thickness. The typical sintering behavior illustrative of these slurries is presented in Table XXV. These results represent only a portion of the sintering tests, since several different sintering treatments were conducted within the temperature ranges summarized previously. The results in Table XXV indicate that the weight losses slightly exceed the nominal concentration of metallic vehicle. This is due to evaporation of the organic vehicle during sintering.

TABLE XXV

SINTERING BEHAVIOR OF IRIDIUM-RHENIUM SLURRIES

Slurry Composition, wt%	Applied Slurry Weight, g	Sintering Weight Loss,		Coating Weight, mg/cm	Coating Thickness,* mils
		g	% +		
Ir-20Re-25Cu	0.995	0.352	26.2	154	2.9
Ir-30Re-25Cu	1.112	0.361	25.1	171	3.2
Ir-20Re-30Cu	1.008	0.487	32.0	155	2.9
Ir-30Re-30Cu	1.562	0.485	31.1	165	3.1
Ir-20Re-35Cu	1.561	0.555	35.6	173	3.2
Ir-30Re-35Cu	1.518	0.541	35.8	162	3.0
Ir-20Re-40Cu	1.528	0.636	41.8	149	2.8
Ir-30Re-40Cu	1.5901	0.659	41.4	155	2.9
Ir-20Re-30Cu-2Al	1.472	0.466	31.7	168	3.1
Ir-30Re-30Cu-2Al	1.692	0.606	35.7	181	3.4

+Calculated from weight loss after sintering.
*Calculated from coating weight after sintering.

The surface appearance of sintered Ir-Re-Cu slurry coatings are shown in Figures 32 through 34. These photographs illustrate the various surface conditions described previously. At 25 w/o copper, surface pitting due to copper bubbles is readily apparent. In 35 w/o copper "craze cracks" are prevalent and inadequate densification is apparent. Furthermore, the higher rhenium slurries were considerably more difficult to sinter than those containing 20 w/o rhenium at all copper concentrations. The best surface condition was obtained on the Ir-20Re-30Cu sintered coating, although some surface pitting was evident. This was correlated by metallographic examination, as shown in the as-sintered coating in Figure 35. The results of sintering studies of Ir-Re coatings correlated with previous information of unalloyed iridium up to at least 20 w/o rhenium; 30 w/o copper is normally used for unalloyed iridium coatings. Accordingly, this process was used for the coating of the tungsten rocket nozzles with the Ir-20Re/Re duplex coating. The Ir-20Re-30Cu-2Al sintered coatings were nearly comparable in surface appearance to the Ir-20Re-30Cu coating. However, it is preferable to avoid the use of aluminum in iridium slurry coatings because it is more difficult to remove by evaporation than copper.

As part of this task, an alternate approach to rhenium slurry coatings was investigated. Application of the rhenium layer by slurry techniques is the most difficult part of the duplex Ir-Re slurry coating process. High-density rhenium coatings are much more difficult to obtain than iridium by the slurry process, particularly on rocket nozzles. This is apparently due to relatively high oxygen content of commercial rhenium powders. CVD rhenium coatings produced by a proprietary process are available from the San Fernando Laboratories. The use of CVD coatings as a substitute for rhenium slurry coatings was therefore investigated in this program.

Test samples of tungsten and Ta-10W were supplied to the San Fernando Laboratories for coating with 3 mils of CVD rhenium. Discussion with San Fernando personnel revealed that, although no

X6

(a) Ir-20Re-25Cu
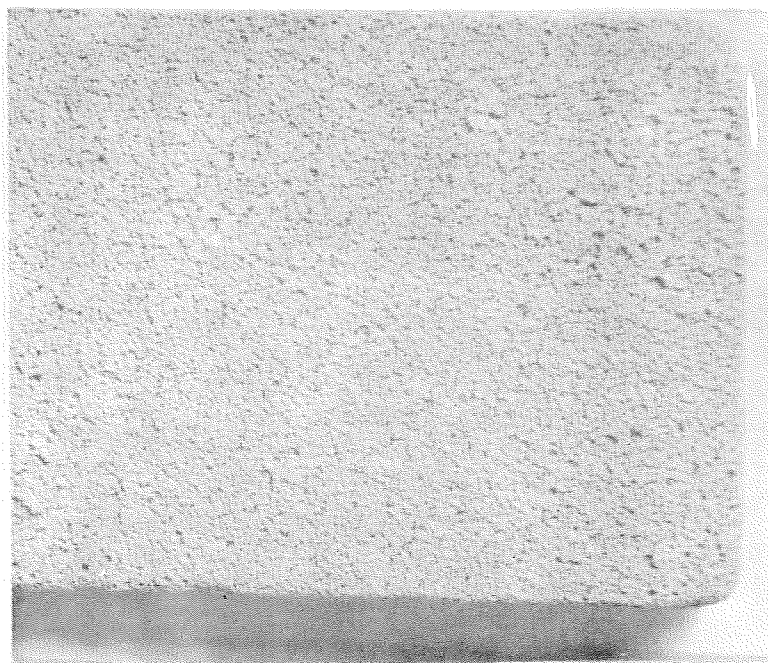
X6

(b) Ir-30Re-25Cu

Fig. 32 - Surface Appearance of Ir-20Re-25Cu and Ir-30Re-25Cu
Slurry Coatings on Tungsten After Sintering.

97

X6

(b) Ir-30Re-30Cu

X6
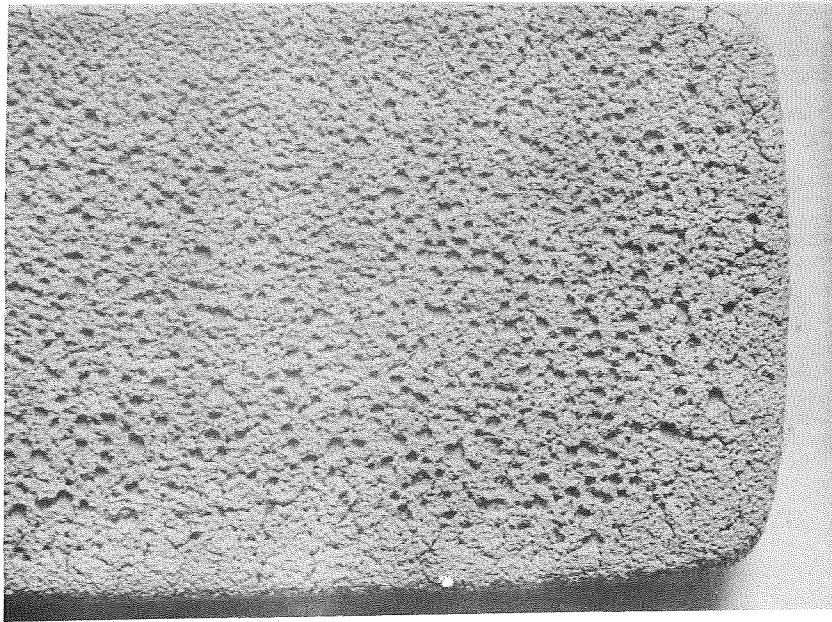
(a) Ir-20Re-30Cu

Fig. 33 - Surface Appearance of Ir-20Re-30Cu and Ir-30Re-30Cu
Slurry Coatings on Tungsten After Sintering.
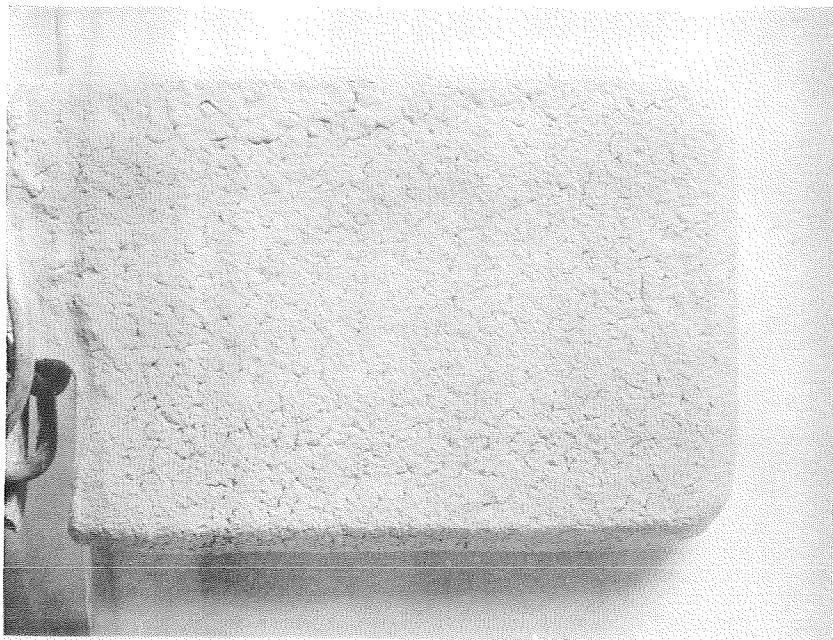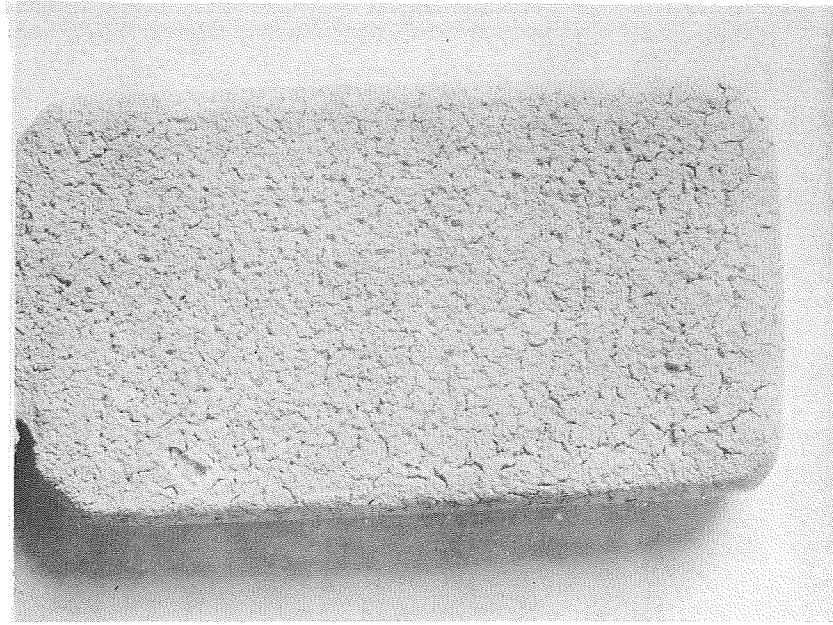
(a) Ir-20Re-35Cu   X5

(b) Ir-30Re-35Cu   X5

Fig. 34 - Surface Appearance of Ir-20Re-35Cu and Ir-30Re-35Cu
Slurry Coatings on Tungsten After Sintering.
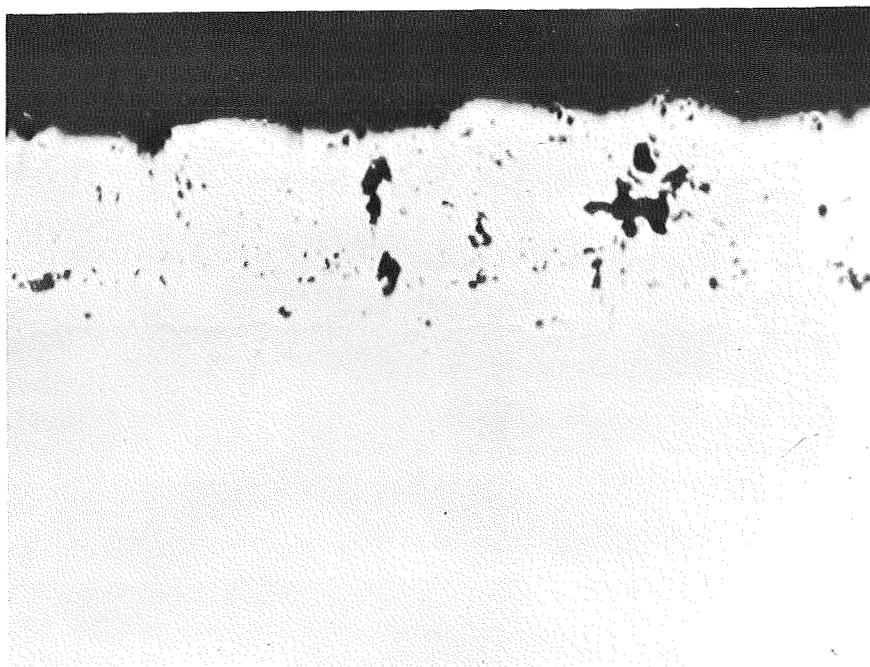
Ir-20Re

W

Neg. No. 37270   X300

Fig. 35 - Microstructure of As-Sintered Ir-20Re
            Slurry Coating on Tungsten.

100

difficulties were anticipated with tungsten, Ta-10W substrates could be subject to attack by the gaseous coating medium.[14] In this event, it was agreed that a 0.1 mil layer of molybdenum, or tungsten, could be applied prior to CVD deposition of rhenium. The molybdenum layer should not be detrimental since molybdenum has extensive solubility in both rhenium and tantalum. The final sintering treatment during application of iridium slurries should result in sufficient interdiffusion to cause alloying of a thin molybdenum layer.

The surface appearance of CVD rhenium coated tungsten and Ta-10W is shown in Figure 36. Rhenium coatings were relatively smooth with only minor edge buildup; the microstructures of these coatings on tungsten and Ta-10W are shown in Figure 37. Metallographic samples were electroplated with nickel prior to polishing. Metallographically, the applied rhenium was uniform over the surface of the test samples and without internal defects, but slightly less than the nominal 3 mils requested, particularly on tungsten. Figure 37b does indicate that a thin layer exists between the rhenium and Ta-10W substrate, suggesting that a molybdenum interlayer was used.

Iridium slurry coatings were applied to CVD rhenium coatings on tungsten and Ta-10W substrates using a Ir-30Cu slurry and the sintering cycle previously shown. The surface appearance of the iridium coating after sintering is shown in Figure 38, and the microstructure in Figure 39. Figure 38 does indicate the uniform iridium coatings that can be obtained on CVD rhenium. Uniform coatings were also produced on tungsten-coated rhenium equivalent to that shown for the Ta-10W sample. The sample in Figure 38b is shown because it illustrates a surface condition described previously during the discussion of the sintering cycle used for iridium coatings. The dark areas on the sample represent areas of segregation of iridium and are due to a complex relationship between the applied coating thickness and the time and the temperature conditions of the first phase of the sintering step. The applied slurry weight on the sample shown in Figure 38b was intentionally greater than that normally applied for the iridium sintering cycle.
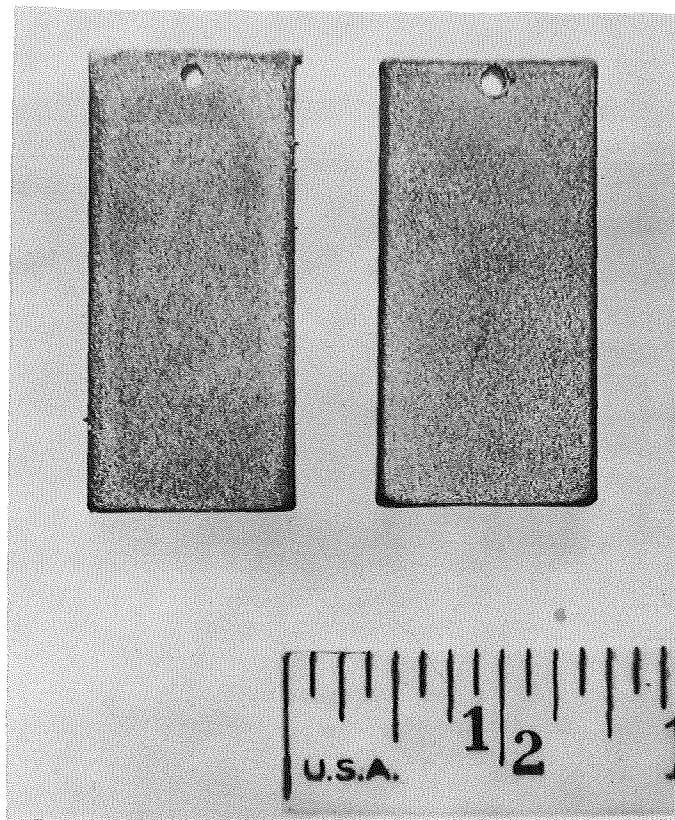
Neg. No. 36709

    (a) Ta-10W   (b) Tungsten

Fig. 36 - Surface Appearance of CVD
        Rhenium Coated Tungsten
        and Ta-10W.
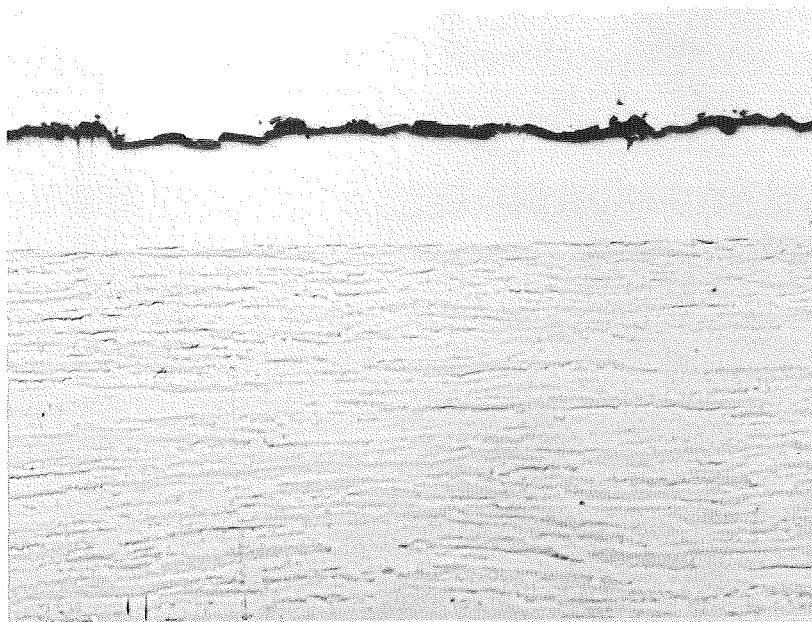
Ni

Re

W

Neg. No. 37356   X500

(a) CVD Re/W
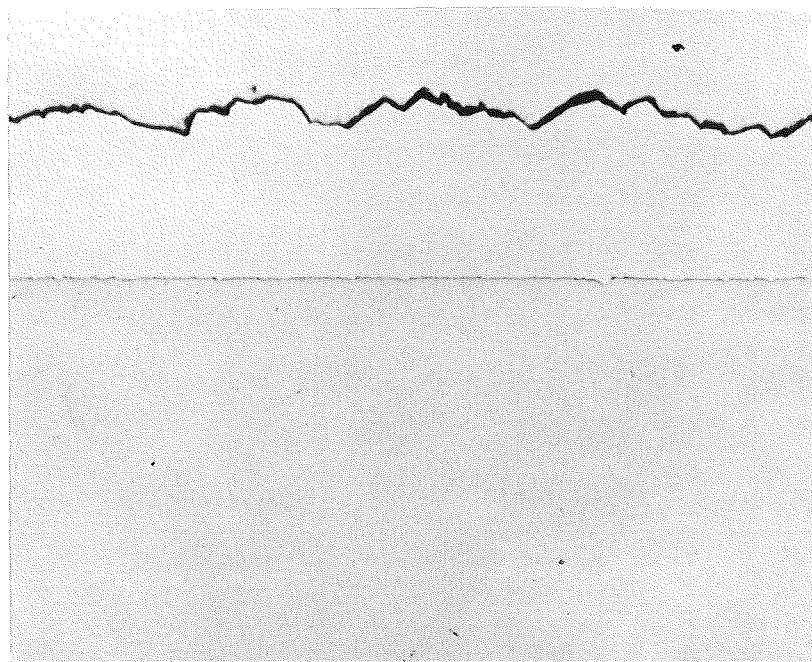
Ni

Re

Ta-10W

Neg. No. 37357   X500

(b) CVD Re/Ta-10W

Fig. 37 - Microstructures of CVD Rhenium
          on Tungsten and Ta-10W.

103
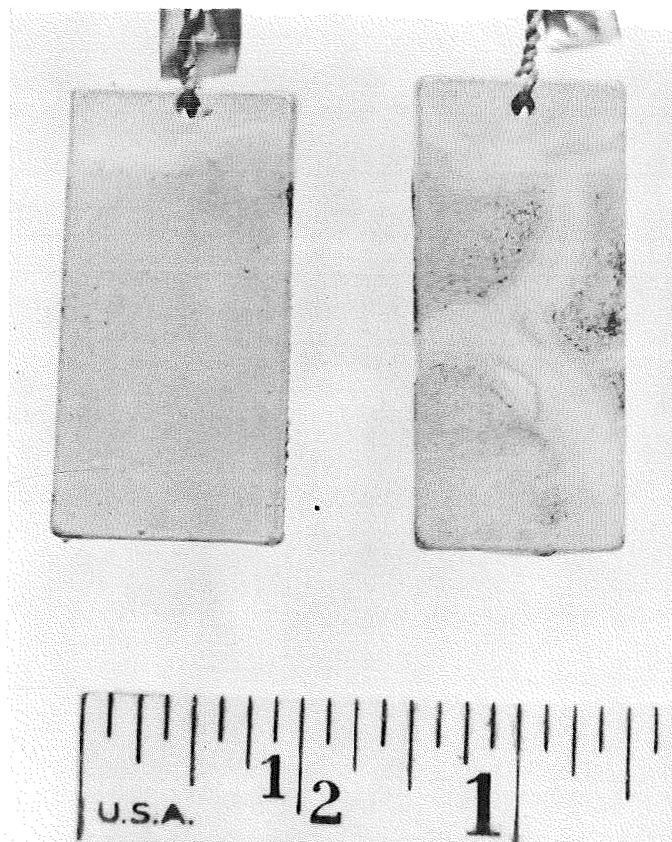
Neg. No. 36707

    (a) Ta-10W   (b) Tungsten

Fig. 38 - Surface Appearance of Ir-30Cu Slurry
Coating on CVD Rhenium Coated Tungsten
and Ta-10W After Sintering.
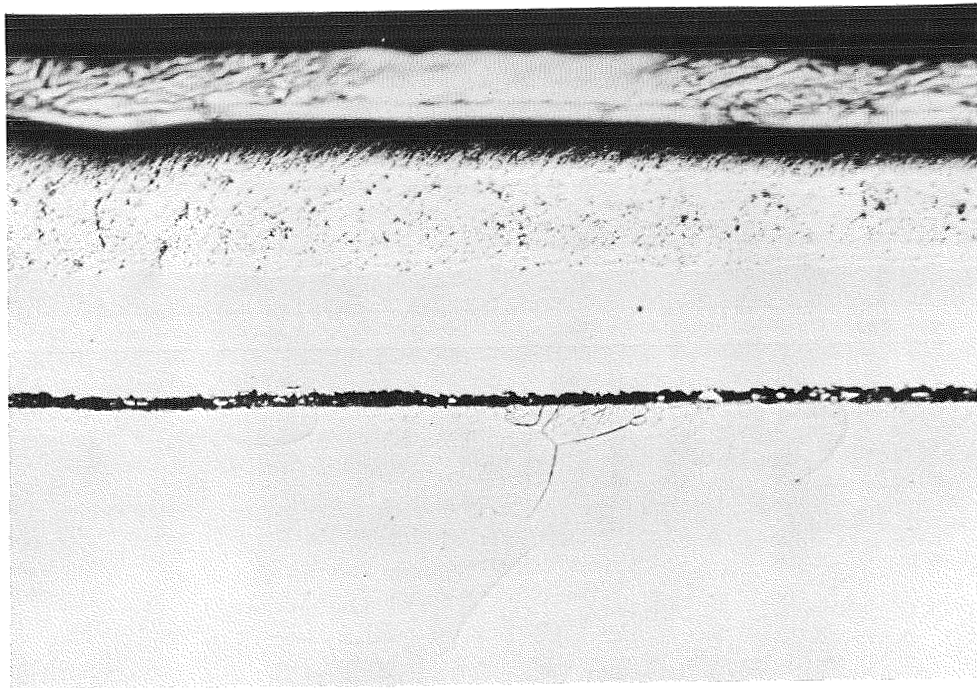
Ni

Ir

Re

W

Neg. No. 37271   X300

(a) Ir/Re/W
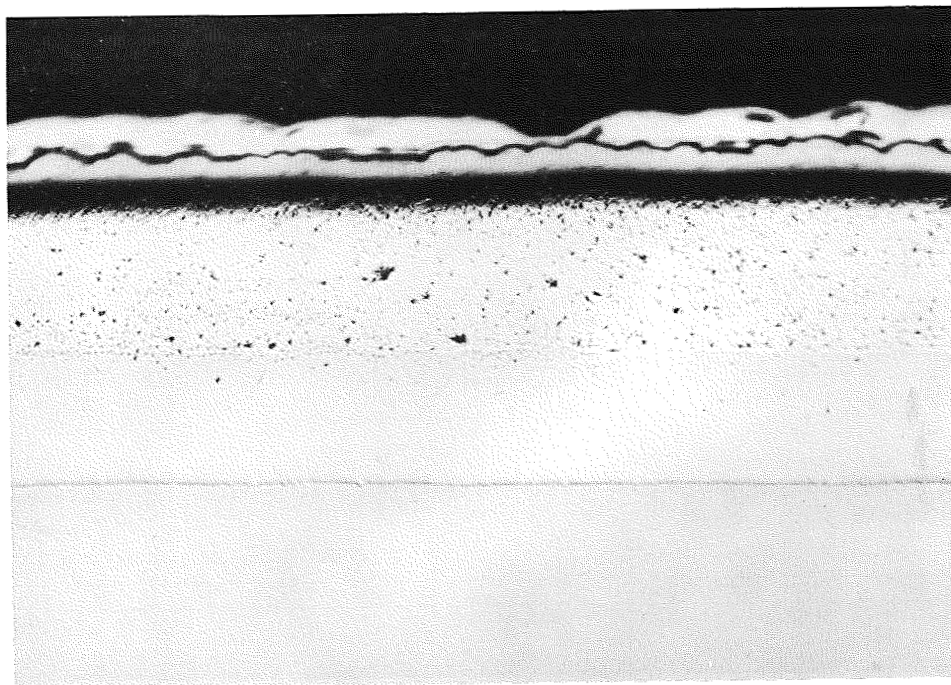
Ni

Ir

Re

Ta-10W

Neg. No. 37272   X300

(b) Ir/Re/Ta-10W

Fig. 39 - Microstructure of Iridium Slurry Coatings
Produced on CVD Rhenium Coated Tungsten
and Ta-10W.

105

The microstructures of the Ir/Re coatings shown in Figure 39 demonstrate that high-density uniform iridium layers can be developed on CVD rhenium with the slurry process. These samples were not given the final high-temperature sintering treatment at 3000°F, so that some very fine porosity is visible in the iridium layers. This is also typical of iridium slurry coatings on tungsten after a comparable sintering treatment. An indication of alloying was evident at the Ir-Re interface in both coatings. The results of sintering iridium slurry coatings on CVD rhenium demonstrated that the CVD process is an acceptable, perhaps preferable, alternative to slurry coating for the rhenium layer in Ir-Re duplex coatings.

A limited study of the workability of Ir-Re alloys was also conducted to determine the feasibility of hot working arc-melted buttons of Ir-20Re and Ir-33Re. Since unalloyed iridium can be warm worked at 1200°-1500°F, the buttons were hot rolled at 1500°F with initial reductions of 1-2%. Both alloys cracked after reduction of about 5%, although some ductile flow was evident on both samples. Cracking was probably due to fracture along the as-cast grain boundaries. Thus, improved rolling characteristics could be expected at 1500°F if the as-cast structure were broken down by upsetting or other techniques prior to warm rolling. While the initial results were encouraging, further study of hot working of iridium-rhenium alloys could not be accommodated in this program.

2. Carbide Coatings

During previous work on this program, the feasibility of developing hafnium-base carbide coatings was established.[2] It was found that Hf-10 w/o Ta coatings with up to 4 w/o carbon could be produced on tantalum by liquid-phase sintering of powders of the individual constituents in argon at 3300°-3500°F. Tantalum was added to improve the oxidation resistance through densification of the oxide developed at high temperatures in oxygen atmospheres. The metallic vehicle used was silicon, which was added in

the range of 0.2 to 0.4 w/o. As the carbon concentration of the coating increased, it was necessary to increase the silicon concentration to obtain dense coatings. Slurries containing greater than about 5 w/o carbon could not be sintered into dense coatings; above 5 w/o carbon sintering occurred, but the resulting coatings contained increasing porosity with increasing carbon concentration. At 6 w/o carbon, the coatings consisted of a porous network of carbides and unreacted carbon.

Work during the current year was intended to further investigate these carbide coatings and to produce coated nozzles for engine firing tests. The previous slurries had been produced using microfine graphite powder. Because of the low density of carbon, the as-applied slurries were very thick at high carbon concentrations. The inability to produce dense coatings at high carbon concentrations (5-6 w/o) may have been due to the excessive amount of shrinkage required during sintering to obtain high-density coatings. Accordingly, current effort was intended to study high-carbon coatings further using the following approaches:

(1) Increasing the carbon particle size in slurries containing 5-6 w/o carbon.

(2) Increasing the silicon concentrations of the slurries at 5-6 w/o carbon.

(3) Carburization of sintered coatings containing 4-4.5 w/o carbon.

Sintering of carbide slurries is much less complex than that of the iridium and rhenium slurry coatings previously described. Like many brazing processes, it consists of simply fusing the powder mixture to the substrate. Silicon is effective in producing liquidation of hafnium-tantalum-carbon mixtures at temperatures above 3300°F. This technique has been used by Lawthers for sintering of Hf-Ta metallic slurry coatings.[15] Since the constituents are added in the slurry as elemental powders, nucleation and growth of the carbide phase must occur. The final sintered structure consists of small spherical particles of carbide in a metallic matrix. Obviously, as the carbon content is increased,

the carbide volume fraction increases reaching about 70 v/o at
4.5 a/o C. The carbon concentration necessary to obtain a stoi-
chiomet   carbide coating is about 6.2 w/o.

Slurries were made by blending elemental powders of the
coating constituents and brushing the slurries on tantalum cou-
pons. During application, the powders were suspended in an organ-
ic vehicle consisting of a mixture of collodion and nitrocellulose
lacquer. All constituents, including graphite, were -325 mesh
powders. The applied slurry weights were intended to develop sin-
tered thicknesses of both 10-15 and 20-25 mils (previous work had
been limited to coatings thicknesses of 10-15 mils). After air
drying, test coupons were sintered in argon at 3300°F and 3500°F
for 2 hr. Weight changes were measured, and the sintered samples
were examined metallographically.

The results of sintering slurries containing 4-6 w/o
carbon and 0.3-1.5 w/o silicon at 3300°F and 3500°F in argon are
summarized in Table XXVI. Previous work had established that high-
density coatings could be produced at 4-4.5 w/o carbon, 0.4 w/o
silicon, and microfine graphite. Similar results were obtained
using -325 mesh graphite. All coatings exhibited some degree of
sintering at both 3300°F and 3500°F, but porosity was present at
5 w/o carbon and the coatings were friable at 6.0 w/o carbon. Gen-
erally, the higher silicon slurries tended to have higher sintered
densities, but none of the coatings approached the high densities
desired. Higher silicon concentrations were probably ineffective
because of the high evaporation rate of silicon at 3300-3500°F.
This was indicated by generally greater weight loss during sinter-
ing at higher silicon concentrations.

The majority of the weight loss during sintering was due
to evaporation of the organic vehicle. For Ir-base slurries,
weight losses due to the organic vehicle were normally in the range
of 1 w/o, while considerably higher weight losses were measured
for many of the carbide slurries. As a result, quantitative de-
termination of weight changes in terms of silicon evaporation
were difficult. Table XXVI shows that the percentage of weight

TABLE XXVI

SINTERING BEHAVIOR OF Hf-10Ta-C-Si SLURRY COATINGS IN ARGON

Applied Slurry Composition, w/o	Sintering Temperature, °F	Weight Loss, mg	Weight Loss, %	Coating Thickness, mils (a)	Results (b)
Hf-10Ta-4.0C-0.4Si	3300	20	1.0	9.5	Sintered
	3500	21	1.0	9.5	Sintered
	3500	50	2.0	21.0	Sintered
Hf-10Ta-4.5C-0.4Si	3300	21	1.0	9.0	Sintered
	3500	17	1.0	10.0	Sintered
	3500	24	1.0	23.0	Sintered
Hf-10Ta-5.0C-0.3Si	3300	12	1.0	9.0	Partial Sintering
	3300	--	--	28.5	Partial Sintering
Hf-10Ta-5.0C-0.4Si	3300	36	2.0	10.0	Partial Sintering
	3300	106	3.6	22.5	Partial Sintering
Hf-10Ta-5.0C-0.5Si	3300	60	3.5	11.5	Partial Sintering
	3300	120	3.5	21.5	Partial Sintering
Hf-10Ta-5.0C-0.6Si	3300	86	4.5	12.0	Partial Sintering
	3300	172	4.5	23.0	Partial Sintering
Hf-10Ta-5.5C-0.3Si	3300	13	1.0	9.0	Partial Sintering
	3300	54	1.5	19.5	Partial Sintering
Hf-10Ta-5.5C-0.4Si	3300	55	3.0	11.5	Partial Sintering
	3300	78	2.5	20.5	Partial Sintering
Hf-10Ta-5.5C-0.5Si	3300	48	2.5	12.0	Partial Sintering
	3300	107	3.0	22.5	Partial Sintering

109

TABLE XXVI (Continued)

Applied Slurry Composition, w/o	Sintering Temperature, °F	Weight Loss, mg	Weight Loss, %	Coating Thickness, mils (a)	Results (b)
Hf-10Ta-5.5C-0.6Si	3300	89	5.0	10.5	Partial Sintering
	3300	123	3.5	21.0	Partial Sintering
Hf-10Ta-6.0C-0.3Si	3300	173	7.5[b]	14.5	Partial Sintering
	3500	41	2.5	9.5	Partial Sintering
Hf-10Ta-6.0C-0.4Si	3300	137	6.0[b]	14.0	Partial Sintering
	3500	9	0.5	10.0	Partial Sintering
Hf-10Ta-6.0C-0.5Si	3300	193	8.5[b]	14.0	Partial Sintering
	3500	64	3.0	13.0	Partial Sintering
Hf-10Ta-6.0C-0.6Si	3300	112	5.0[b]	14.0	Partial Sintering
	3500	121	5.0	14.0	Partial Sintering
Hf-10Ta-6.0C-1.0Si	3300	94	4.0	10.0	Partial Sintering
	3500	70	3.0	9.5	Partial Sintering
Hf-10Ta-6.0C-1.25Si	3300	80	4.0	9.5	Partial Sintering
	3500	125	6.0	10.0	Partial Sintering
Hf-10Ta-6.0C-1.5Si	3300	126	6.0	9.5	Partial Sintering
	3500	--	--	40.0	Partial Sintering

(a) Visual observation and indentation tests.

(b) Slight spalling of powdery surface materials.

losses for the various compositions is generally comparable at both coating thicknesses. At 6 w/o carbon, some spalling of powder may have occurred at low silicon levels, due to partial sintering, resulting in the relatively high weight loss of these coatings. Since all of the powders used for carbide slurries are very reactive, it is possible that reactions with the organic vehicle occurred during slurry application and outgassing of the slurry during the sintering treatment. In fact, the possibility of some additional carbon introduced by decomposition of the organic vehicle during outgassing cannot be discounted. Reaction of the organic vehicle with carbon and/or silicon is a possibility since, in general, weight losses tend to increase with both silicon and carbon concentration.

Further effort on sintering high carbon slurries was discontinued after completion of the sintering studies shown. The results indicated that although some improvement was possible by further sintering studies, a more fruitful approach was carburization of sintered coatings containing 4-4.5 w/o carbon. Accordingly, test samples of Hf-10Ta-4.0C-0.4Si and Hf-10Ta-4.5C-0.4Si were prepared as described above and sintered at 3500°F for 1 and 2 hr. Carburization was accomplished by applying a thin slurry of microfine graphite and heating in argon at 3500°F for 2-4 hr. The results of carburization are summarized in Table XXVII. It was found during these studies that coatings in the range of 20-25 mils developed bubbles during sintering; no evidence of this effect had been observed with 10-15 mil thick coatings. Bubbling was apparently due to entrapment of silicon vapor during sintering, which can also cause isolated spherical porosity in sintered coatings.

Table XXVII shows the weight gains during carburization were measurable, although some additional silicon vaporization may also have occurred, particularly for samples sintered at 3500°F for 1 hr. This is shown by slight roughening of the surface, indicating that partial melting occurred during carburization. For this reason, the weight gains and calculated final carbon concentrations are probably conservative.

TABLE XXVII

BEHAVIOR OF Hf-10Ta-C-Si SLURRIES DURING DUPLEX COATING AND CARBURIZATION AT 3500°F

Slurry Composition, w/o	Sintering Weight Loss, mg	%	Coating Thickness, mils	Carburized Weight Gain, (a) mg	Calculated Carburized Carbon Content, w/o
			Carburized		
Hf-10Ta-4.0C-0.4Si	29(b)	1.5	11.2	9	4.8
	83(c)	4.0	10.5	37	5.6
	43(b)	1.2	22.6	9.5	4.8
Hf-10Ta-4.5C-0.4Si	16(b)	0.85	11.7	14	5.3
	63(c)	1.0	9.3	39	6.2
	56(b)	1.5	23.0	14	5.3
			Duplex Coated		
Hf-10Ta-4.5C-0.4Si	24(c)	1.3	11.4	--	--
	26(c)	1.8	9.1	--	--

(a) Carburized 3500°F - 2 hr.

(b) Sintered 3500°F - 1 hr.
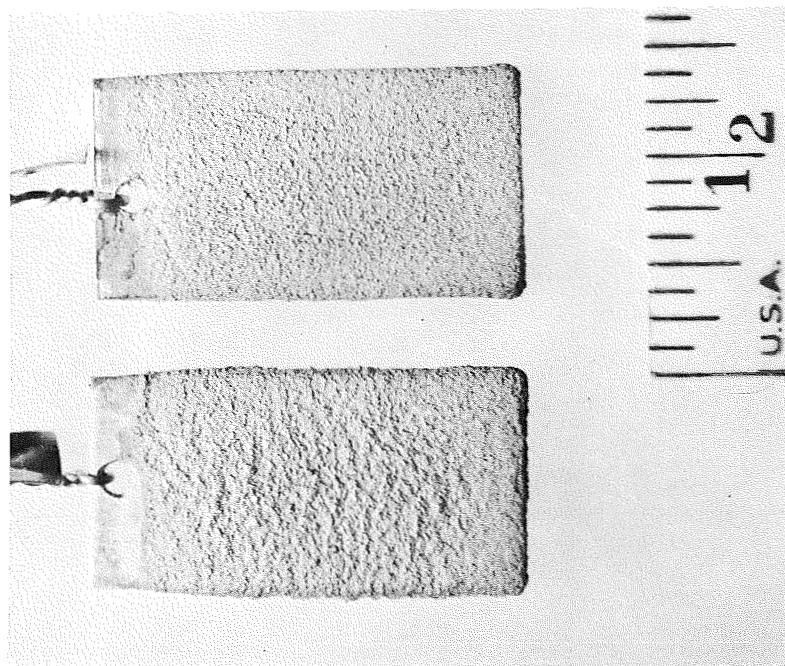
(c) Sintered 3500°F - 2 hr.

112

The typical surface conditions of 10-15 and 20-25 mil Hf-10Ta-4.0C-0.4Si and Hf-10Ta-4.5C-0.4Si coatings as-sintered and after carburization are shown in Figures 40 and 41, respectively. Although not clearly shown, carburization converts the metallic as-sintered coatings to a darker gray surface appearance. Bubbles are readily apparent in 20-25 mil coatings, particularly after carburization.

The microstructures of the Hf-10Ta-4.5C-0.4Si slurry coating after initial sintering and carburization are shown in Figure 42. Both structures appear similar since carburization does not alter the sintered structure; carburization only converts the metal matrix of sintered coatings to a complex Hf-Ta carbide. Although evident in both coatings, porosity was reduced by the carburization treatment. Pores present in the coatings were generally isolated within the coating and are therefore less detrimental than if they were connected to the surface.

It was intended to coat rocket nozzles with a minimum carbide coating thickness of 20 mils. However, the carburization studies revealed that bubbling could be expected for coating thicknesses in the range of 20-25 mils. Accordingly, the possibility of overlaying two 10-mil coatings of Hf-Ta-4.5C-0.4Si was investigated; weight changes during sintering of the duplex process are shown in Table XXVII. The surface appearance and microstructure of a duplex coated 20-mil carbide coating is shown in Figure 43. No evidence of bubbling was apparent and, furthermore, the success of this technique suggested that repair of defects in coated nozzles would be relatively easy. This technique was therefore used for coating the Ta-10W nozzles described in the following section.

C.   Test Nozzle Fabrication

During this year, eight tungsten and Ta-10W rocket nozzles were coated with the systems developed both during the current and previous years. The coated components (nozzle, thrust chamber, and flange) had a maximum overall weight of 6 in. These

113

Neg. No. 36705

(b) Hf-10Ta-4.5C-0.4Si

Neg. No. 36703

(a) Hf-10Ta-4.0C-0.4Si

Fig. 40 - Surface Appearance of 10 mil Hf-Ta-C-Si Slurry Coatings on
Tantalum As-Sintered and After Carburization at 3500°F.

114
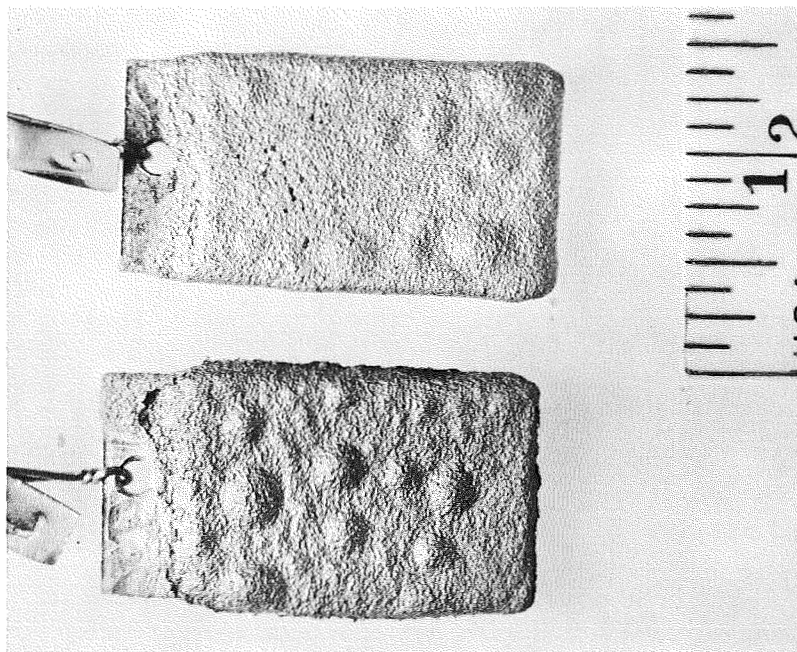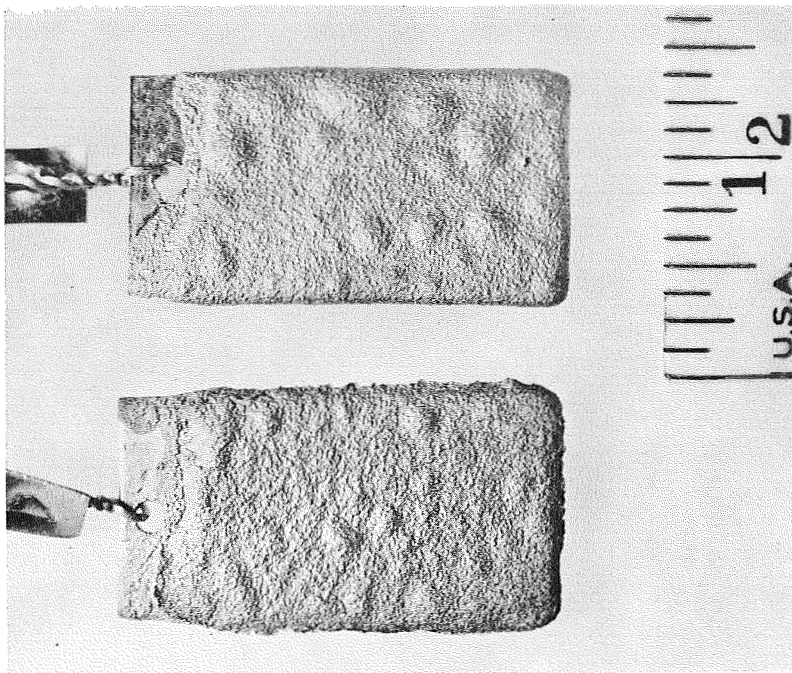
(b) Hf-10Ta-4.5C-0.4Si

(a) Hf-10Ta-4.0C-0.4Si

Fig. 41 - Surface Appearance of 20 mil Hf-Ta-C-Si Slurry Coatings on
Tantalum As-Sintered and After Carburization at 3500°F.

115
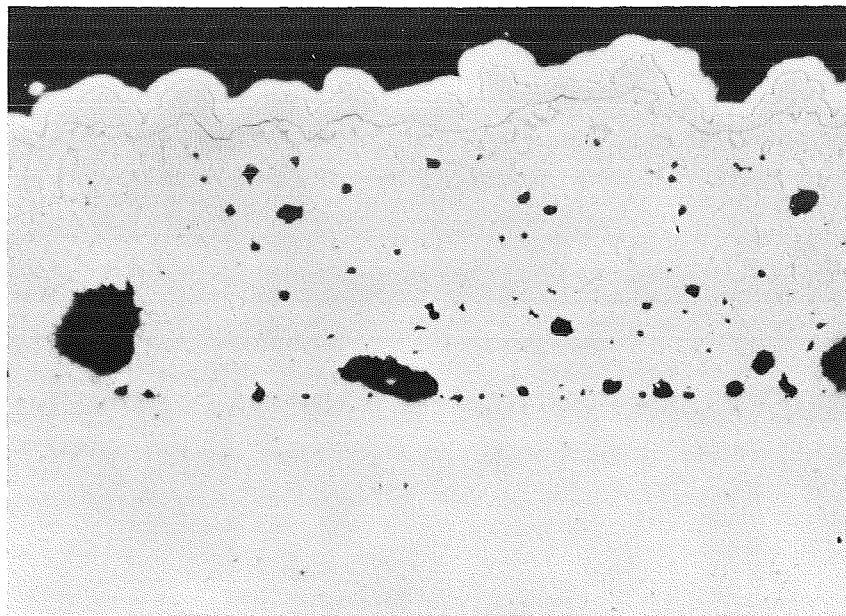
Neg. No. 37268   X125

(a) As Sintered
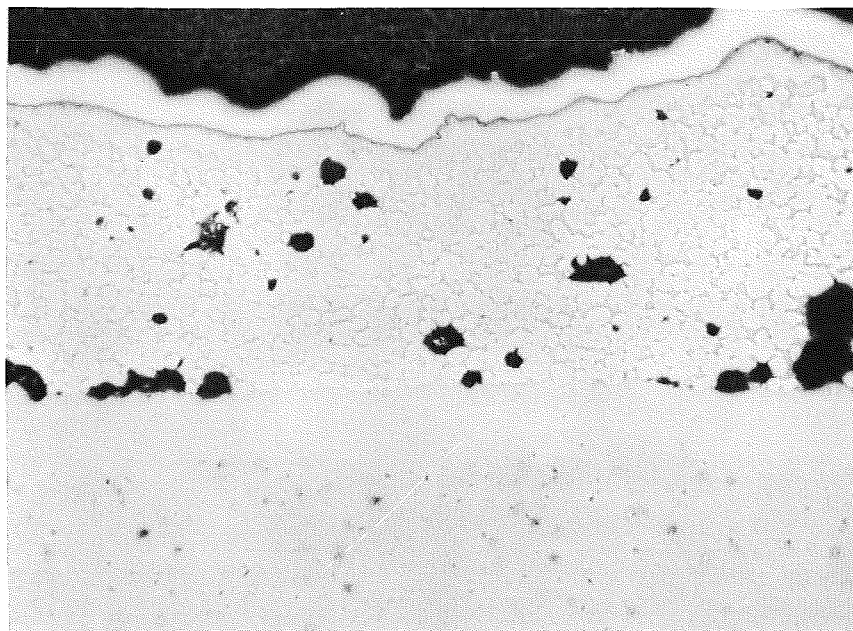
Neg. No. 37526   X125

(b) Carburized at 3500°F-2hr.

Fig. 42 - Microstructures of 10 mil Hf-10Ta-
         4.5C-0.4Si Slurry Coating on Tan-
         talum As-Sintered and After Car-
         burization.

116
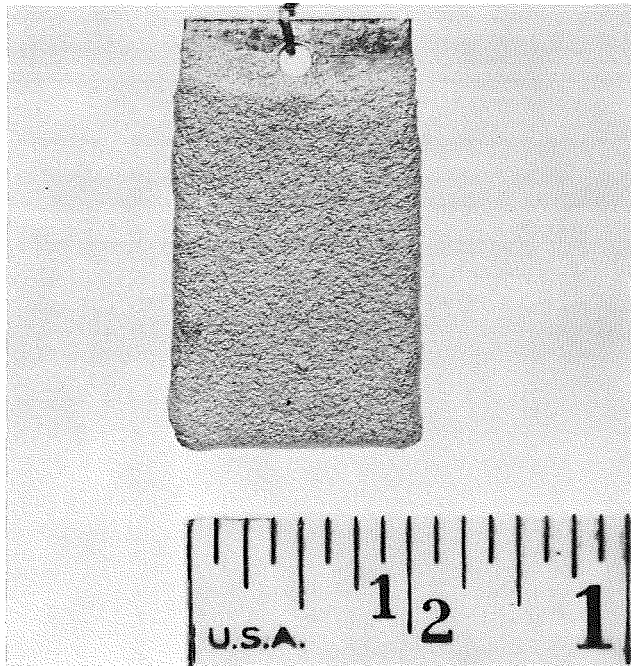
Neg. No. 36708
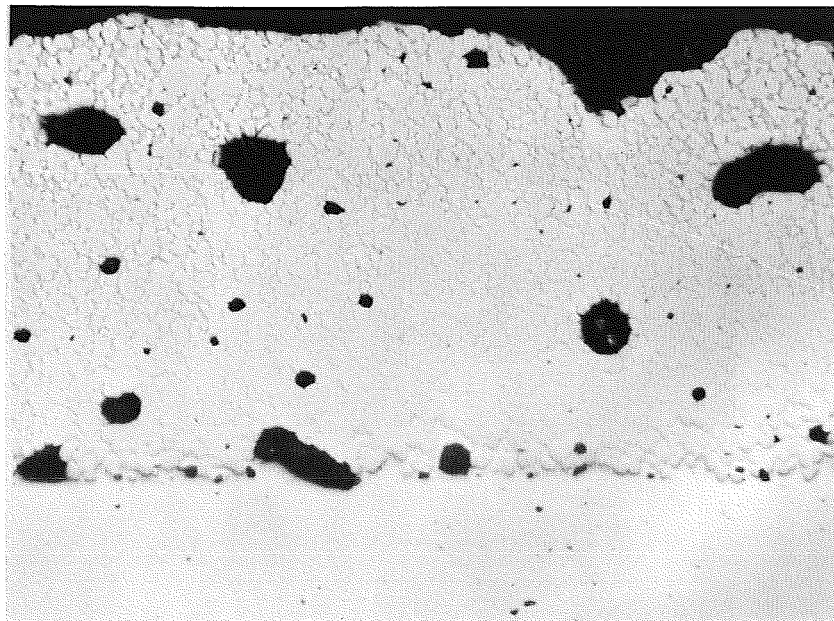
Neg. No. 37308   X125

Fig. 43 - Duplex Hf-10Ta-4.5C-0.4Si Carbide
          Coating on Tantalum As Sintered.

117

nozzles were hot spun by Fansteel Metallurgical Corporation on Contract NAS7-417.[16] Their dimensions were limited to about 6 in. due to the size of the furnace hot zone, 6 in. long x 4 in. in diameter. The actual lengths of nozzles received for coating were about 5 in. for tungsten and 6.1 in. for Ta-10W. These dimensions resulted in an effective coating surface area, including both OD and ID surfaces, of 330 cm^2 (51 in.^{2}) for tungsten and 440 cm^2 (67 in.^{2}) for Ta-10W nozzles. A photograph of a Ta-10W rocket nozzle as received is shown in Figure 44.

The rocket nozzles were coated in two groups. At the beginning of the current work, three Ta-10W and two tungsten nozzles were coated with the Ir-Re duplex coating developed during the previous year.[2] One of the Ta-10W nozzles was sectioned for metallographic examination after coating. The remaining nozzles were scheduled for engine firing tests at the TRW Systems Group, using hydrazine-nitrogen tetroxide propellants, under Contract NAS7-460.[17]

At the completion of the current slurry coating studies, two Ta-10W nozzles were coated with the carburized Hf-10Ta-4.0C-0.4Si slurry coating, and two tungsten nozzles were coated with one Ir-Re and one Ir-20Re/Re slurry coating. These nozzles were to be evaluated in fluorine-containing propellants by the Marquardt Chemical Co. under Contract NAS7-555.

Summaries of the coating thicknesses produced on these nozzles are presented in Tables XXVIII and XXIX. Nozzles C1, C2, B1, and B4 are to be fired on Contract NAS7-460, and nozzles C3, C5, B7, and B8 in fluorine-containing propellants on Contract NAS7-555. The duplex Ir-Re coated nozzle B1 was sectioned for metallographic examination.

1.   Ir-Re Coatings

The Ir-Re duplex coatings were applied by the slurry techniques described in Section II-B. Nozzles and nozzle inserts coated previously in this program did not include the thrust chamber; the maximum length was about 3.5 in. It was found that

118

Neg. No. 34660

Fig. 44- Ta-10W Rocket Nozzle As Received

TABLE XXVII

SUMMARY OF IRIDIUM-BASE COATING THICKNESS ON
ROCKET NOZZLES SCHEDULED FOR ENGINE FIRING TESTS[a]

Nozzle Identi-fication	Substrate	Coating System	Sur-face Area, cm²	Applied Rhenium Coating Weight, g	Applied Iridium Coating Weight, g	Calculated Average Thickness, mils	
						Re	Ir
C1	Tungsten	Ir/Re	330	62.0	47.0	3.3	2.5
C2	Tungsten	Ir/Re	325	53.5	55.0	2.9	3.0
B1	Ta-10W	Ir/Re	435	64.0	74.0	2.6	3.0
B2[b]	Ta-10W	Ir/Re	440	62.0	75.0	2.5	3.0
B4[c]	Ta-10W	Ir/Re	440	53.0	60.0	2.1	2.4
C3[c]	Tungsten	Ir-20 Re/Re	330	50.0	48.0	2.7	2.6
C5[c]	Tungsten	Ir	330	--	54.5	--	2.9

[a] Nominal thickness - 3 mils for both Ir and Re.
[b] Ir applied in two cycles.
[c] Both Ir and Re applied in two cycles.

TABLE XXIX

SUMMARY OF CARBIDE COATING THICKNESS ON
ROCKET NOZZLES SCHEDULED FOR FIRING TESTS

Nozzle Identi-fication	Sub-strate	Applied Coating Weight, g	Calculated Average Thickness, mils	Weight Change During Carburization, g	Calculated Carbon Content, %
B7	Ta-10W	223[a]	19	3	5.5+
B8	Ta-10W	225[a]	19	3	5.5+

[a] Duplex coated; two nominal 10 mil coatings.

larger nozzles in the current work required a modified coating technique. Initially, the rhenium coatings were applied on both the OD and ID surface in one sintering cycle. A similar procedure was used for the subsequent iridium coatings. This technique was used on nozzles C1, C2, B2, and for the rhenium layer coating on nozzle B2.

It was found that a difference in sintering behavior was apparent on the ID and OD surfaces. Generally the OD surface had better surface appearance than coatings on the ID surface, particularly for the rhenium coating. This was apparently due to a difference in surface temperature during sintering. The OD surface was heated by direct radiation from the furnace element, whereas the ID surface was heated by conduction in a vacuum and a combination of conduction and convection during sintering in argon atmospheres. The W/Re control thermocouple was located near the throat on the ID of the nozzle; consequently, the improved sintering behavior of the OD surface was apparently due to a higher surface temperature.

Accordingly, subsequent duplex coatings were applied in a two step process in which OD and ID coatings were applied individually. In addition, a 100°F higher temperature was used as the initial step of sintering (collapse cycle) for ID coatings. This technique was effective in obtaining nearly comparable surface appearance on both OD and ID surfaces. The point of junction for the two coating cycles was located on the OD of the nozzle about 0.5 in. from the nozzle exit. At this point, the individual coatings, as applied, were overlapped for a distance of about 0.25 in. No difficulties were observed with this technique, and it was used for nozzles B4, C3, C5, and for the iridium coating of nozzle B2.

All slurries were applied by brushing in order to conserve both iridium and rhenium powder. First, the slurries were prepared in the appropriate proportions and weight to obtain the desired coating thickness over the total nozzle surface, and blended by tumbling in a glass container for 16 hr. The blended

slurries were then halved, suspended in the organic vehicle, and applied individually to the ID and OD surfaces. Equal slurry weights were applied to both ID and OD. Because of lesser surface area, the average sintered coating thickness was about 10% greater on the ID surface. The nominal coating thickness was 3 mils for both rhenium and iridium-base coatings.

Rhenium slurries were applied by brushing a Re-11.5Cu-3.5Al slurry on the nozzle surface. During slurry application, the nozzle was slowly rotated in a horizontal plane to improve uniformity of the as-applied slurry. This technique was intended to minimize the tendency toward deposition of a thicker slurry at the throat inlet, as was observed in previous slurry-coated nozzles. The sintering cycle for the rhenium slurry coating consisted of an initial sinter in argon at 2300-2400°F followed by a vacuum treatment at 2190-2400°F to remove the Cu-Al metallic vehicle. A final sinter was conducted in vacuum at 3300°F for 1 hr to insure bonding of the rhenium coating to the substrate as well as to provide additional sintering of the coating.

Iridium and Ir-20Re coatings were produced using the Ir-30Cu and Ir-20Re-30Cu slurries described in Section IIB. The slurry application techniques were identical to those used for rhenium. Sintering was conducted at 2200-2300°F in argon followed by vacuum treatment at 2190-2300°F. The final sinter was also conducted in vacuum at 3300°F.

Photographs of Ta-10W nozzles coated with rhenium and the Ir-Re duplex coatings are shown in Figures 45 and 46, respectively. Tungsten rocket nozzles with the iridium, rhenium, Ir/Re, and Ir-20Re/Re coatings are shown in Figures 47, 48, 49, and 50, respectively.

The Ir/Re duplex coated Ta-10W nozzle B1 was sectioned for metallographic examination. This nozzle was selected because it had the roughest ID surface appearance of the three Ta-10W nozzles. Furthermore, it was the first Ta-10W nozzle on which the iridium external coating was applied in a single sintering cycle.

Neg. No, 34855

Fig.45 - Ta-10W Rocket Nozzle B2 Coated
with Rhenium Slurry Coating.
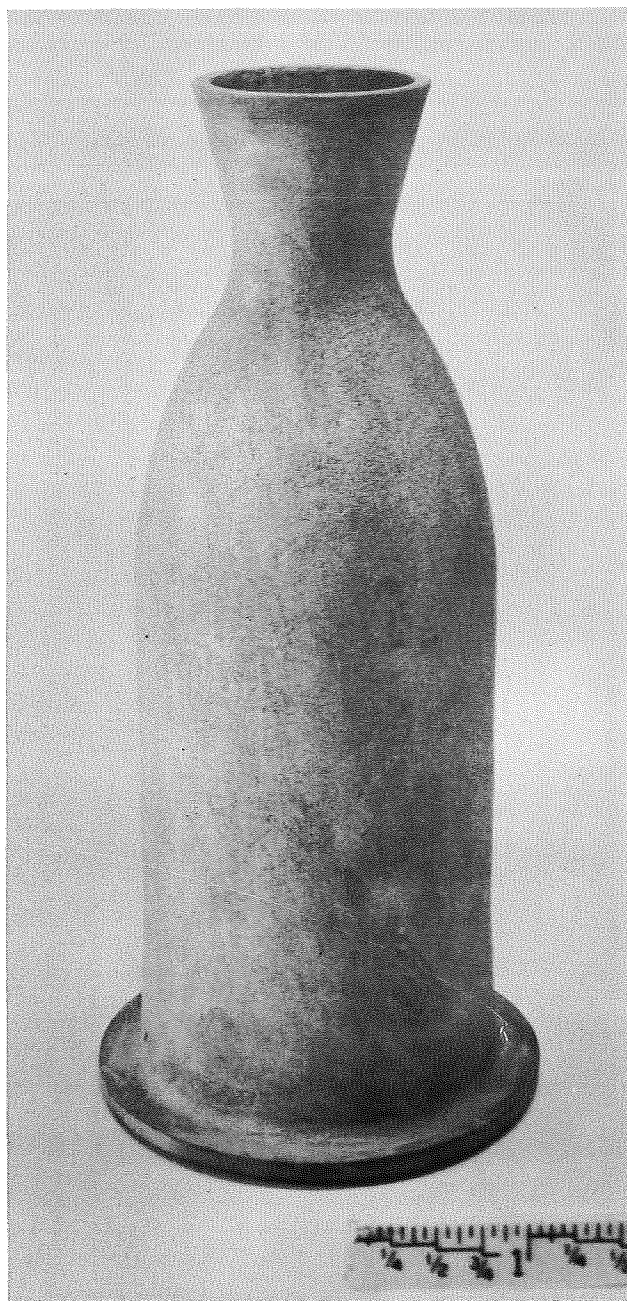
Neg. No. 35447

Fig. 46 - Ta-10W Rocket Nozzle B4
         Coated with Ir/Re Duplex
         Slurry Coating.
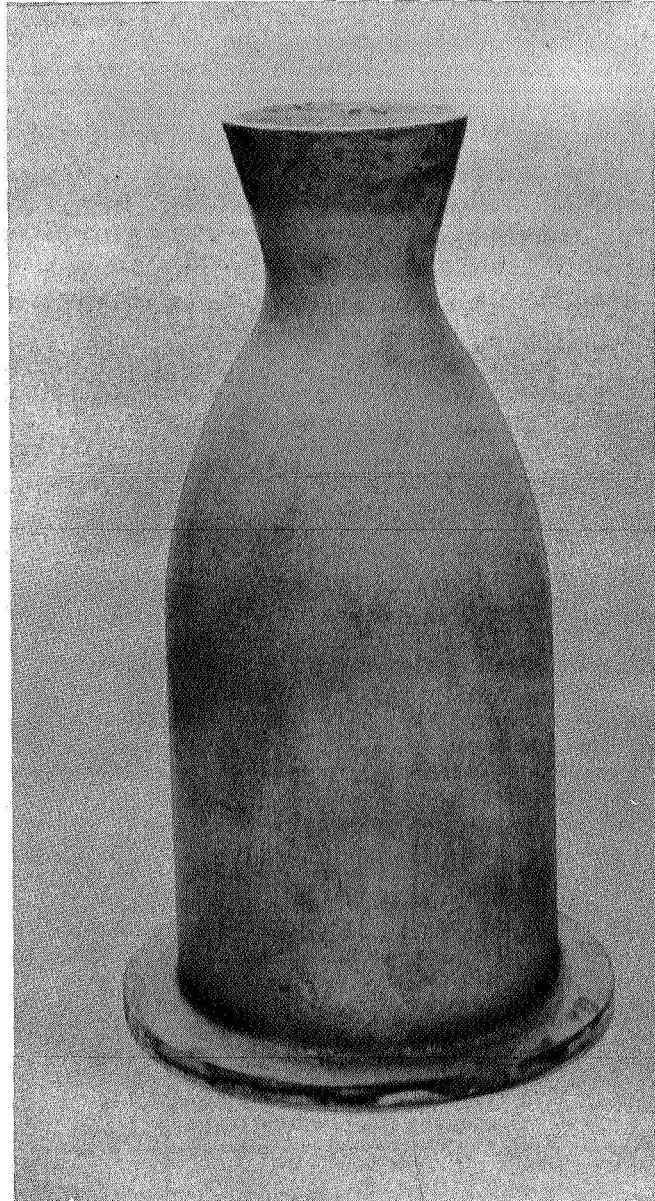
Neg. No. 37034

Fig. 47 - Tungsten Rocket Nozzle C5
Coated with Iridium Slurry
Coating.

Neg. No. 36673

Fig. 48 - Tungsten Rocket Nozzle C3
          Coated with Rhenium Slurry
          Coating.
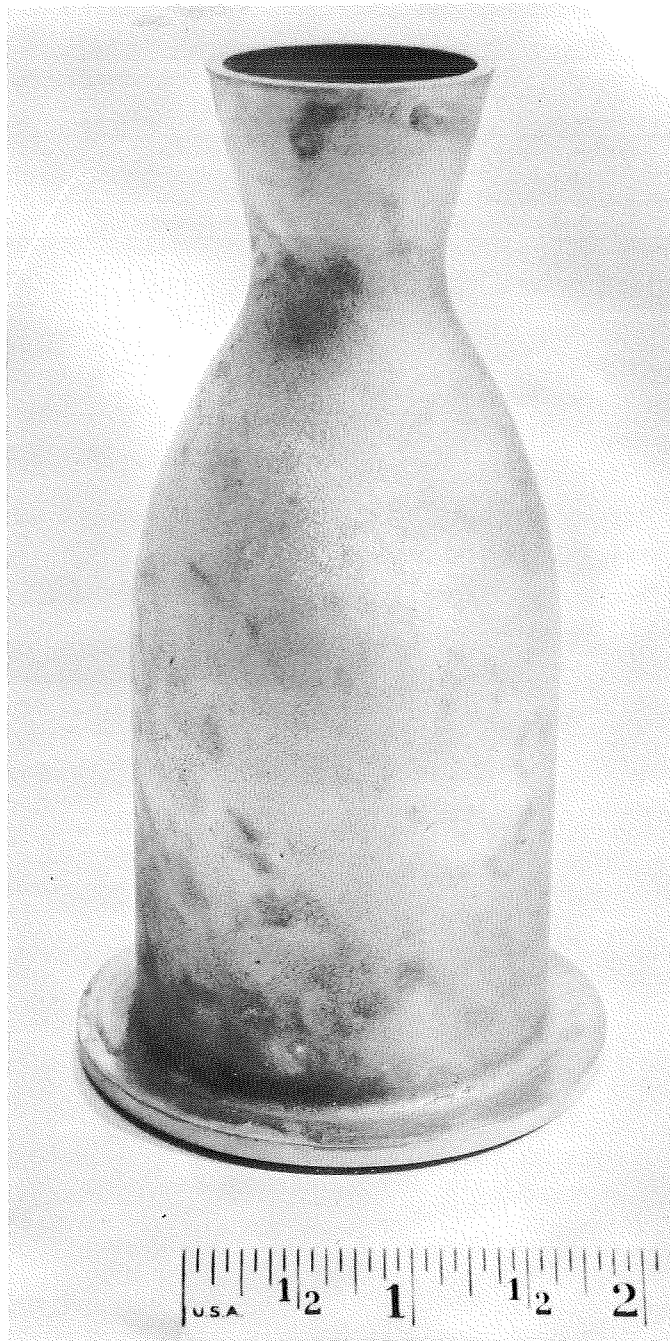
Neg. No. 35148

Fig. 49 - Tungsten Rocket Nozzle C2
Coated with Ir/Re Duplex
Slurry Coating.
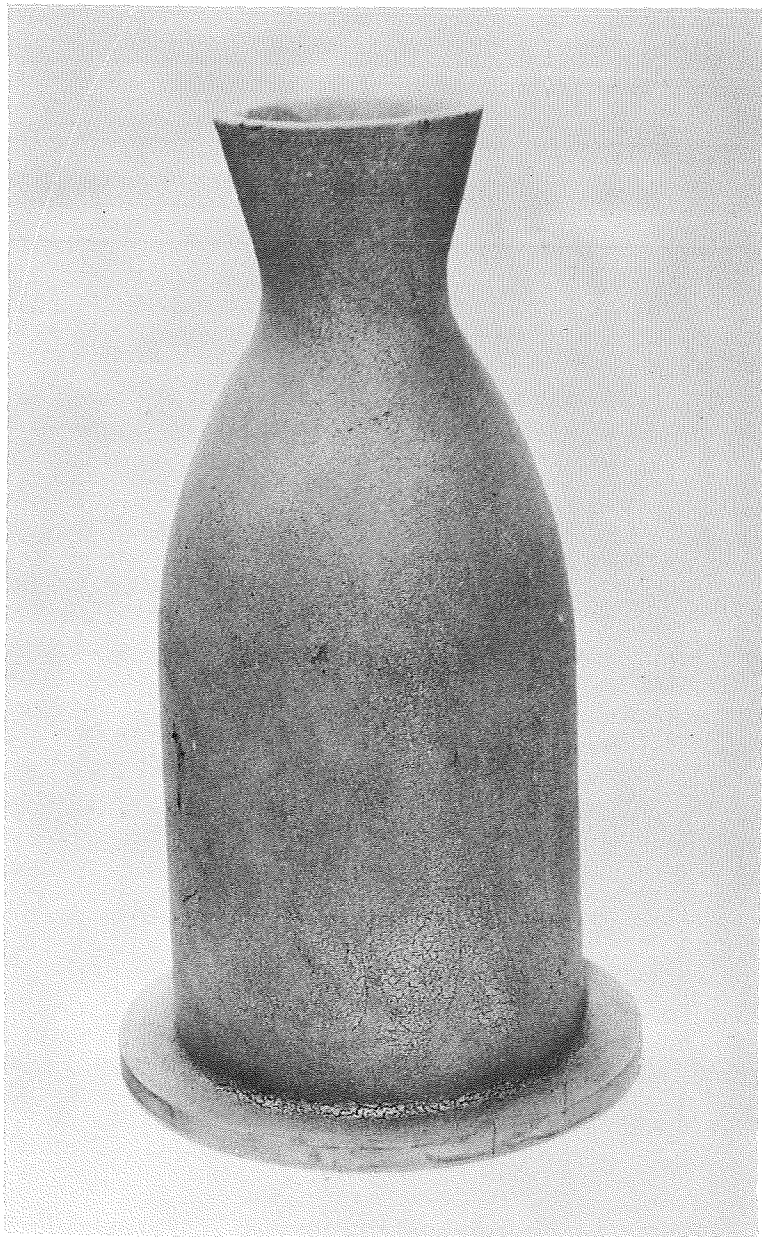
Neg. No. 37033

Fig. 50 - Tungsten Rocket Nozzle C3
         Coated with Ir-20Re/Re
         Duplex Slurry Coating.

The remaining two Ta-10W nozzles to be evaluated in engine firing tests were duplicates as desired, at least in that the external protective iridium coating was applied by the same process.

The B1 nozzle was electroplated with nickel prior to sectioning for metallographic examination. Rather than remove metallographic samples at several locations, the nozzle was initially sectioned transverse to the nozzle axis through the thrust chamber and then parallel to the axis for the full length of the nozzle. One half of the nozzle section was then metallographically polished for examination. This technique permitted examination of the full nozzle cross section from the thrust chamber to the nozzle exit. It did have the disadvantage that the relatively large sample could not be polished easily. Therefore, there was some question whether all of the effects of sectioning were removed by subsequent polishing.

The typical microstructure of the Ir/Re duplex coating on the B1 Ta-10W nozzle is shown in Figure 51. This photomicrograph represents the sintered coating on the ID at the entrance to the nozzle throat. The surface shown is not located at right angles to the substrate, therefore, coating thicknesses cannot be determined accurately from the magnification. Porosity is evident in both the iridium and rhenium layers, although the large pores in the iridium layer may be exaggerated as a result of sectioning. A clearly defined interface is apparent between the iridium and rhenium layers. The rhenium layer contains a relatively uniform distribution of fine porosity. Larger pores exist in the iridium layer, particularly at the interface with the rhenium layer. This is probably due to formation of a Ir-Re alloy layer during the slurry sintering treatments. Other localized defects are also evident in the main body of the iridium layer. As previously discussed, there may have been an increase in pore size in these areas because of sectioning. Furthermore, the use of a separate sintering cycle for the iridium external layer should have provided improved density of the iridium coatings on nozzles B2 and B4.
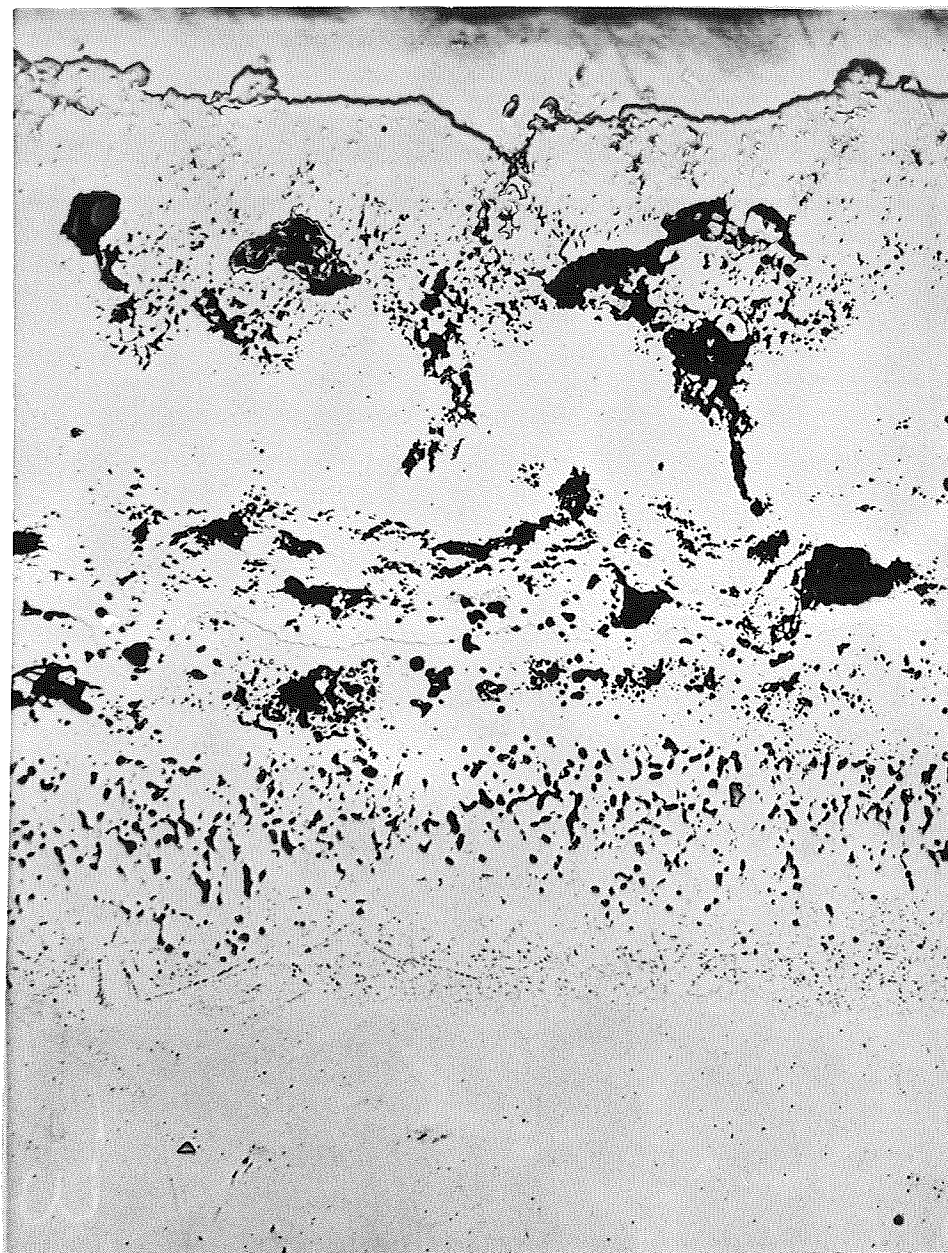
Ni

Ir

Ir/Re

Re

Re-Ta

Ta-10W

Neg. No. 36593

X250

Fig. 51 - Microstructure of Ir/Re Duplex Coated
          Nozzle B3 at ID of Nozzle Throat.

2. Carbide Coatings

Rocket nozzles B7 and B8 were coated with the carburized Hf-10Ta-4.5C-0.4Si coating described in Section IIC. Slurry preparation and application was the same as that used for iridium and rhenium coatings. All powders were-325 mesh and slurries were applied by brushing. Carbide coatings were applied and sintered as two 10 mil layers to eliminate the possibility of blistering observed during sintering of 20-25 mil coatings. Because sintering of carbide is not temperature sensitive above 3300°F, both OD and ID were coated in a single sintering cycle. The maximum stable temperature obtainable in the furnace was 3350°F with the large nozzles. Accordingly, both sintering and carburization was performed in argon at 3350°F (ID temperature) for 2 hr. Finally, the nozzles were cleaned ultrasonically in alcohol to remove residual graphite on the surface prior to weighing for total carbon calculations.

The typical surface condition of the carbide coated nozzles as sintered and carburized are shown in Figures 52 and 53, respectively. Calculated coating thickness on these nozzles was about 19 mils and the final carbon content 5.5 w/o as shown in Table XXIX.

III. SUMMARY

Work during the current year on this program consisted of four areas of investigation. These areas included: (1) oxidation-corrosion studies, (2) development of Ir-Re/Re duplex coatings for tungsten and Ta-10W, (3) development of (Hf-10Ta)C coatings for tantalum base alloys, and (4) coating of rocket nozzles for engine firing tests.

Oxidation-corrosion tests were conducted on eight refractory materials in flowing oxygen, fluorine, hydrogen fluoride, fluorine-oxygen and hydrogen fluoride-oxygen atmospheres at 3000°-5500°F. The materials evaluated included tungsten, iridium, Ir-33 w/o Re, rhenium, ATJ graphite, HfC-33 v/o C, TaC-20 v/o C,
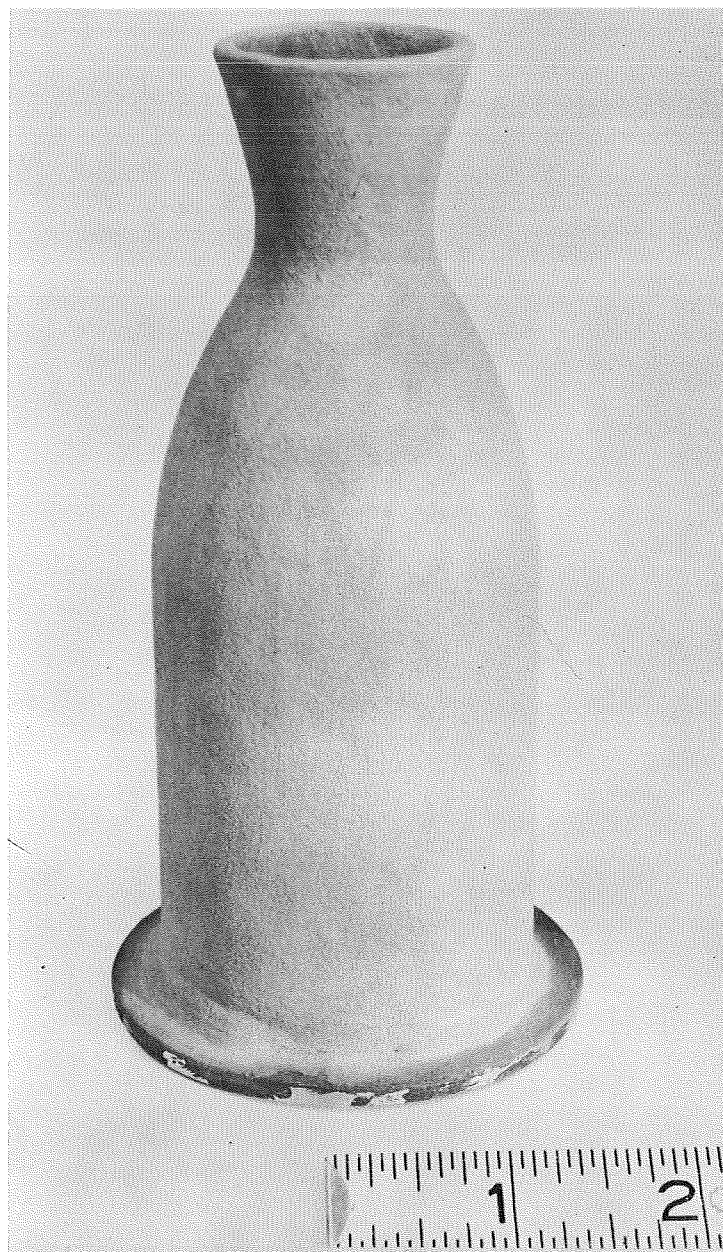
Neg. No. 36376

Fig. 52 - Ta-10W Rocket Nozzle B8 Duplex
          Coated with Hf-10Ta-4.5C-0.4Si
          Slurry Coating.

132
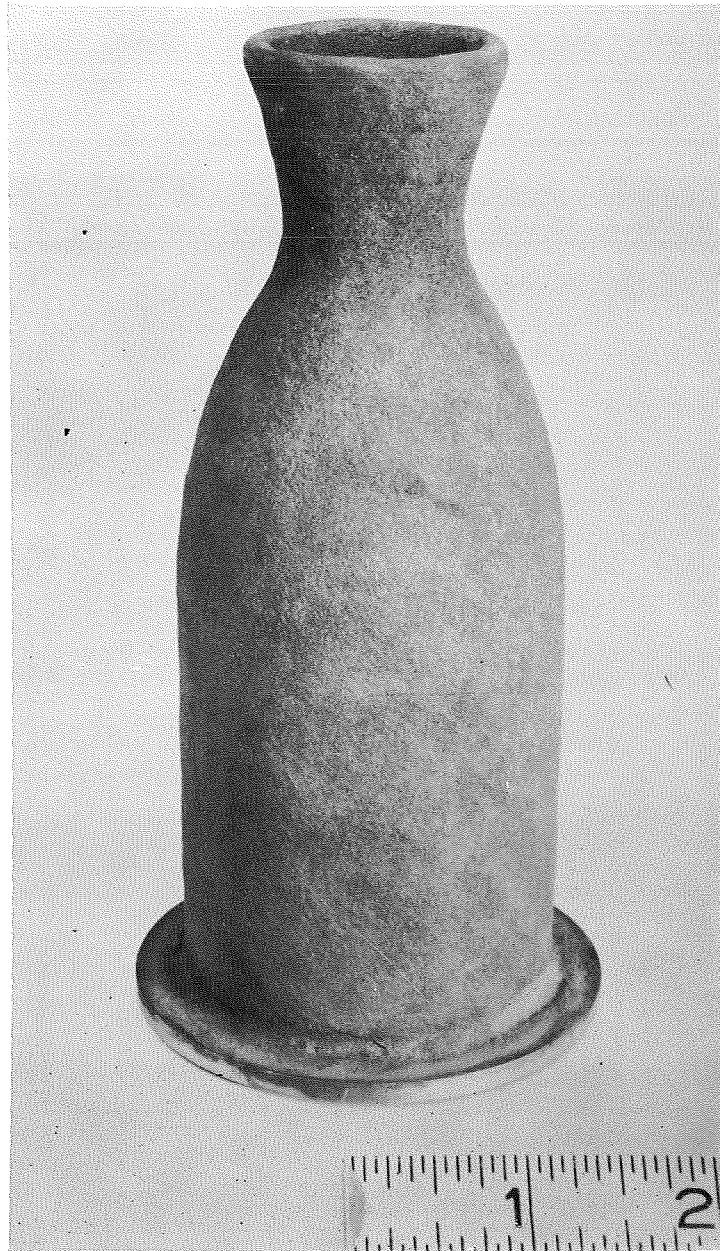
Neg. No. 36375

Fig. 53 - Ta-10W Rocket Nozzle B7 Coated
with Hf-Ta-C-Si Slurry Coating
after Carburization at 3350°F
for 2 hr.

133

and ZrB_2-SiC-C. Surface recession rates in 6.5 v/o fluorine and 10 v/o hydrogen fluoride measured in previous programs were extended to at least 5000°F, or the melting point of the material. Oxidation atmospheres consisted of 2.3 to 5.4 v/o oxygen. The combined environments were 6.5 v/o F_2-4.0 v/o O_2, 6.5 v/o F_2-5.4 v/o O_2, 10 v/o HF-0.56 v/o O_2, and 10 v/o HF-2.3 v/o O_2.

Oxidation-corrosion tests showed that the iridium and Ir-33Re had the lowest recession rates to their respective melting points of 4450°F and 4750°F in all environments. At 5000°F, rhenium had the lowest recession rates in the combined environments. The highest recession rates in fluorine-oxygen at 5000°F were measured for ATJ graphite, HfC-33 v/o C, and TaC-20 v/o C. ZrB_2-SiC-C could not be exposed above approximately 4300°F because of melting of the composite. Oxidation-corrosion tests indicated that, in general, materials which have only gaseous reaction products were resistant to the combined environments only in the temperature range in which they were resistant to the individual environments. The surface recession rates of materials which form solid oxides (carbide and boride composites) were likely controlled by the rate of oxidation, at least above about 3500°F.

Study of the sintering characteristics of Ir-Re/Re slurry coatings was conducted based on previous work on iridium and Ir/Re coatings. It was found that the sintering characteristics of Ir-20Re-30Cu slurry coatings were similar to unalloyed iridium. High density Ir-30Re coatings could not be obtained using a copper vehicle and under the sintering conditions used for iridium and Ir-20Re coatings. Iridium-rhenium coatings were more prone to surface defects and incomplete sintering than were unalloyed iridium coatings. Limited study of Ir/Re duplex coatings produced by iridium application by the slurry technique on CVD rhenium demonstrated that uniform defect free coatings are obtainable by this method.

Investigation of sintered carbide coatings for tantalum-base alloys was based on previous work on these coatings. Carbide

coatings based on Hf-10Ta containing 4-4.5 w/o C and 0.4 w/o Si were produced by sintering in argon at 3300°-3500°F. High densities could not be obtained in Hf-10Ta-C-Si slurry coatings above 4.5 w/o C in slurries containing up to 1.5 w/o Si. It was found that slurry coatings containing 4-4.5 w/o C, greater than 20 mils in thickness after sintering, developed "blisters" during the sintering process. To eliminate this effect, 20 mil carbide coatings were produced by two-step application and sintering of 10 mil coatings. Carburization of 4-4.5 w/o C coatings by solid-state diffusion after sintering was effective in increasing the total carbon content to at least 5.5 w/o. Carburization was accomplished by applying a carbon slurry and heating in argon at 3350°-3500°F for 2 hr.

Eight tungsten and Ta-10W rocket nozzles were coated with the iridium, Ir/Re, Ir-20Re/Re, and carbide slurry coatings for engine firing tests. These nozzles consisted of both nozzle and thrust chamber having an overall length up to 6 in. and 440 cm^2 (68 $in.^2$) coated surface area. Two tungsten and two Ta-10W nozzles coated with the Ir/Re duplex slurry coating were to be fired in hydrazine-nitrogen tetroxide propellant on Contract NAS7-460. The fifth Ir/Re duplex coated Ta-10W nozzle was sectioned for metallographic examination after sintering.

The four remaining coated rocket nozzles are to be evaluated in a fluorine-containing propellant system on Contract NAS7-555. Rocket nozzles prepared for these firing tests included two Ta-10W coated with the carburized Hf-10Ta-4.5C-0.4Si slurry coating. Two tungsten nozzles, one coated with the iridium and the other with the Ir-20Re/Re duplex coating developed in the program, will also be evaluated in the fluorine propellant system.

REFERENCES

1. V. L. Hill, A. Hess, and J. J. Rausch, "Protective Coatings for Refractory Metals in Rocket Engines," Interim Report IITRI-B6058-13, January 1967.

2. V. L. Hill, "Protective Coatings for Refractory Metals in Rocket Engines," Interim Report IITRI-B6058-26, March 1968.

3. I. E. Campbell (ed.), High Temperature Technology, John Wiley & Sons, Inc., New York, 1956.

4. M. A. Tylkina, I. A. Tsyganova, and E. M. Savitskii, Zh. Neorg. Khim., 7, 1962, 1917-1927; Russ. J. Inorg. Chem., 7, 1962, 990-996.

5. Metals Handbook, Vol. 1, Properties and Selection, American Society for Metals, Metals Park, Ohio, 1961.

6. E. Rudy, "Ternary Phase Equilibria in Transition Metal-Boron-Carbon-Silicon Systems," AFML-TR-65-2, Pt. I (Related Binary Systems), Vol. 4, October 1965.

7. E. Rudy and D. P. Harmon, "Ternary Phase Equilibria in Transition Metal-Boron-Carbon-Silicon Systems," AFML-TR-65-2, Pt. I (Related Binary Systems), Vol. 5, January 1966.

8. Y. Harada, "Metal Carbide-Graphite Composites," Summary Report on Contract NASr-65-(09), September 1967.

9. E. V. Clougherty et al., "Research and Development of Refractory Oxidation-Resistant Diborides," Technical Summary Report No. 1 on Contract AF 33(615)-3611, December 1967.

10. M. Ebner, "Stability of Refractories in Hydrogen Fluoride Flames," J. Amer. Chem. Soc., 44, 1961.

11. B. A. Macklin and P. A. LaMar, "Development of Improved Methods of Depositing Iridium Coatings on Graphite," AFML-TR-67-195, Pt. II, Contract AF 33(615)-3617, October 1968.

12. T. R. Wright, T. R. Braeckel, and D. E. Kizer, "The Fabrication of Iridium and Iridium Alloy Coatings on Graphite by Plasma-Arc Deposition and Gas-Pressure Bonding," AFML-TR-68-6, Contract AF 33(615)-3706, February 1968.

13. J. J. Rausch, V. L. Hill, R. J. Van Thyne, and S. Bortz, "Protective Coatings for Refractory Metals in Rocket Engines," IITRI-B237-45, Contract NAS7-113, January 1966.

REFERENCES (Continued)

14. Personal communication with Dr. R. Holzl, San Fernando Laboratories, San Fernando, California.

15. D. D. Lawthers and L. Sama, "Development of Coatings for Protection of High-Strength Tantalum Alloys in Severe High-Temperature Environments," AFML-TR-67-374, November 1967.

16. D. R. Mash, D. C. Brillhart, and D. W. Bauer, "Tantalum-Hafnium Alloys, Metallurgical Processing Technology," Second Interim Report on Contract NAS7-417, April 1968.

17. N. R. Balling and R. I. Batista, "Evaluation Testing of Protective Coatings in Refractory Metals," Contract NAS7-460, in publication.

DISTRIBUTION LIST

Contract NAS7-460, NAS7-431

Jet Propulsion Laboratory
4800 Oak Grove Drive
Pasadena, California 91103

Attn: Richard Cannova

Ames Research Center
Moffett Field
California 94035

Attn: Hans M. Mark

Goddard Space Flight Center
Greenbelt, Maryland 20771

Attn: Merland L. Moseson
Code 620

Jet Propulsion Laboratory
California Institute of Tech.
4800 Oak Grove Drive
Pasadena, California 91103

Attn: Henry Burlage, Jr.
Propulsion Div. 38

Langley Research Center
Langley Station
Hampton, Virginia 23365

Attn: Ed Cortwright
Director

Lewis Research Center
21000 Brookpark Road
Cleveland, Ohio 44135

Attn: Dr. Abe Silverstein
Director

Marshall Space Flight Center
Huntsville, Alabama 35812

Attn: Hans G. Paul
Code R-P+VED

Chief
Liquid Propulsion Technology
Office of Advanced Research
    and Technology
NASA Headquarters
Washington, D.C., 20546

Manned Spacecraft Center
Houston, Texas 77001

Attn: J.G. Thibodaux, Jr.
Chief, Prop. &
Power Division

NASA-Kennedy Space Center
Cocoa Beach, Florida 32931

Attn: Dr. Kurt H. Debus

Aeronautical Systems Division
Air Force Systems Command
Wright-Patterson Air Force
    Base
Dayton, Ohio 45433

Attn: D. L. Schmidt
Code ASRCNC-2

Air Force Missile Develop-
    ment Center
Holloman Air Force Base
New Mexico 88330

Attn: Maj. R.E. Bracken

Air Force Missile Test
    Center
Patrick Air Force Base
Florida

Attn: L. J. Ullian

Contract NAS7-460, NAS7-431

Space and Missile Systems
    Organization
Air Force Unit Post Office
Los Angeles, Calif. 90045

Attn: Col. Clark
      Technical Data Center

      L. N. Hjelm
      SAMCO-SMT/AFML

Arnold Engineering Development
    Center
Arnold Air Force Station
Tullahoma, Tennessee 37388

Attn: Dr. H. K. Doetsch

Bureau of Naval Weapons
Department of the Navy
Washington, D.C. 20546

Attn: J. Kay
      RTMS-41

Defense Documentation Center
    Headquarters
Cameron Station, Building 5
5010 Duke Street
Alexandria, Virginia 22314

Attn: TISIA

Headquarters, U.S. Air Force
Washington 25, D.C. 20546

Attn: Col. C. K. Stambaugh
      AFRST

Picatinny Arsenal
Dover, New Jersey 07801

Attn: I. Forsten, Chief
      Liquid Propulsion
        Laboratory

Air Force Rocket Propulsion
    Laboratory
Research and Technology Div.
Air Force Systems Command
Edwards, California 93523

Attn: RPRPD/Mr. H. Main

U.S. Army Missile Command
Redstone Arsenal
Alabama 35809

Attn: Walter Wharton

U.S. Naval Ordnance Test
      Station
China Lake
California 93557

Attn: Code 4562
      Chief, Missile
      Propulsion Div.

Chemical Propulsion Infor-
    mation Agency
Applied Physics Laboratory
8621 Georgia Avenue
Silver Spring, Maryland 20910

Attn: Tom Reedy

Aerojet-General Corporation
P.O. Box 296
Azusa, California 91703

Attn: W. L. Rogers

Aerojet-General Corporation
P. O. Box 1947
Technical Library, Bldg. 2015
Department 2410
Sacramento, California 95809

Attn: R. Stiff

DISTRIBUTION LIST (CONTD)

Contract NAS7-460, NAS7-431

Space Division
Aerojet-General Corp.
9200 East Flair Drive
El Monte, Calif. 91734

Attn: S. Machlawski

Aerospace Corporation
2400 East El Segundo Blvd.
P.O. Box 95085
Los Angeles, Calif. 90045

Attn: H. M. Blaes
MS-2293

Astrosystems International, Inc.
1275 Bloomfield Avenue
Fairfield, New Jersey 07007

Attn: A. Mendenhall

Atlantic Research Corporation
Edsall Road and Shirley Highway
Alexandria, Virginia 22314

Attn: Dr. Ray Friedman

Avco Systems Division
Wilmington, Massachusetts

Attn: Howard B. Winkler

Beech Aircraft Corporation
Boulder Division
Box 631
Boulder, Colorado

Attn: J. H. Rodgers

Bell Aerosystems Company
P. O. Box 1
Buffalo, New York 14240

Attn: W. M. Smith

Bellcomm
955 L-Enfant Plaza, S.W.
Washington, D.C.

Attn: H. S. London

Bendix Systems Division
Bendix Corporation
3300 Plymouth Road
Ann Arbor, Michigan 48105

Attn: John M. Brueger

Boeing Company
P. O. Box 3707
Seattle, Washington 98124

Attn: R. T. Torgerson

Boeing Company
1625 K Street, N.W.
Washington, D.C. 20006

Attn: Library

Boeing Company
P. O. Box 1680
Huntsville, Alabama 35801

Attn: Ted Snow

Missile Division
Chrysler Corporation
P. O. Box 2628
Detroit, Michigan 48231

Attn: John Gates

Wright Aeronautical Division
Curtiss-Wright Corporation
Wood-Ridge, New Jersey 07075

Attn: G. Kelley

Contract NAS7-460, NAS7-431

Research Center
Fairchild Hiller Corporation
Germantown, Maryland

Attn: Ralph Hall

Republic Aviation Corporation
Fairchild Hiller Corporation
Farmingdale
Long Island, New York

Attn: Library

General Dynamics, Convair Div.
Library & Information Services
P. O. Box 1128
San Diego, California 92112

Attn: J. W. Baer

Missile and Space Systems Center
General Electric Company
Valley Forge Space Technology
     Center
P.O. Box 8555
Philadelphia, Pennsylvania

Attn: F. Mezger
       F. E. Schultz

Grumman Aircraft Engineering
     Corporation
Bethpage,
Long Island, New York 11714

Attn: Joseph Gavin

Honeywell, Incorporated
Aerospace Division
2600 Ridgway Road
Minneapolis, Minnesota

Attn: Gordon Harms

Hughes Aircraft Company
Aerospace Group
Centinela and Teale Streets
Culver City, Calif. 90230

Attn: E. H. Meier
       V. P. and Div. Mgr.
       Research & Devel. Div.

Walter Kidde and Co., Inc.
Aerospace Operations
567 Main Street
Belleville, New Jersey

Attn: R. J. Hanville
       Dir. of Research Engr.

Ling-Temco-Vought Corp.
P. O. Box 5907
Dallas, Texas 75222

Attn: Warren G. Trent

Arthur D. Little, Inc.
20 Acorn Park
Cambridge, Mass. 02140

Attn: Library

Lockheed Missiles and Space
     Company
P. O. Box 504
Sunnyvale, Calif. 94088

Attn: T. H. Dolton

Lockheed Propulsion Company
P. O. Box 111
Redlands, Calif. 92374

Attn: H. L. Thackwell

The Marquardt Corporation
16555 Saticoy Street
Van Nuys, Calif. 91409

Attn: Howard McFarland

Contract NAS7-460, NAS7-431

Baltimore Division
Martin Marietta Corporation
Baltimore, Maryland 21203

Attn: John Calathes (3214)

Denver Division
Martin Marietta Corporation
P. O. Box 179
Denver, Colorado 80201

Attn: Dr. Morganthaler
A. J. Kullas

Orlando Division
Martin Marietta Corporation
Box 5837
Orlando, Florida

Attn: J. Ferm

Astropower Laboratory
McDonnell-Douglas Aircraft Co.
2121 Paularino
Newport Beach, Calif. 92663

Attn: Dr. George Moc
Director, Research

McDonnell-Douglas Aircraft Corp.
P. O. Box 516
Municipal Airport
St. Louis, Missouri 63166

Attn: R. A. Herzmark

Missile and Space Systems Div.
McDonnell-Douglas Aircraft Co.
3000 Ocean Park Boulevard
Santa Monica, Calif. 90406

Attn: R. W. Hallet
Chief Engineer
Adv. Space Tech.

Space & Information
Systems Division
North American Rockwell
12214 Lakewood Boulevard
Downey, California 90241

Attn: Library

Rocketdyne (Library 586-306)
6633 Canoga Avenue
Canoga Park, Calif. 91304

Attn: Dr. R. J. Thompson
S. F. Iacobellis

Northrop Space Laboratories
3401 West Broadway
Hawthorne, California 90250

Attn: Dr. William Howard

Aeronutronic Division
Philco Corporation
Ford Road
Newport Beach, Calif. 92663

Attn: D. A. Garrison

Astro-Electronics Division
Radio Corporation of America
Princeton, New Jersey 08540

Attn: Y. Brill

Rocket Research Corporation
520 South Portland Street
Seattle, Washington 98108

Attn: Foy McCullough, Jr.

Sundstrand Aviation
2421 11th Street
Rockford, Illinois 61101

Attn: R. W. Reynolds

IIT RESEARCH INSTITUTE

DISTRIBUTION LIST(CONTD)

Contract NAS7-460, NAS7-431

Stanford Research Institute
333 Ravenswood Avenue
Menlo Park, California 94025

Attn: Dr. Gerald Marksman

TRW Systems Group
TRW Incorporated
One Space Park
Redondo Beach, Calif. 90278

Attn: G. W. Elverum

Tapco Division
TRW, Incorporated
23555 Euclid Avenue
Cleveland, Ohio 44117

Attn: P. T. Angell

Thiokol Chemical Corporation
Huntsville Division
Huntsville, Alabama 35807

Attn: John Goodloe

Research Laboratories
United Aircraft Corporation
400 Main Street
East Hartford, Conn. 06108

Attn: N. S. Bornstein

Hamilton Standard Division
United Aircraft Corporation
Windsor Locks, Conn. 06096

Attn: R. Hatch

United Technology Center
587 Methilda Avenue
P. O. Box 358
Sunnyvale, Calif. 94088

Attn: Dr. David Altman

Florida Research and
          Development
Pratt and Whitney Aircraft
United Aircraft Corporation
P. O. Box 2691
West Palm Beach, Florida
          33402

Attn: R. J. Coar

Vickers, Incorporated
Box 302
Troy, Michigan

Union Carbide Corporation
Technical Information
          Service
P. O. Box 6116
Cleveland, Ohio 44101

Union Carbide Corporation
Stellite Division
Kokomo, Indiana 46901

Attn: M. Schussler

Universal-Cyclops Steel Corp.
Refractomet Division
Bridgeville, Pa.

Attn: W. A. McNush

Union Carbide Corporation
Nuclear Division
ORGDP Records Dept.
P. O. Box P
Oak Ridge, Tennessee 37830

Attn: A. P. Huber
          Supt., Tech. Div.

Sylvania
Sylcor Division
Cantiague Road
Hicksville
Long Island, New York 11802

IIT RESEARCH INSTITUTE

6

Contract NAS7-460, NAS7-431

Solar Division
International Harvester Co.
2200 Pacific Highway
San Diego, Calif.   92112

Vitro Laboratories
200 Pleasant Valley Way
West Orange, New Jersey

Attn: M. H. Ortner

Wah Chang Corporation
Box 366
Albany, Oregon   97321

Research Laboratories
United Aircraft Corporation
400 Main Street
East Hartford, Conn.   06108

Surface Technology Corporation
3808 North Avenue
Stone Park, Illinois   60165

Attn: R. J. Van Thyne

Super Temp Company
11120 South Norwalk Blvd.
Santa Fe Springs, Calif. 90670

Attn: D. H. Leeds

Reactive Metals Titanium, Inc.
1000 Warren Avenue
Niles, Ohio

Attn: Harold Kessler

Nuclear Materials and Equipment
     Corporation
Apollo, Pennsylvania

Attn: F. B. Michels

National Research Corp.
45 Industrial Place
Newton, Massachusetts 02164

Attn: Dr. M. L. Torti

ManLabs Incorporated
21 Erie Street
Cambridge, Mass.   02139

Attn: Dr. Larry Kaufman

Lockheed Calif. Company
2555 North Hollywood Way
Burbank, Calif.   91503

Attn: G. D. Brewer

Kawecki Chemical Company
Boyertown, Pennsylvania

Lawrence Radiation Lab
Livermore, California

Attn: Dr. W. R. Holman

Commonwealth Scientific
     Corporation
500 Pendleton Street
Alexandria, Virginia   22314

Attn: D. F. Bazzare

Battelle Columbus
     Laboratories
505 King Avenue
Columbus, Ohio   43201

Attn: R. J. Favor